ADVANCES IN HEAT TRANSFER, VOLUME 22

Mathematical Models of Bioheat Transfer

CALEB K. CHARNY

Department of Chemical Engineering, The Cooper Union, New York, NY

I. Introduction

The effects of blood flow on heat transfer in living tissue have been examined for more than a century, dating back to the experimental studies of Bernard in 1876 [8]. Since that time, mathematical modeling of the complex thermal interaction between the vasculature and tissue has been a topic of interest for numerous physiologists, physicians, and engineers. The first quantitative relationship that described heat transfer in human tissue and included the effects of blood flow on tissue temperature on a continuum basis was presented by Harry H. Pennes, a researcher at the College of Physicians and Surgeons of Columbia University [46]. His landmark paper, which appeared in the literature in 1948, is cited in nearly all of the research articles involving bioheat transfer. Appropriately, the equation derived in this paper is often referred to as the "traditional" or "classic" or "Pennes" bioheat equation.

Over the past 40 years, hundreds of research articles have questioned, examined, and utilized the underlying assumptions of the Pennes theory [26, 54]. Even though some aspects of Pennes's work have been convincingly discredited, certain elements have stood up to this intense scrutiny over the years. His work remains essentially the quantitative foundation for the field of bioheat transfer. The objective of this survey is to first present the original work of Pennes, then to examine the subsequent research that questioned Pennes's theory and provided alternate and more sophisticated analyses of bioheat transfer. One of the most important alternates, which will be discussed in depth in this review, was developed by Weinbaum and colleagues in a series of papers over the past decade [24, 34, 55, 56, 59–63, 70]. In a concluding section, the characteristics of the original Pennes theory that are still being used today in bioheat transfer research will be discussed, along with the current understanding and future prospects for advances in bioheat transfer via a bioheat transfer equation.

II. Models Prior to Pennes

A. Thermal Conductances

Prior to the work of Pennes, heat transfer from the body to surroundings was quantified by the product of a thermal conductance and a measured temperature gradient between the tissue and the surroundings. The early work of Gagge *et al.* [27], Hardy and co-workers [29, 30], Bazett and co-workers [5–7], Mendelson [44], and Burton [11] utilized this approach with measurements of temperature gradients between the body surface and the environment under various conditions of environmental and metabolic stress. The heat transfer from the body to the surroundings was modeled based on the radiative, convective, and evaporative conductances with the environment and the temperature difference between the skin and surroundings. The influence of clothing on body heat transfer was modeled by adding an additional conductance for this layer and measuring the clothing surface temperature. These conductances were simply constant physical properties of the particular experimental subject.

B. Effective Conductance Due to Blood Flow

A more difficult problem was to quantify the contribution of blood flow to the thermal conductance of the tissue layer. While it was known from experiments that variations in tissue blood flow rate associated with vascular changes in the skin significantly affected the rate of heat loss from the tissue to the surroundings, the mathematical description of this process was quite simple. Heat transfer from the deep interior region of tissue to the skin surface was modeled by a linear addition of two conductances; one based on tissue blood flow rate and the other based on the inherent thermal conductivity of the tissue under conditions of zero blood flow. The relationship used,

$$q_s = \omega \rho_b c_b \delta (T_b - T_s) + \frac{k_t}{\delta}(T_b - T_s) = K_{eff}(T_b - T_s) \qquad (2.1)$$

states that the surface heat flux from the body to the environment depends on the tissue thermal conductivity, k_t, the thickness of the tissue layer in which a temperature gradient is measured, δ, the volume flow rate of blood to the tissue per unit volume tissue (also known as the blood perfusion rate), ω, and the density and specific heat of the blood, ρ_b and c_b, respectively. The temperature difference between the deep tissue, or body core, and the skin $(T_b - T_s)$, and q_s were usually measured experimentally and in this manner an "effective" tissue conductance, K_{eff}, was determined according to the definition in Eq. (2.1). Rearranging Eq. (2.1), the influence of

blood perfusion in tissue on the heat transfer inside the tissue could be quantified as

$$\frac{K_{\text{eff}}}{K_0} = 1 + \frac{\omega c_b \delta^2}{k_t} \tag{2.2}$$

where K_0 is the tissue conductance in the absence of blood perfusion. Studies were presented which used some form of Eq. (2.1) to quantify the effect of blood flow on tissue heat transfer [5, 27, 29, 30, 44]. Variations in K_{eff} with $(T_b - T_s)$ were identified with the influence of vasomotor control in thermoregulation of body temperature. At large values of $(T_b - T_s)$ the effective conductance was relatively constant, which represented the maximum degree of vasoconstriction in the tissue. As the temperature difference $(T_b - T_s)$ decreased, the effective conductance was observed to rise due to the increased perfusion rate in the tissue at higher ambient temperatures. Numerous experiments seemed to at least qualitatively corroborate this simple mathematical model.

The inadequacies of this formulation were considered by those who utilized it to be due mainly to the use of $(T_b - T_s)$ as the driving force for heat transfer. The temperature difference $(T_b - T_s)$ was usually calculated using the difference between the deep or body core blood (usually the rectal temperature) and the mean skin temperature. Gagge *et al.* [27] were aware that their calculated $(T_b - T_s)$ was a maximum temperature difference and thus the perfusion rate ω in Eqs. (2.1) and (2.2) was the minimum blood perfusion rate required to transfer heat across the tissue layer to the surroundings [27]. As a result, the parameter ω was considered an effective blood perfusion rate in the tissue. Another fundamental assumption of this effective conductance analysis that would be later challenged by Pennes was the existence of a temperature difference between the body and skin surface, $(T_b - T_s)$, that extended only to a depth δ within the tissue. Measurements by these early thermal physiology groups [5, 27, 29, 30, 44] were used along with the mathematical model described by Eqs. (2.1) and (2.2) to estimate that the value of δ was on the order of 2 cm. Pennes's measurements in human limbs, however, indicated the presence of temperature gradients in much deeper regions in the tissue. The importance of Pennes's work on the development of a mathematical model of bioheat transfer was to quantify the first continuous, analytical relationship between tissue temperature and position, or depth from the skin surface.

Prior to 1948, research in bioheat transfer was performed on an experimental basis and the associated quantitative analysis was of the type described in Eqs. (2.1) and (2.2) which used an overall conductivity to describe the heat loss from tissue to the surroundings. The overall thermal gradients measured by these physiologists were related to the overall heat

transfer from the body to the surroundings. Pennes's contribution to the field was stimulated by the lack of rigorous analysis of the local thermal gradients inside the tissue and the effect of blood perfusion on the local heat transfer rate in deep tissue. Preliminary *in vivo* measurements of temperature gradients in human biceps muscle revealed to Pennes that these gradients were present from the surface to the deep region of the muscle layer. These experimental measurements were supported by simple conduction heat transfer theory, which predicts that temperature gradients will exist from the surface down to the axis of a symmetrical body like the human limb, e.g., a cylinder. Recognizing that analytical differential heat transfer theory had not been previously applied to human tissue, Pennes initiated a combined experimental and rigorous theoretical study to examine the governing heat transfer principles in perfused tissue [46].

III. The Pennes Bioheat Equation [46]

A. Experimental Measurements

1. *Description*

Healthy males were used as experimental subjects. They lay on a bed with only a sheet covering their hips. The room and wall temperatures were identical, between 25–27 °C, and typically rose during the 4 to 6 h experimental period by 1 °C. There was essentially no air motion in the laboratory, as measured by an anemometer. Temperature measurements were made on both the surface and deep muscle regions of the unanesthetized pronated right forearm of all subjects. Skin temperatures were determined using both a radiometric device and copper–constantan thermocouples. Deep muscle and brachial artery temperatures were monitored using a similar thermocouple inserted into a thin walled steel needle. The relative precision of the thermocouple measurements was ±0.01 °C, while the radiometric temperatures were accurate to ±0.1 °C.

Skin temperature distributions along the axis of the upper limb, as well as around the circumference of the forearm, were examined by Pennes in 17 subjects. In addition, the effect of circulatory occlusion for 30–40 min at either the distal forearm or upper arm on proximal forearm and hand skin temperatures was quantified. These studies were used to qualitatively analyze the influence of cutaneous blood flow on skin temperature, which was generally a heating effect. The experimental results, however, were not in any way analyzed in a quantitative manner compared to the deep forearm and brachial artery temperature measurements that are described in the following paragraph.

The brachial artery temperature was measured at the elbow while the forearm was in a completely supinated position. The brachial artery temperature was greater than the maximum deep forearm temperature by an average of 0.16 °C for all 10 subjects involved in this part of the experiments. From this result, Pennes hypothesized that the arterial blood supplied to the forearm acts as a heating system for the muscle in this section of the arm. Furthermore, Pennes theorized that the brachial artery temperature at the elbow could be considered equal to the temperature of the blood in the radial artery located 8 cm distal to the elbow. Pennes based this assumption on the earlier observations of Bazett and McGlone [5]. This assumption was critical in the derivation of the Pennes bioheat equation because it allowed the arterial blood supply to the arm to be treated as a heat source that was independent of axial location along the length of the limb.

Steady state temperatures were measured across the muscle layer of nine subjects at an axial location 8.0 cm distal from the tip of the ulna olecranon (an elbow bone) and midway between the superior and inferior surfaces of the forearm. The thermocouple wire was moved in tension across the muscle layer by a mechanical wire-controller so that the position of the thermocouple junction relative to the skin surface was known to a high precision, on the order of a tenth of a millimeter. The number of measurements was greatest near the axis of the limb, where the temperature gradients were small, and temperatures were recorded roughly at 2-mm spacing intervals. Fewer temperatures were measured in the more peripheral region of the muscle layer, with spacing intervals on the order of 10 mm. The temperatures measured by Pennes are shown in Fig. 1.

2. *Basis for the Mathematical Model*

One of the most significant of Pennes's experimental results was that while there was some asymmetry in the temperature profiles, the maximum muscle temperature was located very close to or at the axis of the limb. The asymmetry was explained by Pennes to be due to the asymmetrical temperature distribution around the circumference of the forearm surface. Generally, the medial side of the limb was at a higher level than the lateral side of the limb, due mainly to the medial side's proximity to the warm core section of the human torso.

In addition, the temperature profiles of the different subjects were similarly flat near the limb axis, indicating that in general the tissue temperature was more uniform in this deep central region compared to the peripheral region, with its relatively large spatial gradients. Interestingly, one subject showed a temperature profile with two local maxima, which was accounted for by Pennes as a proximity effect with the radial artery, which would

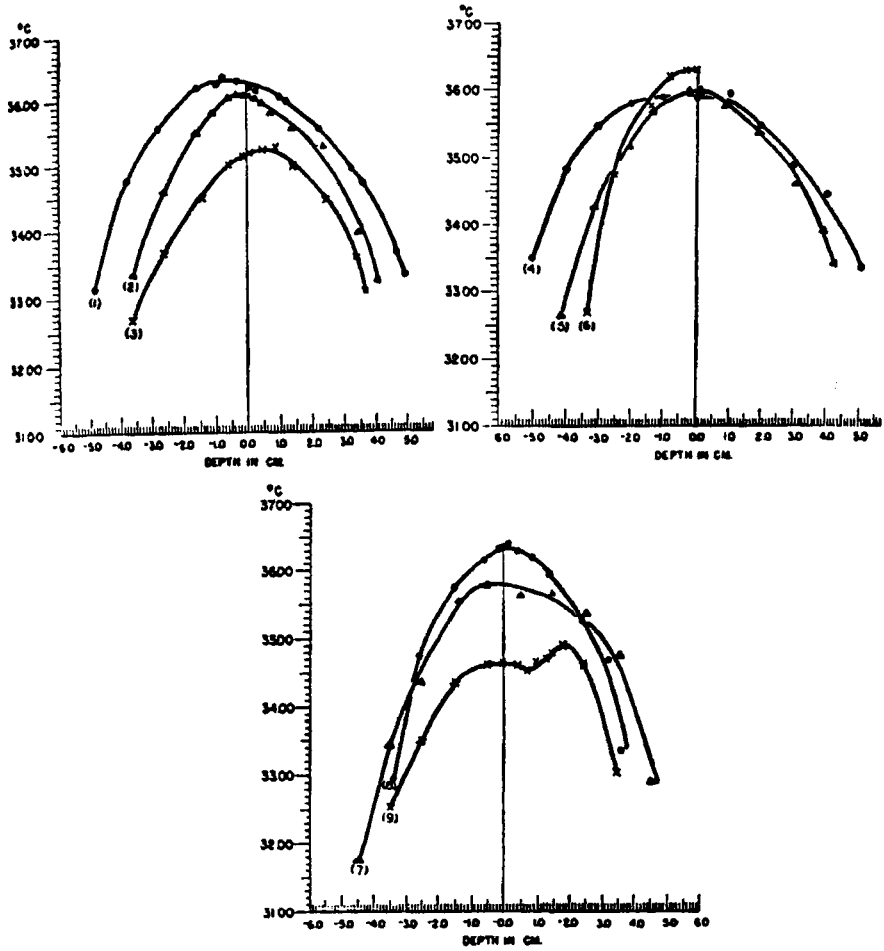

FIG. 1. Tissue temperature profiles in the forearms of nine human subjects. Negative abscissa values represent the lateral side of the forearm, and positive values represent the medial side. The ambient temperatures range from 26.1 to 27.4 °C. (Reproduced from [46], with permission.)

tend to locally heat tissue surrounding its wall. For this particular subject, the thermocouple wire clearly passed close by the wall of this artery. The extent of this local proximity heating, approximately 0.5 °C in this particular subject, is reasonable when compared to the results of bioheat transfer studies conducted much later during the 1980s in which local heating and cooling effects of arteries and veins embedded in muscle tissue were examined both experimentally and theoretically [41, 60].

B. THEORETICAL FORMULATION

1. *Governing Equations and Solution*

Using his experimental results as a basis, Pennes presented his quantitative analysis of heat transfer in the human forearm. For simplicity, a cylindrical geometry was assumed for the pronated forearm, even though its cross section is somewhat elliptical. The rate of metabolic heating in the tissue was assumed to be uniform throughout the forearm despite the observation that metabolic heat production would probably be lower near the forearm surface where temperature gradients are large. Also, the presence of the skin and fat layers, as well as the two forearm bones, was neglected by assuming that their heat production and thermal conductivity were the same as those in the muscle tissue. Pennes justified this latter assumption with his experimental data, which did not reveal any noticeable perturbation in the forearm temperature fields that could have been caused by the presence of the forearm bones.

A more accurate portrayal of the limb geometry and composition was not justified because there were several other simplifications that were more significant, most importantly that the heat transferred from the blood to the tissue was governed by what Pennes termed the "Fick principle." According to this behavior, the rate of mass transfer between the blood and tissue is proportional to the difference between the blood and tissue level of a substance multiplied by the rate of blood flow. Using this concept to describe the rate of heat transfer between blood and tissue, Pennes theorized that the net heat transferred from the blood to the tissue, Q_p, was simply proportional to the temperature difference between the arterial blood entering the tissue and the venous blood leaving the tissue:

$$Q_p = \omega \rho_b c_b (T_a - T_v) \tag{3.1}$$

where ω is the volumetric rate of blood perfusion to the tissue per unit volume of tissue and c_b is the blood specific heat. Since the temperature of the venous blood leaving the tissue depends on the degree of thermal equilibration it undergoes with the surrounding tissue, Pennes introduced a thermal equilibration parameter, k', to account for this effect:

$$T_v = T_t + k'(T_a - T_t) \tag{3.2}$$

For $k' = 0$, i.e., complete thermal equilibration, the venous blood temperature leaving the tissue is T_t, while for $k' = 1$ the venous blood leaves the tissue at a temperature equal to the entering arterial blood temperature. At this point, the Pennes derivation assumes that T_a is uniform throughout the tissue at some T_{a0}, which Pennes set equal to the mean brachial artery

temperature in his experimental subjects, and k' is close to zero everywhere in the muscle layer, thus yielding the familiar Pennes perfusion heat source term

$$Q_p = \omega \rho_b c_b (T_{a0} - T_t) \tag{3.3}$$

The perfusion heat source in Eq. (3.3) essentially assumes that blood enters the smallest vessels of the microcirculation at temperature T_{a0}, where all of the heat transfer between the blood and tissue takes place. The blood will act as a heat source or sink depending upon the algebraic sign of the temperature difference in Eq. (3.3). As blood leaves the capillary bed, it has undergone complete thermal equilibration with the surrounding tissue and enters the venous circulation at this temperature. The complete thermal equilibration is expected in the capillary bed since the blood velocity in these small diameter vessels is very low, corresponding to a Peclet number (the ratio of bulk convection heat transfer to conduction heat transfer) much less than unity. However, the venous blood temperature is assumed to remain at the tissue temperature as it flows from the capillary bed back to the main supply vein, regardless of flow rate or vessel size. Any heat exchange in this region of the microcirculation is neglected. Thus, in a manner analogous to the mass transfer of oxygen from blood to tissue, the Pennes perfusion term neglects all pre- and postcapillary heat exchange between the blood and tissue.

This term has been the focus of attention since its inception over 40 years ago. While computationally simple, several objections have been raised against the assumptions that this term represents [2, 10, 18, 22, 60, 61, 69]. The main argument against this formulation is that the thermal equilibration lengths for precapillary arterioles and postcapillary venules are quite small and thus the blood reaches the capillary bed at the surrounding tissue temperature. All heat exchange between blood and tissue will occur in the larger vessels of the microcirculation before the arterial feed blood reaches the capillaries, and similarly, after blood leaves the capillary bed there can be some heat exchange with the surrounding tissue. These objections and the alternative representations of the effect of blood perfusion on tissue heat transfer will be discussed later in this review.

Assuming angular symmetry and neglecting axial gradients in tissue temperature along the length of the limb, the Pennes equation is

$$\rho c_p \frac{\partial T_t}{\partial t} = \frac{k}{r} \frac{\partial}{\partial r} \left(r \frac{\partial T_t}{\partial r} \right) + \omega \rho_b c_b (T_{a0} - T_t) + Q_m \tag{3.4}$$

where Q_m is the uniform rate of metabolic heat generation in the tissue layer and k is the thermal conductivity of the tissue, also assumed to be uniform. Under steady state conditions, the solution to this second order ordinary

differential equation for the tissue temperature as a function of radial position in the limb is found using a convective boundary condition at the skin surface, radial position R:

$$-k\left.\frac{dT_t}{dr}\right|_{r=R} = h\left(\left.T_t\right|_{r=R} - T_\infty\right) \tag{3.5}$$

where h is the combined convection/radiation heat transfer coefficient between the skin surface and the surroundings, which are at temperature T_∞. The solution of the Pennes bioheat equation in these radial coordinates is

$$T_t = AI_0(ra) + \frac{Q_m}{\omega\rho_b c_b} + T_{a0} \tag{3.6}$$

where

$$a = \sqrt{\frac{\omega\rho_b c_b}{k}} \quad \text{and} \quad A = \frac{T_\infty - \dfrac{Q_m}{\omega\rho_b c_b} - T_{a0}}{\dfrac{ka}{h} I_1(Ra) + I_0(Ra)}$$

Because the perfusion rate, ω, could not be directly measured, Pennes varied this parameter in his model to fit his experimental data to the solution above for a fixed, representative ambient temperature and metabolic heating rate. In addition, the uniform arterial blood temperature T_{a0} was taken to be 36.25 °C, which corresponded to a temperature 0.16 °C higher than the mean maximum temperature measured in the experiments described above. Pennes found that his theory best fit the experimental data for a perfusion rate of between 1.2 and 1.8 ml blood/min/100 g tissue, which is a typical range of values for resting human skeletal muscle. If the equilibration factor k' was not considered to be zero (complete thermal equilibration between the venous blood and surrounding tissue) but 0.25 (partial equilibration), then the values of ω needed to fit the experimental data were higher, in the range 2–3 ml blood/min/100 g tissue. A comparison between the predictions of the Pennes model using various perfusion rates with experimental measurements is shown in Fig. 2.

The results of Pennes were the first predictions of a continuum mathematical model of bioheat transfer in humans. A fundamental conclusion from this study was that the rate of metabolic heat generation in the muscle was not sufficient to heat this tissue to the measured values. In order to qualitatively match experimental data to theory, the warming effect of blood flow in the perfused tissue layer had to be added to the metabolic heating. His model predicted that the maximum tissue temperatures would exceed the ambient tissue temperature by only 2–3 °C if the effects of perfusion were omitted from the bioheat equation. This parametric study

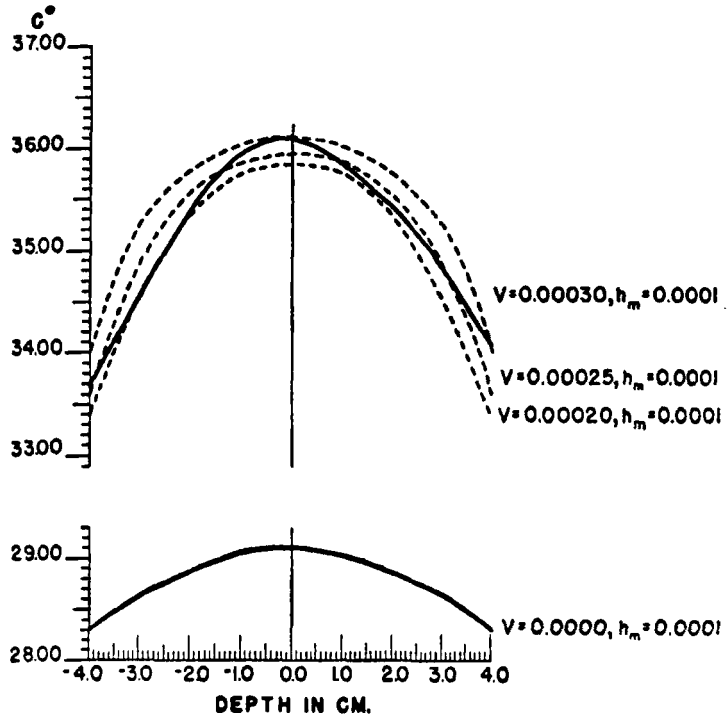

FIG. 2. Mean experimental temperature profile (solid) and theoretical temperature profiles (dashed) based on the Pennes bioheat equation. The parameter V represents perfusion rate in grams blood per cubed centimeter tissue per second, and h_m is the metabolic heat source in calories per second per cubed centimeter tissue. (Reproduced from [46], with permission.)

was invaluable in delineating the heating effects of blood and metabolism. For typical steady state resting conditions, only 25% of the limb heat loss to the environment was produced by tissue metabolic heating. Pennes also observed the effect of blood flow on the shape of the temperature profile. He noted that as the perfusion rate to the tissue increased, the bioheat equation predicted that the temperature profiles across the forearm would become flatter and their level would approach the fixed arterial temperature, T_{a0}. In contrast, earlier calculations in 1938 by Gagge *et al.* [27], which neglected the effects of blood perfusion, overestimated the magnitude of the temperature gradient in the periphery of the muscle layer.

2. *Analysis by Shitzer and Kleiner* [53]

A general analysis of the Pennes bioheat equation and the solution given above by Eq. (3.6) was performed by Shitzer and Kleiner in 1976 [53].

Their computations showed that the steady state temperature profile in the deep regions of the tissue, i.e., radial positions smaller than one-half the radius of the limb, was relatively insensitive to variations in the physiological parameters that appear in the solution to the Pennes equation, namely the perfusion rate ω and metabolic heating rate Q_m, as long as these two parameters changed in the same proportion. These theoretical studies also revealed that the computed temperatures in the deep regions of the tissue were not strongly dependent upon the rate of heat transfer from the surface of the cylindrical limb as characterized by the heat transfer coefficient h. As constructed, the Pennes model assumes that the arterial blood bathes the tissue at the same temperature everywhere in the limb cross section. In the deep region of the muscle layer, blood perfusion dominates the heat transfer because the surface boundary is relatively far away. The temperature difference between the blood and tissue in the deep region is relatively uniform, resulting in a temperature profile that is flat in the core of the limb. Shitzer and Kleiner also showed in their general analysis that the role of the perfusion term was that of a source in the cooler peripheral tissue and a sink in the warm core region of the cylindrical limb model. As the perfusion rate increases, the arterial blood acts like a heat source in a larger portion of the deep tissue. In the theoretical limit of infinite perfusion rate, the Pennes equation predicts that the entire cylindrical limb model will be at a uniform temperature equal to T_{a0}.

3. *Model Shortcomings*

Pennes acknowledged the inherent simplicity of his bioheat transfer model, for example, assuming uniform metabolic heating, perfusion rate, and thermal conductivity [46]. In addition, venous return from the distal part of the forearm could have an important effect on the tissue temperature of the deep muscle in which these vessels were located. To observe this effect, he suggested that a series of experiments in which the distal venous return was occluded would be useful. However, the underlying assumption of the model regarding the isotropic perfusion heat source itself was not mentioned as a possible source of error. As explored by many researchers in subsequent studies, this assumption is critical to the formulation of Pennes's equation. Without consideration of the vascular architecture, especially the countercurrent arrangement of the circulatory network and the gradually tapering characteristics of the vascular bed, the bioheat equation of Pennes neglected important anatomical features of the circulatory system that can have a profound effect on tissue bioheat transfer.

While the Pennes model has been applied with great success as an analytical tool with which blood perfusion rate can be determined from

experimentally measured local temperature gradients and heat flows, the basic formulation of the model is still questionable. The shortcomings of the Pennes model and improvements that have been proposed to overcome the deficiencies inherent to this model have been the subject of a large body of research over the past 40 years. An examination of these studies yields some very interesting observations, including not only the flaws and limitations of the Pennes model, but also the applicability of this relatively simple bioheat equation as an analytical tool for bioheat transfer.

These successes include implementation of the Pennes model in mathematical simulations of procedures such as therapeutic hyperthermia for the treatment of cancer [15, 16, 23, 26, 33, 42, 49, 54], estimation of tissue perfusion by heat clearance methods [9, 14, 21, 25, 35, 43, 47, 48], as well as in whole body thermal models of man under conditions of environmental stress [28, 31, 32, 57, 65]. Many of these formulations have yielded realistic predictions, in some cases with experimental verification. In most of these theoretical studies, the temperature of the blood that perfuses the tissue is assumed to be uniform and fixed at the body core temperature. Some of the whole body thermal models mentioned above include a spatial variation in blood temperature between body segments [16, 65]. However, within a body segment, the Pennes assumptions are usually applied. While many of these simulations were in good agreement with experimental data obtained clinically, the questionable assumptions upon which the Pennes equation are based continue to be examined. In many of these cases, the neglect of heat transfer in the prearteriole and postvenule blood vessels of the circulatory system can be used to explain the discrepancy between experimental measurements and Pennes bioheat equation-based theoretical calculations.

IV. Wulff Continuum Model [69]

A. Criticism of the Pennes Model

In 1974 a paper by Wulff appeared which was one of the first papers that directly criticized the fundamental assumptions of the Pennes bioheat equation and provided an alternate analysis [69]. Three different aspects of the Pennes theory were faulted. Consider the unsteady version of the Pennes equation in its original form, before any assumptions are made regarding the thermal equilibration of blood in the microcirculation:

$$\rho c_p \frac{\partial T_t}{\partial t} = \nabla \cdot (k \nabla T_t) + \omega c_p (T_{a,in} - T_{v,out}) + Q_m \tag{4.1}$$

where $T_{a,in}$ and $T_{v,out}$ represent the temperature of the blood upon entering and leaving the tissue region via the arteriole–venule network. Wulff states that one flaw in the Pennes equation is that it contains both local and global control systems. The capacitance term on the left-hand side of Eq. (4.1), along with the diffusion and metabolic heat generation terms on the right-hand side of Eq. (4.1), all represent local control volume heat sources, that is, net heat deposition at a specific location in the tissue at a given time. The perfusion term, as represented by the second term on the right-hand side of Eq. (4.1), however, is what Wulff terms a "global" heat source. The Pennes perfusion term in Eq. (4.1) models heat exchange between the blood and tissue on an overall, or global, basis, where the heat deposited in the tissue per unit volume tissue is proportional to the total, or global, change in the blood temperature accomplished during its travel through the tissue medium. Such a combination of local and global control volume terms is physically inconsistent.

The second major criticism by Wulff is that the original form of the Pennes equation, as shown in Eq. (4.1), actually contains three unknown temperatures: the tissue temperature T_t, the entrance arterial temperature $T_{a,in}$, and the exit venous temperature $T_{v,out}$. Based upon this equation, there are three different materials occupying the same space at any given location and time: the solid tissue as well as two flowing blood streams, arterial and venous. Therefore two more equations must be written and then solved simultaneously with Eq. (4.1) in order to completely define the system both mathematically and physically.

Another faulty aspect of the Pennes equation according to Wulff is the representation of the heat transfer between the solid tissue and moving fluid blood streams. Since blood is moving through the tissue, it may convect heat in any direction, not just in the direction of the local tissue temperature gradient. In addition, the magnitude of the heat transfer between the solid tissue and flowing blood should be proportional to the temperature difference between these two media, rather than between the two blood stream temperatures, $T_{a,in}$ and $T_{v,out}$. Based upon this principle, the convective transport of energy by the flowing blood is

$$\rho_b h_b v_h = \frac{1}{4\pi} \int_\Omega \rho_b h_b v \, d\omega' \tag{4.2}$$

where h_b is the specific enthalpy of the blood, ω' represents the solid angle across the control surface of the blood vessel, Ω represents the entire solid angle, equal to 4π, and v_h represents a local mean apparent blood velocity. This energy flux by the flowing blood will either augment or diminish the effect of the conductive energy flux on overall tissue heat

transfer. Wulff argues that the isotropic perfusion term that appears in the Pennes equation does not account for the convective heat transfer by the flowing blood described in Eq. (4.2). Another inconsistency in the Pennes theory, according to Wulff, is that the presence of arterial and venous blood streams within the solid tissue medium renders the existence of the continuous gradients in tissue temperature implied by the conduction term in Eq. (4.1) physically impossible. Wulff also points out that the actual tissue contains a microcirculatory network in which a single stream of arterial blood flows through capillaries and in this manner gradually becomes converted into a single stream of venous blood over a finite space. The Pennes perfusion term, however, essentially assumes that two different blood temperatures, the inlet arterial and outlet venous temperatures, coexist at the same spatial location within the tissue continuum.

Wulff's three areas of criticism are directed towards the inherent physical incongruities of the original form of the Pennes equation, before any assumptions are made regarding the thermal equilibration effects in the microcirculation. The approximations of thermal equilibration in the microcirculation are also shown to be faulty. Wulff contends that the simplification of the perfusion heat source term from its form in Eqs. (3.1) and (4.1) to Eq. (3.3) is arbitrary since the blood will be thermally equilibrated with the surrounding tissue before it reaches the capillary level. While it is reasonable to equate the blood and tissue temperatures, Wulff states that it is arbitrary to choose only the venous blood stream and not the arterial blood as the fluid stream that becomes equilibrated with the tissue. Of course, if both arterial and venous blood temperatures are equilibrated with the tissue only a very small distance from the main supply artery and drainage vein, the magnitude of the Pennes perfusion term in Eqs. (3.1) and (4.1) will be zero. Wulff concludes his physical arguments by stating the form of the Pennes perfusion term in Eq. (3.4), which had been used in previous studies of bioheat transfer, was the result of numerous deficiencies in its derivation.

B. Derivation of an Alternate Bioheat Equation

1. *Anisotropic Blood Flow Term*

In response, Wulff presents his own formulation which corrects the physical violations in the Pennes model described above. In conjunction with Eq. (4.2), the energy flux at any point in the tissue region is

$$q = -k \nabla T_t + \rho_b h_b v_h \tag{4.3}$$

The specific enthalpy of the blood h_b is formulated to account for both the sensible enthalpy plus the enthalpy of reaction that is represented by the Q_m term in Eq. (4.1):

$$h_b = \int_{T_0}^{T_b} c_p(T_b^*)\, dT_b^* + \frac{P}{\rho_b} + \Delta H_f(1 - \varepsilon) \tag{4.4}$$

where P is the system pressure, ΔH_f is the specific enthalpy of the metabolic reaction, ε is the extent of reaction, and T_0 and T_b are the reference and blood temperatures, respectively. Since the energy capacitance of the tissue in the control volume is equal to the negative gradient of the net energy flux into the control volume, the energy balance equation can be written as

$$\rho c_p \frac{\partial T_t}{\partial t} = -\nabla \cdot q \tag{4.5}$$

Substituting Eq. (4.4) into Eq. (4.5)

$$\rho c_p \frac{\partial T_t}{\partial t} = \nabla \cdot \left\{ k \nabla T_t - \rho_b v_h \int_{T_0}^{T_b} c_p(T_b^*)\, dT_b^* + \frac{P}{\rho_b} + \Delta H_f(1 - \varepsilon) \right\} \tag{4.6}$$

Note that Eq. (4.6) neglects the fact that the heat capacity product ρc_p on the left-hand side should actually be taken as a volume average for the tissue and blood properties since both media comprise the control volume under consideration. However, the volume of blood relative to tissue in the control volume is considered small enough so that the contribution of the blood to the heat capacity of this mixture may be neglected. Using the continuity condition, Eq. (4.6) can be simplified for a system with no fluid accumulation. This is a reasonable assumption if the effect of lymph accumulation and drainage is neglected. By setting the divergence of the product $(\rho_b v_h)$ to zero, neglecting the mechanical work term P/ρ_b, and assuming constant physical properties within the control volume, Eq. (4.6) becomes

$$\rho c_p \frac{\partial T_t}{\partial t} = k \nabla^2 T_t - \rho_b v_h (c_p \nabla T_b - \Delta H_f \nabla \varepsilon) \tag{4.7}$$

The metabolic reaction term can be substituted with its usual form since the last term on the right-hand side of Eq. (4.7) is equivalent to Q_m.

2. *Complete Blood–Tissue Equilibration*

Wulff assumes that the gradient in blood temperature in Eq. (4.7) is equivalent to the gradient of the surrounding tissue temperature, an assumption that will be encountered later in this review as other mathematical models of bioheat transfer are introduced [61, 63]. Actually, in his formulation

Wulff simply assumes that T_b is equivalent to T_t in the tissue control volume based upon the argument that blood in the microcirculation will be thermally equilibrated with the surrounding tissue not far from its exit from the main arterial supply blood streams. According to Wulff, this concept was overlooked in Pennes formulation, which he claimed arbitrarily chose the venous blood to be thermally equilibrated with the surrounding tissue, while a similar argument could be made for the arterial blood as it leaves the main supply vessel and enters the tissue via the microcirculatory network. The final form of the "correct" form of the bioheat equation as derived by Wulff is

$$\rho c_p \frac{\partial T_t}{\partial t} = k \nabla^2 T_t - \rho_b v_h c_p \nabla T_t + Q_m \tag{4.8}$$

C. Solution to the Wulff Model—Parameterization and Comparison with Pennes

The main difficulty in solving this energy balance equation is in the evaluation of the local blood mass flux $\rho_b v_h$. This determination is more complicated than the evaluation of the volumetric perfusion bleed-off parameter, ω, which appears in the Pennes equation. For a relatively simple geometry, however, this mass flux term may be reduced to an easily managed form. For a one-dimensional slab geometry, there is only one nonzero component of blood velocity, v_x. At steady state with zero metabolic heating, this one-dimensional problem is easily solved. Wulff enforces a fixed temperature boundary condition at the two boundaries of the slab, and solves both Eq. (4.8) and the Pennes bioheat equation. In dimensionless form, the fundamental difference between the two equations is readily apparent. The Pennes bioheat equation reduces to

$$\frac{\partial^2 \theta}{\partial^2 z} - a\theta = 0, \qquad a = \frac{\omega \rho_b c_b L^2}{k} \tag{4.9}$$

The energy balance in Eq. (4.8) under these same conditions is

$$\frac{\partial^2 \theta}{\partial^2 z} - b\frac{\partial \theta}{\partial z} = 0, \qquad b = \frac{\rho_b c_b L v_x}{k} \tag{4.10}$$

where L is the length of the slab, z is a dimensionless position within the slab, and θ is the dimensionless temperature $(T_t(x) - T_t(0))/(T_t(L) - T_t(0))$. Both Eqs. (4.9) and (4.10) are subject to the fixed temperature boundary conditions $\theta(0) = 0$ and $\theta(1) = 1$. Note that Eq. (4.9) was derived by setting the boundary value temperature $T(0)$ equal to the value of T_{a0} in the perfusion term of the Pennes bioheat equation. This dimensionalization

transforms the Pennes bioheat equation from a nonhomogeneous to a homogeneous differential equation which can be solved independently of the arterial blood temperature T_{a0}.

The solution to Eq. (4.9) for the conditions stated above is

$$\theta = \frac{\sinh(\sqrt{a}\, z)}{\sinh(\sqrt{a})}, \qquad 0 \le z \le 1 \tag{4.11}$$

while the solution to Eq. (4.10) under these same conditions is

$$\theta = \frac{e^{zb} - 1}{e^{b} - 1}, \qquad 0 \le z \le 1 \tag{4.12}$$

Solutions to both the Pennes and Wulff models are shown in Fig. 3.

With zero blood flow, the temperature profile is linear according to both the Pennes and Wulff models, since under these conditions ω and v_h are both zero and thus the tissue slab is a one-dimensional pure conduction field. As the blood flow increases from zero, the temperature profiles become skewed away from a linear profile. It is important to realize that for a constant value for v_x, the ratio of the coefficient a and b has a magnitude of unity because the products $\omega\rho_b L$ and $\rho_b v_x$ both represent the mass flux of blood flowing through the tissue. However, Wulff shows that while the Pennes bioheat equation is insensitive to the direction of blood flow (the isotropic perfusion parameter ω is by definition always positive), the predictions of Eq. (4.12) will include the consequences of blood flow direction. Thus the coefficient a that appears in the Pennes bioheat equation is always positive, while the coefficient b in Eq. (4.12)

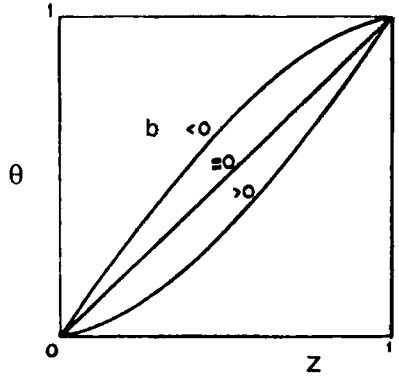

FIG. 3. Temperature profiles across a one-dimensional slab as predicted by the Wulff bioheat equation. The parameter b, defined in Eq. (4.10), corresponds to the perfusion velocity of blood in the tissue. (Reproduced from [69], with permission, © 1974 IEEE.)

may be positive or negative, depending upon the direction of blood velocity. This directionality effect is missing from the Pennes bioheat equation and is clearly a major deficiency of this model. The degree of error introduced into the Pennes equation computations depends mainly on the magnitude of the perfusion bleed-off parameter, ω. It is interesting to note that under resting conditions, the value of the coefficient a across a 5-cm-thick slab of skeletal muscle tissue is on the order of 5-10. For the case $a = b = 10$, the dimensionless temperatures predicted by the Pennes and Wulff models at the midpoint of the one-dimensional slab are 0.1974 and 0.0067, respectively. Also, with $b = -10$, the dimensionless temperature at this same midpoint location as predicted by the Wulff model is 0.9933, which is four times greater than the value predicted by the Pennes bioheat equation. Clearly, directionality of blood flow plays an important part in the heat transfer within the perfused tissue.

The study by Wulff represented one of the earliest investigations of alternatives to the Pennes bioheat equation. One of the major criticisms of the Pennes model, the omission of blood flow directionality, was shown to be of great significance because the errors introduced by this omission were on the same order as the effect of blood flow itself. Wulff also concluded that blood flow could be properly modeled only if spatial variations in the local blood velocity where known. For the one-dimensional slab case described above, no variations were considered. For the *in vivo* case, however, these considerations of blood flow variations become very complicated. Finally, Wulff revealed that there were several physical inconsistencies inherent to the Pennes bioheat equation, including the combination of local and distributed heat source terms. The control volume approach to analyzing bioheat transfer between solid tissue and flowing blood within the solid tissue that was used by Wulff in 1974 was similarly implemented in series of studies by Klinger [37-39].

V. Klinger Continuum Model [37-39]

In 1974, Klinger [37-39] presented an analytical model of heat diffusion with convection that did not use the Pennes assumptions and was conceptually similar to that of Wulff. The formulation of Klinger was developed primarily to describe thermal clearance experiments in which tissue perfusion rate was related to the rate at which deep tissue temperature changed during point source heating [47, 48]. Klinger argued that in utilizing the Pennes model to interpret these heat clearance experiments, the effects of nonunidirectional blood flow were being neglected and thus significant errors were being introduced into the computed results. In order to correct

this lack of directionality in the formulation, Klinger proposed that the convection field inside the tissue should be modeled based upon the *in vivo* vascular anatomy. A combination of "convection multipoles" could be used to represent the thermal influence of the blood vessels, based upon not only the magnitude of the blood flow, but also its direction.

A. Governing Equations

The differential energy balance for this system contains capacitance, convection, conduction, and heat source terms:

$$\rho c \frac{\partial T_t}{\partial t} + \rho c \mathbf{v} \cdot \nabla T_t = k_t \nabla^2 T_t + Q \tag{5.1}$$

This model assumes that the tissue physical properties are constant and the flowing blood is incompressible so that $(\nabla \cdot \mathbf{v}) = 0$. This equation is similar to that derived by Wulff [69], except it is written for the more general case of a spatially and possibly temporally nonuniform velocity field $\mathbf{v}$ and heat source Q. This general heat transport equation can be written in terms of spatially dimensionless quantities as

$$\frac{\partial T_t}{\partial \tau} + \mathrm{Pe}\, \mathbf{v}^* \cdot \bar{\nabla} T_t = \bar{\nabla}^2 T_t + \frac{QL^2}{k_t} \tag{5.2}$$

where the $\mathbf{v}^*$ is the fluid velocity relative to a characteristic velocity, Pe is the Peclet number for flow based upon the characteristic velocity, $\bar{\nabla}^2$ is a dimensionless Laplacian operator based upon the characteristic length L, and τ is the time relative to a characteristic time, L^2/α, where α is the tissue thermal diffusivity. Note that this time characterization is equivalent to a Fourier number of unity. Klinger introduces another dimensionless velocity $\bar{\mathbf{v}}$, which is the product of the Peclet number and $\mathbf{v}^*$. In this manner, the energy balance equation is written as

$$\psi T_t + \frac{QL^2}{k_t} = 0 \tag{5.3}$$

where ψ is the dimensionless operator $[\bar{\nabla}^2 - (\mathrm{Pe}\, \mathbf{v}^* \cdot \bar{\nabla}) - \partial/\partial\tau]$. Assuming an instantaneous point source, the heat source term QL^2/k_t is replaced by a Dirac delta function that vanishes everywhere except at the location $\mathbf{r}_1$.

B. Green's Function Solution

Klinger uses a Green's function formulation to solve the differential equation above. The solution to Eq. (5.3) is given by the relationship

$$\psi G_v(\mathbf{r}, \mathbf{r}_1, \tau, \tau_1) = \delta(\mathbf{r} - \mathbf{r}_1)\delta(\tau - \tau_1) \tag{5.4}$$

where the solution of G_v is the Green's function, which depends upon $\mathbf{r}_1$, the nondimensional location of the point source (normalized by length L), the general position $\mathbf{r}$, which is a nondimensional radial position, and time τ. The time τ_1 represents the time when the point source is turned on. For a small heat source, the surrounding tissue can be considered an infinite medium, and the heat flux will therefore be zero as $\mathbf{r}$ approaches infinity. The value of $\mathbf{r}_1$, however, must be finite. The initial conditions are based upon a uniform temperature field inside the tissue before time τ_1. Equation (5.4) is solved according to the conditions

$$G_v(\mathbf{r}, \mathbf{r}_1, \tau, \tau_1) = 0 \qquad \tau < \tau_1 \tag{5.5}$$

$$\frac{\partial}{\partial r} G_v(\mathbf{r}, \mathbf{r}_1, \tau, \tau_1) = 0 \qquad r \to \infty \tag{5.6}$$

For the case of a noninfinite tissue medium, the boundary condition described by Eq. (5.6) can be modified to account for the heat flux at the tissue surface using a superposition method with the method of images. Klinger shows that the solution to the nonhomogeneous heat conduction aspect of this problem, with no convection effects, has the form

$$T_t(\mathbf{r}, \tau) = -\int_\Omega d^3\mathbf{r}_1 \int_0^\tau G_v(\mathbf{r}, \mathbf{r}_1, \tau, \tau_1) Q^*(\mathbf{r}_1, \tau_1)\, d\tau_1 \tag{5.7}$$

where $Q^* = QL^2/k_t$. The symbol Ω stands for the control volume of integration. Klinger calculates the Green's function by treating the effect of convection near the point source as a small perturbation of the temperature field in the absence of convection. This can be justified by considering that the temperature gradient near the point source is very large during a time interval that is much smaller than the characteristic time for heat conduction, L^2/α. During this period, the conduction heat flow is much more significant that the effect of convection and the Green's function can be written

$$G_v = G_{v0} + G_{v1} \tag{5.8}$$

where G_{v0} is the Green's function for heat transfer by pure conduction and G_{v1} is the perturbation due to heat transfer by convection. Substituting this expression for the Green's function into the governing energy balance equation (5.4) and utilizing the condition that

$$\left[\bar{\nabla}^2 - \frac{\partial}{\partial \tau}\right] G_{v0} = \delta(\mathbf{r} - \mathbf{r}_1)\delta(\tau - \tau_1):$$

$$-\mathbf{v} \cdot \bar{\nabla} G_{v0}(\mathbf{r} - \mathbf{r}_1, \tau - \tau_1) + \left[\bar{\nabla}^2 - (\bar{\mathbf{v}} \cdot \bar{\nabla}) - \frac{\partial}{\partial \tau}\right] G_{v1}(\mathbf{r}, \mathbf{r}_1, \tau, \tau_1) = 0 \tag{5.9}$$

Neglecting the small convection term $\bar{\mathbf{v}} \cdot \bar{\nabla} G_{v1}$, the solution for G_{v1} is given by Eq. (5.7). Consequently, the convection term $G_{v2} = (\bar{\mathbf{v}} \cdot \bar{\nabla} G_{v1})$ can be considered a small perturbation term in the solution for G_{v1}, and so on, implying that the exact solution to Eq. (5.4) is an infinite series of terms

$$G_v(\mathbf{r}, \mathbf{r}_1, \tau, \tau_1) = \sum_{i=0}^{\infty} G_{vi}(\mathbf{r}, \mathbf{r}_1, \tau, \tau_1) \tag{5.10}$$

Klinger uses similar perturbation methods to show that the series solution in Eq. (5.10) is appropriate not only for the time intervals much smaller than the characteristic time, but also for all times τ. The expressions for G_{vi} are

$$\left[\bar{\nabla}^2 - \frac{\partial}{\partial \tau}\right] G_{v0} = \delta(\mathbf{r} - \mathbf{r}_1)\delta(\tau - \tau_1) \tag{5.11}$$

$$\left[\bar{\nabla}^2 - \frac{\partial}{\partial \tau}\right] G_{vi} = \bar{\mathbf{v}} \cdot \bar{\nabla} G_{v(i-1)}, \qquad \text{where } i = 1, 2, 3, \ldots \tag{5.12}$$

The solution to Eq. (5.11) with boundary conditions (5.5) and (5.6) is the Green's function for pure conduction heat transfer with no convection.

$$G_{v0}(\mathbf{r} - \mathbf{r}_1, \tau - \tau_1) = \frac{\exp[-(\mathbf{r} - \mathbf{r}_1)^2/4(\tau - \tau_1)]}{[4\pi(\tau - \tau_1)]^{3/2}} \tag{5.13}$$

The $i \neq 0$ terms in Eq. (5.10) are computed successively using the $(i-1)$th solution for each Green's function. Klinger shows that the term on the right-hand side of Eq. (5.12) can be interpreted as a distributed heat source that influences the pure conduction field described by the Green's function G_{v0}. While each calculation of G is performed without including the effect of convection in the operator on the left-hand side of Eq. (5.12), the right-hand side acts as a higher order correction. In this manner, the effect of convective heat transfer due to the circulatory system is treated as a correction term in the perturbation solution, and the total convective heat transfer between tissue and flowing blood is modeled as an infinite number of successively smaller magnitude heat sources that may be both spatially and temporally variable. The terms in this infinite series are uniformly and absolutely convergent, as shown by Klinger [37].

The temperature field is thus determined by implementing Eq. (5.7) to solve for G_{vi}, which represents the temperature distribution inside the nonhomogeneous conduction field

$$G_{vi} = -\int_{\tau_1}^{\tau} \int_{\Omega} G_{v0}(\mathbf{r} - \mathbf{r}_2, \tau - \tau_2)\bar{\mathbf{v}}(\mathbf{r}_2, \tau_2) \cdot \bar{\nabla} G_{v(i-1)}(\mathbf{r}_2, \mathbf{r}_1, \tau_1, \tau_2)\, d^3\mathbf{r}_2\, d\tau_2 \tag{5.14}$$

Klinger shows that by combining Eqs. (5.10) and (5.14), the Green's function solution can be written as

$$G_v = G_{v0}(\mathbf{r} - \mathbf{r}_2, \tau - \tau_2)\bar{v}(\mathbf{r}_2, \tau_2) - \int_{\tau_1}^{\tau}\int_{\Omega} G_{v0}(\mathbf{r} - \mathbf{r}_2, \tau - \tau_2)\bar{v}(\mathbf{r}_2, \tau_2) \cdot \bar{\nabla} G_{v(i-1)}(\mathbf{r}_2, \mathbf{r}_1, \tau_1, \tau_2)\, d^2\mathbf{r}_2\, d\tau_2 \tag{5.15}$$

C. COMPUTATION OF MEAN TISSUE TEMPERATURE

In order to relate the predictions of this analytical solution to experimental measurements, Klinger defines a macroscopic temperature based upon a spatial average of the microscopic temperatures predicted by his mathematical model over a finite volume. This averaging procedure is necessary because the experimental measurements are made with temperature probes that have some finite dimension, and an associated spatial resolution, and thus measure temperatures over a macroscopic length scale. The spatial averaging procedure also reduces the amount of information regarding vascular geometry that is required to solve the analytical model. The details of the vascular architecture can be replaced by a repeating pattern of vessels in the tissue that are represented mathematically by a set of convection multipoles.

1. *Multipole Models of Blood Perfusion*

Klinger computes a mean temperature over a finite volume of tissue based on an average Green's function [38]

$$\langle G_v \rangle \equiv \frac{1}{V_0}\int_{V_0} G_v\, d^3\mathbf{r} \tag{5.16}$$

Substituting Eqs. (5.10) and (5.14) into the definition above

$$\langle G_v \rangle \equiv \frac{1}{V_0}\sum_{i=0}^{\infty}\int_{V_0} d^3\mathbf{r}\int_{\tau_1}^{\tau}\int_{\Omega} G_{v0}(\mathbf{r} - \mathbf{r}_2, \tau - \tau_2) q_i(\mathbf{r}_2, \mathbf{r}_1, \tau_1, \tau_2)\, d^3\mathbf{r}_2\, d\tau_2 \tag{5.17}$$

where q_i represents the heat source effect of perfusion based on the $(i - 1)$th Green's function

$$q_i = -\bar{v}(\mathbf{r}_2, \tau_2) \cdot \bar{\nabla} G_{v(i-1)}(\mathbf{r}_2, \mathbf{r}_1, \tau_1, \tau_2) \tag{5.18}$$

The volume V_0 is chosen to be on the order of the volume resolution of the temperature probe. Outside the control volume V_0, the contribution of

convection to the temperature field inside the volume V_0 can be written as

$$\langle G_{vi} \rangle = \sum_j \frac{1}{V_0} \int_{V_0} d^3\mathbf{r} \int_{\tau_1}^{\tau} \int_{V_j} G_{v0}(\mathbf{r} - \mathbf{r}_0, \tau - \tau_2) q_i(\mathbf{r}_2, \mathbf{r}_1, \tau_1, \tau_2)\, d^3\mathbf{r}_2\, d\tau_2 \tag{5.19}$$

where V_j represents the volume of the region outside V_0 in which blood flow influences the temperature profile inside volume V_0.

Klinger uses the q_i perfusion correction terms to account for variations in vascular geometry and their effect on the mean tissue temperature field. By introducing the vector ξ to relate spatial positions inside each volume V_j to $\mathbf{r}$, the Green's function solutions for the temperature field inside the control volume V_0 can be written in terms of a series of heat multipoles, whose moments represent the influence of the blood flow convection effect. The components of the resulting moment tensor depend upon the geometry of the flow field inside the volume elements V_j. The mean temperature distribution predicted by this method is valid as long as the characteristic distance between adjacent blood vessels is smaller than the length scale of the control volume V_0 over which the mean temperature is determined, i.e., the temperature probe's spatial resolution. Under this condition, the mean temperature distribution is given by the Green's function solution

$$G_v(\mathbf{r}, \mathbf{r}_1, \tau, \tau_1) = \sum_{i=0}^{\infty} \int_{\tau_1}^{\tau} \int_{\Omega} \sum_{\nu=1}^{3} \bar{\nabla}_\nu G_{v(i-1)}(\mathbf{r}_2, \mathbf{r}_1, \tau_1, \tau_2) \cdot \sum_{l=0}^{\infty} \left(\frac{\partial}{\partial \mathbf{r}_2}\right)^l G_{v0}(\mathbf{r} - \mathbf{r}_2, \tau - \tau_2) \cdot \begin{pmatrix} l & \mathbf{r}_2 \\ \xi^l & \bar{v}_\nu \end{pmatrix} d^3\mathbf{r}_2\, d\tau_2 \tag{5.20}$$

where $\xi = \mathbf{r}_2 - \mathbf{r}_{2,0j}$ with $\mathbf{r}_{2,0j}$ representing the position of the center of the element j with volume V_j, the parameter ν is one of the three primary spatial directions, and l is the order of the moment tensor described below.

The tensor term on the right-hand side of Eq. (5.20) as derived by Klinger is a moment tensor representation of the blood flow velocity field in the tissue based upon the local perfusion field in the volume element V_j. The moment, of order l, depends upon the blood velocity and geometry:

$$\begin{pmatrix} l & \mathbf{r}_2 \\ \xi^l & \bar{v}_\nu \end{pmatrix} = \frac{1}{V_j} \begin{pmatrix} \sum_{k=1}^{3} n_k & j \\ \xi_1^{n_1}, \xi_2^{n_2}, \xi_3^{n_3} & \bar{v}_\nu \end{pmatrix} \tag{5.21}$$

When the moment order is zero, the effect of blood flow on tissue temperature is one-dimensional, and the tensor specifies a monopole moment. With $l = 1$, the tensor yields the dipole moments in each of the three spatial dimensions.

2. *Variations in Vascular Geometry*

Klinger shows that the multipole moments of several different convection patterns are determined by the relationship

$$\begin{pmatrix} l = n_1 + n_2 + n_3 & j \\ n_1, n_2, n_3 & \bar{v}_\nu \end{pmatrix} = \int_{V_j} \bar{v}_\nu \prod_{k=1}^{3} \xi_k^{n_k} \, d^3\xi \tag{5.22}$$

for the tissue element with volume V_j containing a repeating pattern of blood vessels. Klinger considers three different flow arrangements, one cocurrent, and two countercurrent, as shown in Fig. 4. In case 1, flow is cocurrent and the monopole moment, from Eq. (5.22), is

$$\begin{pmatrix} 0 & j \\ 0 & \bar{v}_\nu \end{pmatrix} = \int_{V_j} \bar{v}_\nu \, d^3\xi \tag{5.23}$$

or

$$\begin{pmatrix} 0 & \mathbf{r}_2 \\ 0 & \bar{v}_\nu \end{pmatrix} = \frac{1}{V_j} \frac{\lambda}{L} \bar{V} \tag{5.24}$$

where $\bar{V}$ is the volume flow rate in all vessels that are embedded in the tissue element, λ is the length of the side of the cube over which the average tissue temperature is determined, and L is the characteristic length of the macroscopic temperature field. The nondimensional volume of the cubic element V_j is $(\lambda/L)^3$. In this manner, Klinger illustrates that the monopole moment for this vascular arrangement is equivalent to an average flow velocity based upon the volume flow rate per unit area normal to flow. Similar evaluations are made for the multipole moments related to cases 2 and 3.

In all three vascular arrangements, Klinger observes that the multipole moment is directly proportional to the total volumetric flow rate in the blood vessels within a repeating tissue element. The influence of each of these multipole moments is influenced also by the ratio (λ/L), which is less than unity, to some power between unity and 5, depending on the moment order and the vascular geometry. The multipole moments for the cocurrent arrangement described by case 1 are on the order of magnitude of (λ/L) or smaller, while for the countercurrent flows in cases 2 and 3 the multipole moments vary with $(\lambda/L)^2$ or smaller. Thus Klinger concludes that the effect of countercurrent flow on tissue heat transfer is at most a second order effect. Klinger also points out that the monopole moment for all cases is independent of the number density of blood vessels in the tissue as well as the velocity profile inside the vessels and depends instead on a D'Arcy type mean blood flow velocity as described by Eq. (5.24). The higher order multipole moments, however, depend on the vessel density. The influence of blood flow on tissue heat transfer will decrease as the number density

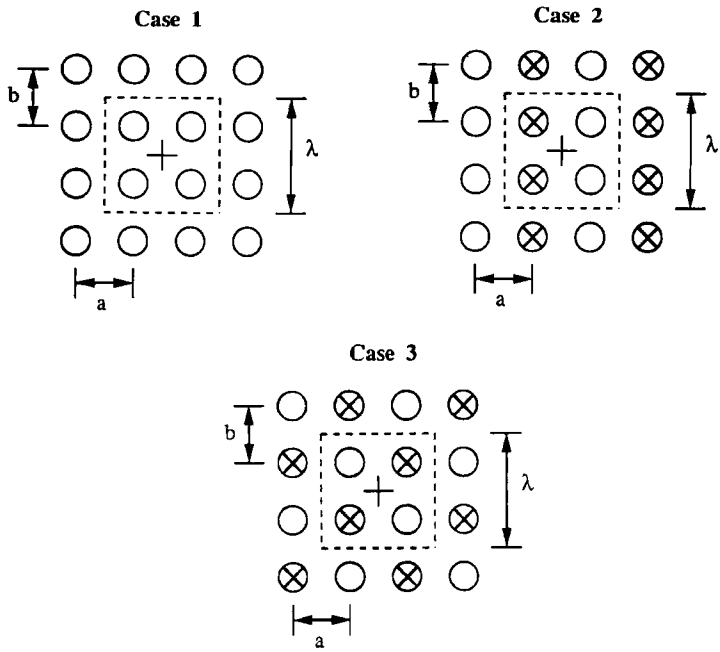

FIG. 4. Three different vascular arrays considered by Klinger. The "×" signifies a vessel with flow countercurrent to a vessel with no ×. (Reproduced from [39], with permission of the publisher, Plenum Publishing Corporation.)

of blood vessels increases for a fixed total blood flow rate $\dot{V}$. Klinger shows that, in the limit of an infinite vessel density, his mathematical model predicts that the countercurrent arrangement will have no effect on tissue heat transfer since the flow paths of all adjacent vessels will over overlap and cancel each other.

Klinger derived the influence of the countercurrent flow arrangement on tissue temperature by considering case 2 in Fig. 4, in which the blood flow effect can be modeled as a dipole (i.e., $l = 1$ in Eq. (5.20)), neglecting the higher order effect of the octopole moment (i.e., $l = 3$). Note that in this case the monopole and 2^4-pole moments are both zero due to symmetry. The tissue temperature profile can be written for this case as

$$G_v(\mathbf{r}, \mathbf{r}_1, \tau, \tau_1) = \sum_{i=0}^{\infty} \int_{\tau_1}^{\tau} \int_{\Omega} \sum_{\nu=1}^{3} \frac{\partial}{\partial x_2} G_{v(i-1)}(\mathbf{r}_2, \mathbf{r}_1, \tau_1, \tau_2) \times \sum_{\mu=1}^{3} \frac{\partial}{\partial x_2} G_{v0}(\mathbf{r} - \mathbf{r}_2, \tau - \tau_2) \cdot \begin{pmatrix} 1 & \mathbf{r}_2 \\ \xi_\mu & \bar{v}_\nu \end{pmatrix} d^3\mathbf{r}_2 \, d\tau_2 \tag{5.25}$$

where the dipole moment tensor in Eq. (5.25) is determined from Eq. (5.22):

$$\begin{pmatrix} 1 & \mathbf{r}_2 \\ \xi_\mu & \bar{v}_\nu \end{pmatrix} = \frac{1}{V_j} \int_{V_j} \xi_\mu \bar{v}_\nu(\xi)\, d^3\xi \tag{5.26}$$

By assuming that the integral in Eq. (5.26) is the same for each element j, i.e., the dipole moment is independent of $\mathbf{r}_2$, Klinger derives a new expression for the Green's function solution for the tissue temperature profile:

$$G_v(\mathbf{r}, \mathbf{r}_1, \tau, \tau_1) = G_{v0}(\mathbf{r} - \mathbf{r}_1, \tau - \tau_1) - \int_{\tau_1}^{\tau} \int_{\Omega} G_{v0}(\mathbf{r} - \mathbf{r}_2, \tau - \tau_2)\, d\tau_2\, d^3\mathbf{r}_2$$
$$\times \frac{1}{V_j} \int_{V_j} (\bar{\nabla}_2, \bar{\nabla}_2)(-\bar{v}(\xi)) G_v(\mathbf{r}_2, \mathbf{r}_1, \tau_2, \tau_1)\, d^3\xi \tag{5.27}$$

Klinger rewrites this equation as a differential equation for the Green's function solution as a function of space and time using the governing equations (5.4) and (5.8):

$$\bar{\nabla}^2 G_v + \frac{1}{V_j} \int (\bar{\nabla}, \bar{\nabla}) \bar{v} G_v(\mathbf{r}, \mathbf{r}_1, \tau, \tau_1) \xi\, d^3\xi - \frac{\partial G_v}{\partial \tau} = \delta(\mathbf{r} - \mathbf{r}_1)\delta(\tau - \tau_1) \tag{5.28}$$

3. *Calculation of an Effective Thermal Conductivity*

Equation (5.28), the energy balance equation for the tissue element V_j, contains an integral term for the effect of convective perfusion on tissue heat transfer which contains a tensor of second derivatives of the Green's function solution [39]. Klinger shows that these tensor terms may be combined with the first term on the left-hand side of Eq. (5.28), which represents the pure conduction heat transfer. By defining the tensor elements,

$$a_{ij} = \frac{1}{V_j} \int (\xi_i \bar{v}_j + \bar{v}_j \xi_i)\, d^3\xi \tag{5.29}$$

Klinger introduces an anisotropic effective conductivity for the tissue into the energy balance equation (5.28)]:

$$\frac{\partial G_v}{\partial \tau} = \nabla k_{\text{eff}} \nabla G_v - \delta(\mathbf{r} - \mathbf{r}_1)\delta(\tau - \tau_1) \tag{5.30}$$

where

$$k_{\text{eff}} = \begin{pmatrix} 1 + a_{11} & a_{12} & a_{13} \\ a_{21} & 1 + a_{22} & a_{23} \\ a_{31} & a_{32} & 1 + a_{33} \end{pmatrix} \tag{5.31}$$

Based upon the definition of a_{ij} in Eq. (5.29), the effective conductivity tensor in Eq. (5.31) is symmetric about the diagonal, as required. The influence of blood flow on tissue heat transfer in this case depends on the magnitude of the dipole moments contained within Eq. (5.29). For the countercurrent flow configuration in Fig. 4, Klinger shows that the dipole moment is given by

$$\begin{pmatrix} 1 & \mathbf{r}_2 \\ \xi_\mu & v_\nu \end{pmatrix} = \frac{1}{V_j} \int_{V_j} \xi_\mu \bar{v}_\nu(\xi)\, d^3\xi \tag{5.32}$$

$$\propto \frac{1}{V_j} \left(\frac{\lambda}{L}\right)^2 \frac{\bar{V}}{N} \tag{5.33}$$

where N is the characteristic spacing between adjacent vessels. According to this mathematical model, the change in tissue conductivity due to countercurrent blood flow will depend on the blood flow rate in the countercurrent vessels and the number density of the vessels.

Klinger's mathematical model was significant in that it introduced the concept of an enhancement of tissue thermal conductivity due to the presence of flowing blood in the tissue via a conduction tensor. Using the Green's function solution, Klinger quantified the importance of vessel number density, blood perfusion rate, and vessel architecture on this enhancement of tissue conduction. His most important observations were (1) the temperature field was most influenced by the geometric arrangement of the blood vessels, (2) a cocurrent flow structure results in a mean velocity analogous to the D'Arcy velocity that enhances conductivity in the flow direction, while the enhancement is independent of vessel density, and (3) a countercurrent system of blood vessels influences the tissue conductivity in an anisotropic manner and the magnitude of this effect is inversely proportional to the vessel density and proportional to the total volumetric flow rate of blood in the tissue. These results were important because they emphasized the importance of the geometry and flow direction of the microcirculation, which was not considered by the Pennes bioheat transfer model. The use of an enhanced conductivity tensor in the bioheat transfer model that Klinger introduced would be applied several years later by Weinbaum and Jiji in their mathematical model of bioheat transfer [34, 61]. Prior to the work of Weinbaum and Jiji, however, Chen and Holmes [22] developed a bioheat transfer model that included the effects of blood flow direction and vessel orientation relative to the tissue and examined the anisotropic effect of blood flow on a "perfusion" conductivity that was similar in concept to the effective conductivity derived by Klinger [39].

VI. Continuum Model of Chen and Holmes [22]

The modeling work of Chen and Holmes [22] employs a continuum description of the tissue-blood control volume in a manner similar to that of Wulff [69] and Klinger [39]. This is justified by the presence of a large number of blood vessels in a tissue volume whose characteristic dimension is much larger than those of the individual blood vessels. The effect of these numerous small blood vessels on the heat transfer of the tissue is based upon a statistical grouping of the vessels and is incorporated into the physical parameters that govern the system heat transfer. The theoretical relationship between the microvascular network structure and tissue thermal properties and perfusion bleed-off rate into the tissue is examined in this study. Similar to the analysis of Wulff and Klinger, the bioheat transfer analysis of Chen and Holmes is a microvascular model, with the effects of large blood vessels with diameters on the order of 1 mm or greater omitted from the energy balance. The presence of these large vessels in this type of model would violate the continuum assumption that the length scale of the tissue temperature variations is much larger than the dimensions of the individual blood vessels.

A. Governing Equations

Chen and Holmes divide the control volume occupied by the tissue and blood vessels into two separate volumes: one consisting of solid tissue only, with differential volume dV_s, the other, with differential volume dV_b, comprised of only blood in the vascular space within the blood vessels. Although there is some mass transfer between the blood and the tissue control volumes, the fluid lost from the vascular space is assumed to be compensated for by the flow of lymph from the tissue to the vascular space. Since the flow rate of lymph is slow compared to the flow of blood in the vascular space, it is reasonable to assume that all lymph that remains in the tissue space has the same temperature as the tissue itself and is therefore indistinguishable from the tissue.

For a relatively small vascular control volume dV_b, and a total control volume dV that is small compared to the scale of macroscopic temperature gradients, yet large compared to the scale of microscopic temperature gradients, volume-averaged local temperatures can be defined for both the tissue (subscript "s" for solid tissue volume) and blood:

$$T_s = \frac{1}{dV_s} \int_{dV_s} T \, dv \tag{6.1}$$

$$T_b = \frac{1}{dV_b} \int_{dV_b} T \, dv \tag{6.2}$$

Using these local mean temperatures, an energy balance equation can be written for both the tissue and vascular spaces. In the solid tissue space

$$dV_s \rho_s c_s \frac{\partial T_s}{\partial t} = dQ_{ks} + dQ_{bs} + dQ_m \tag{6.3}$$

where dQ_{ks} is energy gain in the control volume by conduction, dQ_{bs} is energy gain in the control volume from the blood compartment, and dQ_m is energy gain from metabolic heating. The energy balance equation for the vascular space is similar, but with an added term due to the bulk fluid flow in this space:

$$dV_b \rho_c c_b \frac{\partial T_b}{\partial t} = dQ_{kb} - dQ_{bs} + \int_S \rho c_b T \mathbf{v}\, ds \tag{6.4}$$

where dQ_{kb} is energy gain by conduction in the vascular space, and the integral term represents the convective energy gain due to blood flow at velocity $\mathbf{v}$ across the surface area S. The addition of Eqs. (6.3) and (6.4) and division of the result by dV yields an energy balance for the continuum tissue space:

$$\rho c \frac{\partial T_t}{\partial t} = q'_k + q'_m + q'_p \tag{6.5}$$

where ρ, c, and T_t represent the local mean density, specific heat, and temperature of the continuum tissue based upon a volume average

$$T_t = \frac{1}{\rho c}\left(\left(1 - \frac{dV_b}{dV}\right)\rho_s c_s T_s + \frac{dV_b}{dV}\rho_b c_b T_b\right) \tag{6.6}$$

$$\rho = \left(1 - \frac{dV_b}{dV}\right)\rho_s + \frac{dV_b}{dV}\rho_b \tag{6.7}$$

$$c = \frac{1}{\rho}\left(\left(1 - \frac{dV_b}{dV}\right)\rho_s c_s + \frac{dV_b}{dV}\rho_b c_b\right) \tag{6.8}$$

Note that as the ratio of blood to total tissue volume dV_b/dV approaches zero, the tissue temperature T_t approaches the solid medium temperature T_s.

1. *Conduction and Metabolic Terms*

The thermal capacitance term on the left-hand side of Eq. (6.5) is balanced by three sources of heat in the total control volume: conduction, metabolic, and convective heat gain. The conduction gain can be written in terms of an effective thermal conductivity, k_k, which represents the thermal transport associated with molecular energy diffusion of the combined tissue and vascular spaces:

$$q'_k = \frac{Q_{ks} + Q_{kb}}{dV} = \nabla \cdot k_k \nabla T_t \tag{6.9}$$

Note that this effective thermal conductivity is not associated with the bulk flow of blood in the vascular space, an effect that is considered later in the development of this model. Because the vascular volume is much smaller than the tissue volume, Chen and Holmes assume that the value of k_k is equal to the thermal conductivity of the solid tissue medium, k_s.

While the metabolic heat deposition per unit volume term, q'_m, is straightforward in its significance, the perfusion, or bulk flow term, q'_p, must be further examined.

2. *Blood Flow Terms*

The integral equation

$$q'_p = \frac{1}{dV} \int_S \rho_b c_b T \mathbf{v}\, d\mathbf{s} \tag{6.10}$$

is complicated by the condition that the temperature T within the integral is not simply equal to T_s, as was assumed by the bioheat transfer model of Wulff [69]. In Wulff's formulation, complete thermal equilibration between blood and solid tissue medium was assumed at all locations within the control volume. Under these conditions, the ratio of the integral in Eq. (6.10) to the tissue volume reduced to the familiar convection term $\rho_b c_b \mathbf{v} \cdot \nabla T_s$. In this case, a single equation was derived by Wulff [69] to describe solid tissue temperature variations with spatial position without including the effect of spatial variations in the blood temperature.

In contrast, Chen and Holmes [22] consider the effect of blood flowing within the tissue matrix at a temperature different than the tissue temperature. The convective heat flow across a differential surface area dS is written by Chen and Holmes as the sum of the contributions of individual blood vessels crossing this surface:

$$\int_{dS} \rho_b c_b T \mathbf{v}\, d\mathbf{s} \cong \rho_b c_b \sum_i T_{bi} v_i A_i \sin \theta_i \tag{6.11}$$

where A_i is the cross-sectional area of the ith vessel, θ_i is the angle formed between the vessel axis and the surface area dS, v_i is the mean velocity in the blood vessel, and T_{bi} is the flow-weighted, or "mixing cup" average temperature of blood inside the vessel:

$$v_i = \frac{1}{A_i} \int_{A_i} u\, dA \tag{6.12}$$

$$T_{bi} = \frac{1}{u_i A_i} \int_{A_i} Tu\, dA \tag{6.13}$$

a. *Thermal Equilibration Effects in the Microcirculation.* Evaluating the summation in Eq. (6.11) is difficult due to the unknown mean blood temperature in the blood vessel. At this point in their model formulation, Chen and Holmes examine the effect of thermal equilibration length on this mean blood temperature as blood passes through the circulatory system [22]. The thermal equilibration effect between flowing blood and the surrounding solid tissue medium will be used to evaluate the perfusion heat transfer term, q_p', as described by Eqs. (6.10) and (6.11).

Based upon a one-dimensional steady state analysis, where the time rate of change of the mean blood temperature is small compared to the convective effect, the governing energy balance equation for the blood temperature T_{bi} as a function of axial position x is

$$A_i \rho_b c_b u_i \frac{dT_{bi}}{dx} = U_i P_i (T_s - T_{bi}) \tag{6.14}$$

where U_i represents the overall heat transfer coefficient between the flowing blood and surroundings, and P_i is the perimeter of the blood vessel. The solution to this first order equation is an exponential mean blood temperature profile along the length of the vessel.

Chen and Holmes define the thermal equilibration length of a blood vessel as the length of blood vessel over which the temperature difference between the blood and the solid tissue surroundings decreases by a factor e. Based upon the solution to Eq. (6.14), the thermal equilibration length is

$$L_{eq} = \frac{A_i \rho_b c_b u_i}{U_i P_i} \tag{6.15}$$

When L_{eq} is small relative to the spatial scale of solid tissue temperature gradients, then the mean blood temperature can be considered equal to the solid tissue temperature T_s. Conversely, when L_{eq} is large compared to the characteristic length of the solid tissue temperature gradients, the mean blood temperature will be independent of T_s. This second condition was not considered in the bioheat transfer model of Wulff [69].

In order to calculate the values of the thermal equilibration lengths in various regions of the circulatory system, it is necessary to estimate the overall heat transfer coefficient U_i. The thermal resistance represented by the inverse of U_i is comprised of two components: conduction resistance through the tissue and convective resistance in the blood. Using a cylindrical geometry, the former depends upon the logarithmic ratio of the characteristic distance of the tissue from the blood vessel wall to the radius of the blood vessel itself. Chen and Holmes suggest that this characteristic distance is half the distance between adjacent vessels. The convective

resistance is inversely proportional to the Nusselt number, Nu. Therefore the overall resistance is

$$\frac{1}{U_i} = \frac{r_i \ln(l_i/r_i)}{k_s} + \frac{r_i}{k_b \, \mathrm{Nu}} \tag{6.16}$$

where l_i is the distance midway between adjacent vessel walls. Chen and Holmes argue that because the Nusselt number for fully developed tube flow is on the order of 4, and because the ratio l_i/r_i is typically on the order of 10 in the microcirculation, it is reasonable to assume that the overall thermal resistance is dominated by the conduction term since the ratio of the thermal conductivities of the blood and solid tissue is near unity. Subsequently, Chen and Holmes combine the effect of these two resistances into a parameter Λ which represents the combined effects of blood and solid tissue thermal conductivities, vascular geometry, and blood velocity on the overall blood–tissue resistance.

$$U_i = \frac{k_s}{\Lambda r_i} \qquad \text{where } \Lambda = \ln(l_i/r_i) + \frac{k_s}{k_b \, \mathrm{Nu}} \tag{6.17}$$

Assuming the ratio l_i/r_i is 10 and the Nusselt number is 4, the value of Λ will be approximately 3. The expression for thermal equilibrium length in Eq. (6.15) is transformed for a circular blood vessel to

$$L_{eq} = \frac{\Lambda r_i^2 \rho_b c_b u_i}{2k_s} \tag{6.18}$$

Using the vascular data from a 13-kg dog shown in Table I [13, 64], Chen and Holmes utilized Eq. (6.18) to compute the thermal equilibration lengths of various blood vessels in the circulatory system. Because the blood velocity in the circulatory system is roughly proportional to the vessel radius [64], the thermal equilibration length depends on approximately the third power of the radius, which is a very high sensitivity. For the larger vessels such as the aorta and large arteries and veins, the thermal equilibration length is on the order of meters, implying that blood in these large vessels can be at a mixing cup temperature that is much different than the surrounding tissue temperature. Conversely, the thermal equilibration lengths of the blood vessels that comprise the microcirculation, i.e., the arterioles, venules, and capillaries, are on the order of microns, which implies that blood flowing in these small vessels will be completely equilibrated with the surrounding tissue. These equilibrium effects are shown schematically in Fig. 5.

The main assumption of the Pennes formulation, that all tissue–blood heat transfer occurs in the capillary bed, is clearly contradicted by this result. Chen and Holmes also estimated that the terminal arteries, with a

TABLE I

VASCULAR PARAMETERS [22]

j	Vessel	% Vascular volume	r_j (μm)	x_{ej}[a] (m)	l_j/x_{ej}[a]	k_{pj}/k_s[a] ($1/\beta \leq 10$)
1	Aorta	3.30	5000	190	0.002	0.1
2	Large artery	6.59	1500	4	0.05	2
3	Arterial branch	5.49	500	0.3	0.3	15
4	Terminal branch	0.55	300	0.08	0.1	4
5		1.00	175	0.009	1	10
6	Arteriole	2.75	10	5×10^{-6}	400	0.04
7	Capillary	6.59	4	2×10^{-7}	6000	0.00008
8	Venules	12.09	15	2×10^{-6}	800	0.002
9	Terminal veins	3.30	750	0.1	0.1	4
10	Venous branch	29.67	1200	0.3	0.3	14
11	Large veins	24.18	3000	5	0.04	2
12	Vena cava	5.49	6250	190	0.002	0.09

[a] Symbols: % vascular volume: compartment percent of total vascular volume.
x_{ej}: equilibrium length.
l_j/x_{ej}: vessel length/equilibration length.
k_{pj}/k_s: perfusion thermal conductivity/solid tissue thermal conductivity.

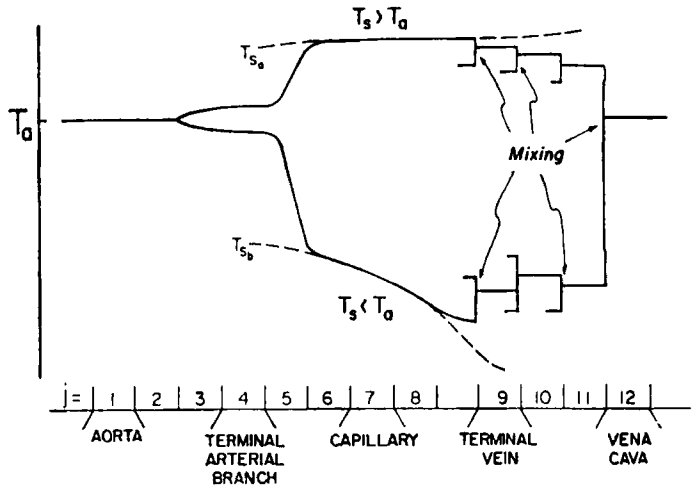

FIG. 5. A schematic view of the blood temperature throughout the systemic circulation. Blood at arterial temperature T_a is distributed to solid tissue that is either warmer (T_{sa}) or cooler (T_{sb}) than T_a. Thermal equilibration occurs after the terminal arterial branches ($j = 5$). Past the venules ($j = 8$), blood temperature changes are due to mixing effects in venous drainage branches. The vena cava blood returns to the heart at T_a. (Reproduced from [22], with permission of the Publisher, the Annals of the New York Academy of Sciences.)

diameter of approximately 0.2–0.5 mm, would have a thermal equilibration length equal to their own length, and on the venous side, terminal veins with a diameter of 0.3–0.8 mm would similarly be as long as their thermal equilibration length.

Using a length scale analysis, Chen and Holmes illustrated an important new concept in bioheat transfer modeling: all of the tissue–arterial blood heat exchange must occur along the circulatory network after the blood flows through the terminal arteries and before it reaches the level of the arterioles, and consequently there can be no significant heat transfer between tissue and capillary blood. Downstream from the arterioles, the blood temperature will be equal to the surrounding tissue temperature until the blood reaches the terminal veins. Here the thermal equilibration length of the veins is significant compared to their length, and there will be little heat transfer between the solid tissue and venule blood. Mixing effects, however, will be important as cool blood from the cutaneous regions drains into the veins. Chen and Holmes also show that the thermal equilibration constant k', used by Pennes to account for any incomplete thermal equilibration between tissue and blood in the capillaries (see Eq. (3.2)), must be zero, since the thermal equilibration length of these vessels is several orders of magnitude smaller than their actual length.

b. *Subdivision of Perfusion Term.* Applying these results, Chen and Holmes were able to determine the microvascular contributions to tissue heat transfer as represented by the term in Eq. (6.11). Following the flow of blood along a vessel axis position x, the differential energy balance equation is given by Eq. (6.14). Substituting the expression for vessel thermal equilibration length:

$$L_{eq} \frac{dT_b}{dx} = T_s - T_b \tag{6.19}$$

Equation (6.19) is solved by setting the mean blood temperature at the entrance to the circulatory network, i.e., $x = 0$, equal to the core arterial temperature, T_{a0}, typically 37 °C. Note that L_{eq} and T_s are both functions of x, the location along the circulatory network. In order to solve the problem, Chen and Holmes introduce a Fourier integral representation for the solid tissue temperature T_s:

$$T_s(x) = T_s(x_0) + \int_0^\infty C(\eta) \sin \eta(x_0 - x)\, d\eta \tag{6.20}$$

where x_0 represents the location downstream from position x where the vessel crosses the control surface dS, η is the spatial wavenumber, and the coefficient $C(\eta)$ is determined according to the given solid tissue temperature distribution $T_s(x)$. The sinusoidal variation in $T_s(x)$ is justified by the

structural periodicity of the blood vessels embedded in the tissue. The blood vessels can be depicted as an array of identical repeating units crossing the control surface at the position x_0. Based upon the linear property of both the governing energy balance equation (6.19) and its boundary condition at $x = 0$, Chen and Holmes separate the solution to the energy balance equation (6.19) into three independent parts:

$$T_b(x) = T_1 + T_2 + T_3 \tag{6.21}$$

where three "subproblems" are defined:

$$L_{eq}\frac{dT_1}{dx} = -T_1 \tag{6.22}$$

$$T_s(x_0) = T_2 \tag{6.23}$$

$$\int_0^\infty T_\eta \, d\eta = T_3 \tag{6.24}$$

where

$$L_{eq}\frac{dT_\eta}{dx'} = T_\eta - C \sin \eta x' \qquad (x' = x_0 - x) \tag{6.25}$$

subject to the following boundary conditions

$$T_1(0) = T_{a0} - T_s(x_0) \tag{6.26}$$

$$T_\eta(x') = T_\eta\left(\frac{x' + 2\pi}{\eta}\right) \tag{6.27}$$

The T_1 subproblem represents the thermal equilibration of the blood with a uniform solid temperature, while the T_2 subproblem is just the contribution of the solid tissue temperature to the blood temperature, and the T_3 subproblem models the thermal equilibration of the blood with the spatial variations in the solid tissue temperature. Note that if the solid tissue temperature is assumed independent of x, i.e., a constant, the solution for T_b is just $(T_1 + T_2)$, as the coefficient C will be zero, and subsequently the temperature T_3 will be zero.

The solution for temperature T_1 is the exponential relationship

$$T_1 = [T_{a0} - T_s(x_0)] \exp\left(-\int_0^x \frac{1}{L_{eq}}\, dx\right) \tag{6.28}$$

The integral in Eq. (6.28) can be estimated by considering the thermal equilibration length of the various blood vessels in the circulatory system. As blood passes through the major arteries into the large arteries, the thermal equilibration lengths are so large that the integral remains essentially at

zero. In this part of the circulation, T_1 will be equivalent to the temperature difference $[T_{a0} - T_s(x_0)]$. Past the terminal arteries, however, the magnitude of this integral will increase substantially, so that T_1 will approach zero in this region of the microcirculation between the terminal arteries and arterioles.

At this point Chen and Holmes show that the perfusion heat source term in the blood-tissue composite energy balance equation (6.5), q'_p, can be interpreted based upon the above results for the first subproblem. For a control volume dV much smaller than the scale of macroscopic temperature gradients in the tissue, the large arteries and veins will have little influence on the value of q'_p. The effect of blood flow on tissue temperature around these large vessels can be accounted for by examining heat transfer between the tissue and blood in the vessels on an individual basis. At some generation of branching within the vascular network, however, this procedure becomes too complex for an individual analysis. At this location, the j^*th generation of branching, the blood temperature is defined as T_a^*. Note that T_a^* will not be equal to T_{a0}, the blood temperature as it enters the circulatory system in the aorta. The difference between T_a^* and T_{a0} will depend upon the blood flow rate, vessel wall heat transfer coefficient, and vessel-tissue geometry and architecture.

Chen and Holmes next argue that if the control volume dV is large enough that it contains the portion of vascular network that includes all vessels between the terminal arteries and arterioles, then for the first subproblem the blood that leaves this control volume will be at the solid tissue temperature. Under these conditions, the summation of $(v_j A_j \sin \theta_j)$ in Eq. (6.11) is equivalent to the total volume of blood that flows through the tissue per unit time. Consequently, the integral in Eqs. (6.10) and (6.11) can be simplified so that q'_p for this subproblem looks quite similar to the Pennes perfusion heat source:

$$q'_{p(1)} = \omega_j^* \rho_b c_b (T_a^* - T_s) \tag{6.29}$$

Chen and Holmes emphasize the differences between the perfusion heat source term in Eq. (6.29) and that of Pennes in Eq. (3.3). First, the term ω_j^* is the total perfusion bleed-off to the tissue only from the microvessels past the j^*th generation of branching. The Pennes term ω includes bleed-off from all generations of the vasculature. Second, the perfusion heat source term derived by Chen and Holmes is proportional to the temperature difference $(T_a^* - T_s)$, which, as stated above, is not the same as $(T_{a0} - T_s)$. According to their calculations, the difference between these two temperature differences can be on the order of 10–50%, based upon the thermal equilibration lengths of these large vessels compared to their actual lengths.

The second subproblem simply states that the blood temperature is equal to the solid tissue temperature everywhere in the control volume. This was the assumption made by Wulff [69] in his derivation of the bioheat equation, as discussed above. In this case, Chen and Holmes show that the perfusion term described by Eqs. (6.10) and (6.11) can be reduced to the familiar convective heat transfer term

$$q'_{p(2)} = -\rho_b c_b \mathbf{v}_p \cdot \nabla T_s \tag{6.30}$$

where $\rho_b \mathbf{v}_p$ is the mass flux of blood flowing through the tissue. This expression for the tissue-blood heat transfer and its derivation from Eq. (6.10) is identical to that described by Wulff and described in Eq. (4.8).

The third subproblem involves variations in T_b due to a temperature difference between the blood and the various components of $T_s(x)$. The solution to Eq. (6.25) when combined with the periodicity prescribed by Eq. (6.27) is

$$T_\eta(0) = \frac{-\eta L_{eq} C}{\eta^2 L_{eq}^2 + 1} \tag{6.31}$$

Since $T_\eta(0)$ represents the net temperature difference between the blood and the solid tissue at $x = x_0$, there is added heat transfer between the blood and tissue due to the contribution of this temperature component with wavenumber η. This extra contribution is included in the integral in Eq. (6.10) which quantifies the total heat transfer between blood and tissue due to bulk flow. Chen and Holmes also show that the amplitude of this wave component, $C(\eta)$, is related to the temperature gradient at $x = x_0$, so that the effect of the term $T_\eta(0)$ on q'_p is analogous to that of a heat conduction term. In this manner, the effect of blood flow can be characterized by a perfusion or effective thermal conductivity, k_p.

c. *Effective (Perfusion) Conductivity.* The analysis of k_p is simplified by assuming that the differential surface area is normal to the temperature gradient and that the tissue is isotropic. In this case k_p can be considered a scalar quantity. Under these conditions, Chen and Holmes derive the relationship between the perfusion conductivity and the vessel thermal equilibration length, wavenumber, blood velocity, and vascular geometry. Using the definition

$$q'_{p,\eta i} = -\nabla k_{p,\eta i} \nabla T \tag{6.32}$$

and the definitions of $C(\eta)$, η, L_{eq}, along with Eqs. (6.10) and (6.11), Chen and Holmes show that the value of the effective or perfusion conductivity

for the wavenumber η in blood vessel i is

$$k_{p,\eta i} = \frac{\Lambda^2}{4k_s} \rho_b^2 c_b^2 \frac{v_i^2 r_i^2 \lambda_i}{L_{eq}^2 \eta^2 + 1} \sin^2 \theta_i \tag{6.33}$$

where λ_i is the area fraction of the ith blood vessel.

Chen and Holmes note several important characteristics of their derived perfusion conductivity parameter, k_p. First, for the smaller vessels of the microcirculation the quantity $L_{eq}^2 \eta^2$ in the denominator of Eq. (6.33) is negligible and the value of $k_{p,i}$ is independent of wavenumber. Second, the perfusion conductivity depends significantly on the vessel inclination angle, but not on the direction of flow (positive or negative) in the vessel, as the velocity term v_i is squared. However, the contribution of the blood vessel to the perfusion heat transfer does depend on the direction of the temperature gradient. As a result, tissue with an isotropic array of blood vessels will yield an isotropic increase in conduction due to the blood flow. Using the superposition principle to sum the influence of all the individual vessels and wavenumbers, Chen and Holmes define an overall perfusion thermal conductivity k_p by the expression

$$q'_{p(3)} = -\nabla k_p \nabla T \tag{6.34}$$

While the value of k_p is necessarily a complicated function of vessel geometry and architecture, estimates can be made of the individual vessel k_{pi} values by approximating the wavenumber as the inverse of the vessel length, and using vessel number density measurements to compute λ_i. In addition, the inclination angles θ_i can be approximated from vascular anatomical studies. For example, a terminal branch artery with a radius of 0.03 cm and velocity of 7.4 cm/s will have a thermal equilibration length of approximately 8.0 cm, assuming a value of 3 for Λ. Since the number density of a 600-μm terminal branch artery in the systemic circulation is approximately 1 vessel/cm^2 tissue, the area fraction λ is 2.8×10^{-3}. Using Eq. (6.33) with an inclination angle of 90° (i.e., vessel axis normal to the control surface), and a wavenumber of 1 cm^{-1} (i.e., the inverse length of a terminal branch artery), the resulting value of the perfusion conductivity is 1.5 W/m-°C, which is three times the thermal conductivity of solid tissue.

Based on Eq. (6.33), the effect of perfusion on tissue heat transfer will be important in blood vessels larger than the terminal artery branches and terminal venous branches, where thermal equilibration lengths are much larger than the lengths of the vessels themselves. In the small vessels of the microcirculation, the thermal equilibration lengths of the arterioles, venules, and capillaries are so small that the contribution to tissue conductivity by perfusion is negligible. Chen and Holmes emphasize, however,

that despite the large ratio of perfusion conductivity to tissue conductivity in the larger vessels of the circulation, it is preferable to analyze the heat transfer around these large vessels on an individual basis rather than in a continuum model. The low number density of these large vessels is not compatible with the assumptions of a continuum model where the size of the individual blood vessels is assumed to be much smaller than the length scale of the macroscopic temperature gradients.

B. FINAL BIOHEAT EQUATION

Substituting the three components of perfusion heat transfer derived in the three subproblems and described by Eqs. (6.29), (6.30), and (6.34) into Eq. (6.5), Chen and Holmes derive a "new" bioheat equation:

$$\rho c \frac{\partial T_t}{\partial t} = \nabla \cdot k_t \nabla T_t + \nabla \cdot k_p \nabla T_t + \omega_j^* \rho_b c_b (T_a^* - T_t) - \rho_b c_b \mathbf{v}_p \cdot \nabla T_t + q'''_m \tag{6.35}$$

where T_s, the temperature of the solid tissue component of the tissue–blood continuum model, is replaced by T_t, the volume-weighted continuum temperature (see Eq. (6.6)). This replacement is reasonable as long as the ratio of vascular volume to total (tissue plus blood) volume is small, i.e., $dV_b/dV \ll 1$. Similarly, since the vascular volume is much smaller than the tissue volume, Chen and Holmes assume that the thermal conductivity of the total control volume is equal to that of the solid tissue medium. Equations (6.7) and (6.8) can be used to determine the values of ρ and c, which are also volume-weighted quantities.

Several new terms appear in this energy balance equation for a tissue control volume perfused by flowing blood. The second term on the right-hand side of Eq. (6.35) models the enhancement of thermal conductivity in the tissue due to the flow of blood within blood vessels with thermal equilibration lengths of the same order of magnitude as the lengths of the blood vessels themselves. Chen and Holmes show that this term acts like an "eddy" conduction due to the random flow of blood through the tissue. The third term on the right-hand side of Eq. (6.35) looks very much like the familiar Pennes perfusion heat source term, but, as mentioned above, T_a^* is the temperature of the arterial blood in the first generation that can be legitimately represented in the continuum model, the j^*th generation. Similarly, ω_j^* is the blood perfusion rate only from blood vessels beyond the j^*th generation. In order to model bioheat transfer from the larger vessels upstream from the j^*th generation, Chen and Holmes propose that these arteries and veins should be examined on an individual basis as macroscopic entities. The fourth term on the right-hand side of Eq. (6.35) is the usual

convection transport term that accounts for the effect of the direction of blood flow within the tissue on tissue heat transfer. This concept was included in the earlier model of Wulff [69].

In the absence of the anatomical data that are needed to determine k_p, ω_f^*, and $\mathbf{v}_p$, the bioheat equation of Chen and Holmes can be reduced to the familiar Pennes bioheat equation. Neglecting the second and fourth terms on the right-hand side of Eq. (6.35), and assuming that the equation applies to all vessels in the circulatory network, i.e., $T_a^* = T_{a0}$ and $\omega_f^* = \omega$, the Chen and Holmes bioheat equation simplifies to the Pennes bioheat equation. When applied to a lumped parameter model, where conduction is neglected inside the control volume and consequently there are no spatial variations in temperature within a tissue region, the governing bioheat transfer equation simplifies further to a balance between thermal capacitance and the two heat source terms: perfusion and metabolic heating.

The model of Chen and Holmes [22] offered a new perspective on bioheat transfer in several manners. While the bioheat transfer model of Wulff [69] introduced the concept of bulk convective transport into bioheat transfer analysis, Chen and Holmes [22], as well as Klinger [39], generalized this effect to a much greater extent. Rather than simply assuming complete thermal equilibration in all vessels of the circulation as Wulff had done, Chen and Holmes implemented the concept of thermal equilibration length into their analysis to account for bulk flow convection heat transfer. As a result, their model defined an effective thermal conductivity in order to quantify the enhancement of thermal conductivity in the tissue by the convection transport associated with blood flow. Similarly, Klinger [39] derived an effective thermal conductivity that was dependent on the blood vessel spatial arrangement.

Another important aspect of the bioheat transfer model of Chen and Holmes [22] was the observation that thermal equilibration between blood and tissue takes place in the terminal branches of the arteries and the arterioles. Chen and Holmes demonstrated that the main assumption of Pennes's bioheat equation, no precapillary heat transfer, was not possible due to this equilibration effect in the microcirculation. While their bioheat transfer equation contains a term similar to that of the Pennes bioheat equation, T_a^* and ω_f^* are defined differently, so that the microcirculatory perfusion heat transfer in Eq. (6.35) accounts for heat exchange only within the region defined by the continuum model.

An aspect of bioheat transfer that was not examined by Chen and Holmes was the effect of countercurrent heat transfer between closely spaced, paired arteries and veins. The bioheat transfer model of Chen and Holmes considered the heat transfer between essentially isolated vessels and the surrounding tissue, without accounting for countercurrent exchange between

adjacent vessels in the microcirculation. Klinger [39] included the effects of countercurrent flow in his continuum model in order to quantify the importance of flow direction on the perfusion multipole solution. This continuum model, however, did not investigate the variation of blood temperature within the blood vessels as a function of vessel geometry and the heat transfer between blood flowing in vessels and the tissue that surrounds these vessels. These phenomena have been considered in mathematical models of bioheat transfer that may be categorized as vascular, as opposed to continuum, models [3]. In vascular models, the heat transfer between tissue and blood is examined by deriving the governing energy balance equations between individual blood vessels and the surrounding tissue [3]. The next section of this review will present several important vascular models, which provided a theoretical basis for the interpretation of bioheat transfer in countercurrent flow systems.

The thermal significance of countercurrent flow of closely spaced arteries and veins positioned alongside each other was first observed over 100 years ago by Claude Bernard [8]. This structure has been observed in many parts of the circulatory system, including retia in the limbs of many animals and paired artery-vein networks in the fins of whales. In addition, the deep-seated arteries and veins that supply blood to and drain blood from the extremities of many animals, including humans (e.g., the femoral artery and vein in the upper leg), are similarly arranged in a countercurrent manner. The countercurrent arrangement is a mechanism by which heat losses from the body to the environment are reduced. As warm arterial blood flows towards an extremity such as a limb or tail, it exchanges heat with cooler venous blood which flows in the opposite direction, back towards the body core. In this manner, arterial blood can be supplied to the extremity without significant heat loss to the surroundings [45].

Another view of the countercurrent heat exchange mechanism involves the mean tissue temperature of the extremity. As heat is shunted from the artery to the countercurrent vein via this mechanism, the arterial and mean tissue temperatures in the limb or tail are reduced since some of this heat would be otherwise transferred to the surrounding tissue. In this manner, the temperature difference between the extremity and the environment, which is the driving force for heat loss from the extremity, is reduced. This heat conserving property of the countercurrent mechanism can be bypassed during periods of thermal stress such as exercise by shunting blood from the deep veins to the cutaneous venous system. Without significant blood flow in the deep veins, the countercurrent heat exchange is reduced and, as a result, heat can be shed from the body. Control of venous blood flow is accomplished by the thermoregulatory system according to the thermal state of the whole body [45].

VII. Countercurrent Bioheat Transfer

A. EARLY STUDIES

1. *Bazett* [5–7]

One of the earliest examinations of countercurrent heat exchange in the circulatory system was performed by Bazett and co-workers [5–7] in a series of experimental studies. Longitudinal temperature gradients were measured in the large arteries and veins of the limbs of humans. Under conditions of very low ambient temperature, the axial gradient in the limb artery was shown to be an order of magnitude greater than under normal ambient conditions. When venous return in the limbs was interrupted by occlusion the temperature of the artery increased significantly, indicating that a portion of the arterial temperature gradient was due to heat transfer with the parallel vein. Bazett and colleagues proposed the concept of venous shunting to the periphery, whereby heat could be readily shed from the body by reducing countercurrent exchange in the deep vasculature and at the same time directing venous blood to the cutaneous circulation where the venous blood is in close proximity to the surroundings. These qualitative examinations of thermal physiology by Bazett and colleagues were significant in bringing attention to the role of countercurrent heat exchange in bioheat transfer. These studies by Bazett did not attempt to mathematically model the effects of countercurrent heat exchange, but within several years these concepts were incorporated by other physiologists in their research.

2. *Scholander* [50–52]

The work of Scholander and colleagues [50–52] was an early example of mathematical modeling of biotransport phenomena in countercurrent systems. In 1954, Scholander and van Dam [50, 51] presented a quantitative study of gas diffusion in the swim bladder of fishes in which the mass transfer of oxygen in countercurrent systems was examined theoretically. These theoretical studies were useful in providing the basis for a subsequent report by Scholander and Krog [52] which applied the same concepts of transport in countercurrent systems to an investigation of heat transfer between paired arteries and veins in the vascular bundles of sloths.

The theoretical countercurrent heat transfer model of Scholander and Krog [52] assumed that the axial temperature profiles in both the paired artery and vein were linear, with a constant temperature difference between the artery and vein along their axes. This is the "perfect" countercurrent heat exchange assumption, whereby all heat that leaves the warm fluid

enters the cool fluid with no heat exchange with the surroundings. Under these conditions, Scholander and Krog showed that the heat transfer from the warm fluid to cool fluid per unit length tube, Q', is simply proportional to the product of the tube flow rate and the slope of the temperature profile. This relationship can be written as

$$Q' = \frac{mc_b(T_{in} - T_{out})}{L} = UA' \Delta T \tag{7.1}$$

where m is the fluid mass flow rate, $(T_{in} - T_{out})$ is the total fluid temperature change along the length of the tube with length L (the same for both the warm and cool fluids according to the perfect countercurrent assumption), ΔT is the constant temperature difference between the warm and cool fluid, and UA' is the overall heat transfer coefficient per unit length for the countercurrent system.

In order to verify this simple analysis, Scholander and Krog built an experimental apparatus which attempted to physically model the countercurrent heat exchange system. Two 1-cm-diameter thin-walled copper tubes were used to simulate an artery–vein pair. Warm water passed through one tube and after a 10-cm distance passed through a copper spiral which was immersed in a cold water bath. The cooled water emerged from the spiral and flowed through the second tube in a countercurrent direction alongside the tube containing the flowing warm water. The two tubes were bundled together and insulated from the surroundings. Temperature profiles along the axes of both tubes were measured at various flow rates and the results seemed to corroborate the theoretical analysis shown in Eq. (7.1). Scholander and Krog subsequently used their model to evaluate the experimental measurements of temperatures taken in the vascular bundles in sloth extremities.

A linear temperature gradient was measured in an isolated sloth rete that was much greater in magnitude than the temperature gradient measured by Bazett *et al.* in the human brachial artery [6]. This result supported Scholander and Krog's hypothesis that an efficient countercurrent heat exchange system would yield a steep temperature gradient in the blood vessel, thus reducing heat transfer from the limb to the surroundings. This concept was further supported by experimental measurements of the rete temperature gradient when the venous flow was occluded. In this case, the temperature gradient along the length of the rete was significantly decreased, demonstrating the importance of countercurrent heat exchange in these vascular bundles. Additional experiments by Scholander and Krog showed that the rate of rewarming an ice-chilled sloth limb was significantly slower than that of other animals which did not have retia in their limbs [52]. This effect was explained by the rete countercurrent system which

supplies arterial blood to the extremities that are substantially cooler than the core body temperature. Other measurements revealed that the flow rate in the rete was reduced during extremity cooling which resulted in a large temperature gradient along the length of the limb due to the increased efficiency of the countercurrent heat exchange mechanism under conditions of low blood flow rate.

B. ANALYSIS OF MITCHELL AND MYERS [45]

These combined theoretical and experimental studies by Scholander and Krog were valuable in demonstrating the importance of countercurrent heat exchange in bioheat transfer. While their model was simple, it provided a reasonable guide to the factors governing this heat-conserving phenomenon. Their theoretical model was substantially improved, however, in a study by Mitchell and Myers [45] that appeared 10 years later in 1968. Mitchell and Myers criticized the model of Scholander and Krog on several grounds. First, the assumption of perfect countercurrent exchange is not the general case for all artery–vein pairs and represents an idealization of their heat exchange. Second, the use of copper tubes by Scholander and Krog to physically model the artery and vein added a significant conductive heat transfer component along the length of the tube walls that does not exist *in vivo*.

1. *Governing Equations*

The analysis of countercurrent heat exchange in animals by Mitchell and Myers mathematically modeled this important bioheat transfer phenomenon in a more general manner than that presented by Scholander and Krog. The steady state model of Mitchell and Myers, shown schematically in Fig. 6, was derived under the following conditions. First, a one-dimensional vessel was assumed so that artery and vein temperatures depended only upon the axial location of blood in the vessel. Radial variations within the vessel were neglected. Second, heat conductance between the artery and vein, as well as the individual vessels and the environment, were considered constant with axial position in the blood vessels. Another assumption of this model was that there was no significant vessel branching or perfusion bleed-off from the artery or to the vein. Thus the mass flows of blood in the artery and vein were considered equal and independent of axial position. Finally, the effect of metabolic heat generation in the tissue was neglected compared to the countercurrent heat transfer terms. For convenience, all tissue and blood physical properties were considered constant.

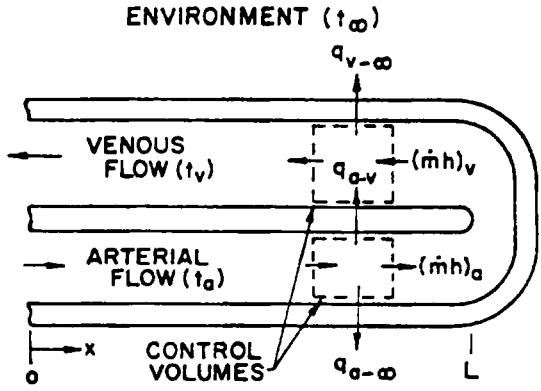

FIG. 6. A schematic view of countercurrent heat exchange between vessels and the surroundings used in the mathematical model of Mitchell and Myers. (Reproduced from [45], the *Biophysical Journal* **8**, 897–911, by copyright permission of the Biophysical Society.)

Separate energy balance equations are written for the differential control volumes of both the artery and vein. The differential energy balance for a segment of the artery of length dx is

$$mh_{ax} = mh_{a(x+dx)} + [(UA')_a(T_a - T_\infty) + (UA')_c(T_a - T_v)]\,dx \quad (7.2)$$

where h_a is the enthalpy of the arterial blood, m is the mass flow rate (assumed constant with x-location), and $(UA')_c$ and $(UA')_a$ are the overall heat transfer coefficient-surface area per unit length products for total heat transfer between the countercurrent artery and vein, and artery and surroundings, respectively. Assuming that the enthalpy of the arterial blood is the product of the blood specific heat and temperature, i.e., no pressure variations, Eq. (7.2) can be written as

$$mc_b \frac{dT_a}{dx} = (UA')_c(T_v - T_a) + (UA')_a(T_\infty - T_a) \quad (7.3)$$

The differential energy balance for the venous fluid is similarly

$$-mc_b \frac{dT_v}{dx} = (UA')_c(T_a - T_v) + (UA')_v(T_\infty - T_v) \quad (7.4)$$

Note that the left-hand side of Eq. (7.4) is written with a negative sign because flow is countercurrent and the venous flow is defined to be in the negative x-direction. The two boundary conditions used to solve Eqs. (7.3) and (7.4) are

$$T_a(0) = T_{a0} \qquad \text{and} \qquad T_a(L) = T_v(L) \quad (7.5)$$

The position $x = L$ physically represents the "turnaround" point for the artery and may be viewed schematically as the region of the microcirculation where the arteriole, venule, capillary, and tissue temperatures are all completely equilibrated.

Mitchell and Myers nondimensionalize the problem using the definitions

$$N_a = \frac{(UA')_a L}{mc_b}, \qquad N_v = \frac{(UA')_v L}{mc_b}, \qquad N_c = \frac{(UA')_c L}{mc_b} \tag{7.6}$$

$$\theta_a = \frac{T_a - T_\infty}{T_{a0} - T_\infty}, \qquad \theta_v = \frac{T_v - T_\infty}{T_{a0} - T_\infty} \tag{7.7}$$

and $z = x/L$. Note that the parameters N_a, N_v, and N_t are equivalent to the number of "heat transfer units" that characterize countercurrent heat exchangers. Based upon these definitions, the governing equations and boundary conditions for the countercurrent flow system are

$$\frac{d\theta_a}{dx} = N_c(\theta_v - \theta_a) - N_a\theta_a \tag{7.8}$$

$$-\frac{d\theta_v}{dx} = N_c(\theta_a - \theta_v) - N_v\theta_v \tag{7.9}$$

$$\theta_a(0) = 1 \qquad \text{and} \qquad \theta_a(1) = \theta_v(1) \tag{7.10}$$

These two first order ordinary differential equations are easily solved analytically by using Eq. (7.8) to write θ_v as a function of θ_a and its derivative and substituting this expression into Eq. (7.9). The result is a second order equation for θ_a as a function of x. The final solution is obtained by using the boundary conditions in Eq. (7.10) to solve for the dimensionless artery and vein temperature profiles

$$\theta_a = \exp(N_v - N_a)\frac{z}{2}\frac{C_2 \cosh C_1(1 - z) + \sinh C_1(1 - z)}{C_2 \cosh C_1 + \sinh C_1} \tag{7.11}$$

$$\theta_v = \exp(N_v - N_a)\frac{z}{2}\frac{C_2 \cosh C_1(1 - z) - \sinh C_1(1 - z)}{C_2 \cosh C_1 + \sinh C_1} \tag{7.12}$$

where

$$C_1 = \tfrac{1}{2}\sqrt{(N_a + N_v + 4N_c)(N_a + N_v)}$$

and (7.13)

$$C_2 = \sqrt{(N_a + N_v + 4N_c)/(N_a + N_v)}$$

2. *Model Solutions*

Mitchell and Myers present the solutions to this model under two different conditions that each resemble anatomical *in vivo* conditions. In the first case, the artery and vein are considered to be paired within a tissue cylinder such that there is symetry with respect to the cylinder axis and therefore the thermal conductance between the artery and environment $(UA')_a$ is equal to the thermal conductance between the vein and the environment $(UA')_v$. This structure resembles the major supply artery and vein pair that are embedded in the core of an extremity (e.g., the paired femoral artery and vein in the upper leg). This situation is also approximated by the rete structure observed in the sloth extremity by Scholander and Krog in which a bundle of arteries and veins are grouped together in the core of the limb. Under these conditions, the dimensionless temperature profiles depend only upon two parameters N_c and N_v.

$$\theta_a = \frac{C_2 \cosh C_1(1 - z) + \sinh C_1(1 - z)}{C_2 \cosh C_1 + \sinh C_1} \tag{7.14}$$

$$\theta_v = \frac{C_2 \cosh C_1(1 - z) - \sinh C_1(1 - z)}{C_2 \cosh C_1 + \sinh C_1} \tag{7.15}$$

where

$$C_1 = N_v\sqrt{1 + 2(N_c/N_v)} \quad \text{and} \quad C_2 = \sqrt{1 + 2(N_c/(N_v)} \tag{7.16}$$

Figure 7 shows the profiles for countercurrent systems for various ratios of N_c/N_v with N_v equal to zero, 0.1, and unity. Note that $N_v = 0$ represents the limiting case of $mc_p/L \gg (UA')_v$, in which there is no temperature change along the length of the artery or vein and thus no countercurrent heat transfer between the adjacent vessels. As N_v increases from zero to 0.1, temperature gradients along the length of the vessels can be seen, but there is still relatively little heat lost to the surroundings and thus only a small degree of blood temperature change. For large values of N_v the temperature change in the artery can be significant, which provides a large driving force for heat transfer between the artery and countercurrent vein. Whether or not adequate reheating of the blood occurs depends on the ratio N_c/N_v. For values of N_c/N_v greater than 10, this rewarming is significant. Mitchell and Myers also point out that for the cases where N_c/N_v is low (i.e., less than unity), there is still some heat transfer between the artery and vein which acts to increase the return temperature of the venous blood relative to the case where there is no countercurrent heat transfer at all $(N_c = 0)$. Because the total heat loss from the extremity is proportional to the difference between inlet artery temperature T_{a0} and the return venous

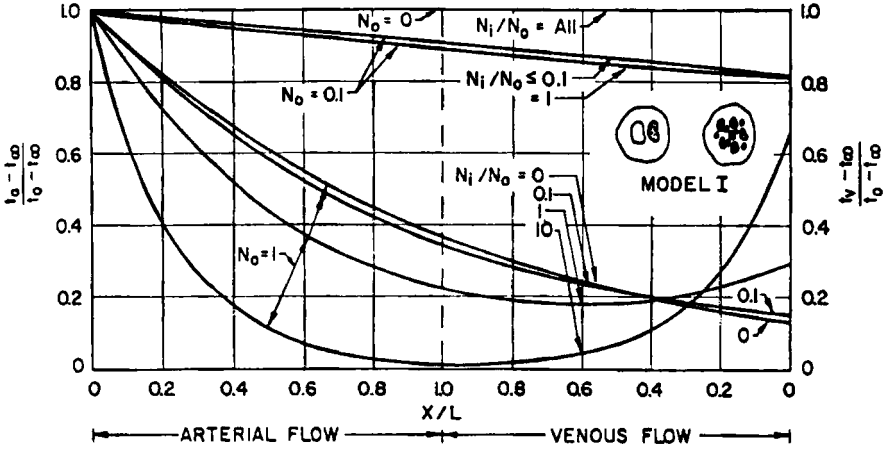

FIG. 7. Normalized arterial and venous blood temperature profiles along the length of a limb or rete with a symmetrical vascular arrangement of type I that implies $N_a \cong N_v$, as modeled by Mitchell and Myers. The parameters N_0 and N_i correspond to N_v and N_c, respectively. (Reproduced from [45], the *Biophysical Journal* **8**, 897–911, by copyright permission of the Biophysical Society.)

temperature $T_v(0)$, the Mitchell and Myers model successfully demonstrates that any finite amount of countercurrent heat exchange will reduce heat loss from the extremity to the surroundings [45].

The second case examined by Mitchell and Myers models the vascular arrangement in the fins of porpoises and tails of some animals. The artery is completely surrounded by smaller veins so that the heat transfer between the artery and the surroundings is negligible relative to the heat exchange between the artery and vein. Interestingly, this arrangement is similar to that in the human digits, where cutaneous veins surround the main supply artery. Setting the parameter N_a to zero, the Mitchell and Myers model depends again in the two parameters N_v and N_c:

$$\theta_a = \exp\left(N_v \frac{z}{2}\right) \frac{C_2 \cosh C_1(1 - z) + \sinh C_1(1 - z)}{C_2 \cosh C_1 + \sinh C_1} \tag{7.17}$$

$$\theta_v = \exp\left(N_v \frac{z}{2}\right) \frac{C_2 \cosh C_1(1 - z) - \sinh C_1(1 - z)}{C_2 \cosh C_1 + \sinh C_1} \tag{7.18}$$

where

$$C_1 = \frac{N_v}{2}\sqrt{1 + 4(N_c/N_v)} \quad \text{and} \quad C_2 = \sqrt{1 + 4(N_c/N_v)} \tag{7.19}$$

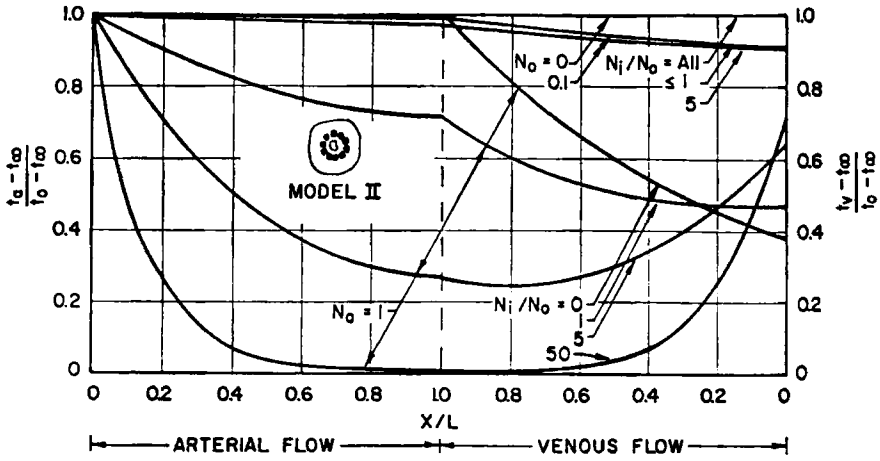

FIG. 8. Normalized arterial and venous blood temperature profiles along the length of a fin with the vascular arrangement of type II that implies $N_a \cong 0$, as modeled by Mitchell and Myers. The parameters N_0 and N_i correspond to N_v and N_c, respectively. (Reproduced from [45], the *Biophysical Journal* **8**, 897-911, by copyright permission of the Biophysical Society.)

The results for this second anatomical case are shown in Fig. 8. As in the first anatomical case, when N_v is low there is little heat lost to the environment and therefore little change in the blood temperature with axial position. When both N_v and N_c are large, there will be significant countercurrent exchange due to large gradients in the artery and vein temperatures. Similar to the first case, venous rewarming may or may not occur, depending on the ratio N_c/N_v, but countercurrent heat exchange will always act to increase the temperature of the vein at $x = 0$ relative to the case of zero countercurrent heat transfer, thereby reducing heat loss from the extremity to the surroundings. Mitchell and Myers show that for a given set of values for N_c and N_v, the second anatomical case is more effective in reducing the extremity heat loss than the first anatomical case. This difference is caused by the lack of heat transfer allowed between the artery and surroundings in the second anatomical model. Again, it is interesting to note that this second configuration is observed in the digits of humans, which presumably are most vulnerable to heat loss due to their large surface area to volume ratio. In this manner, the veins protect the arterial blood from excessive heat loss as blood flows towards the tip of the extremity. In contrast, the anatomical configuration of the main supply artery and vein in the limbs more closely resembles the first case of Mitchell and Myers [45].

3. *Parameter Estimation*

Using a resistance analysis similar to that employed by Holmes and Chen, Mitchell and Myers estimate the numerical values of N_v and N_c for a human extremity, sloth rete, and porpoise fin. The total thermal resistance $[(UA')_c]^{-1}$ depends on three resistances: the convective resistance from the arterial blood to the artery wall, the conduction resistance through the tissue, and the convective resistance from the venous wall to the venous blood. For this geometry, the conduction resistance per unit length vessel, R_{k1}, derived analytically for equal size vessels using a source–sink superposition in a cylindrical conduction field, is

$$R_{k1} = \frac{\cosh^{-1}[2(s/d)^2 - 1]}{2\pi k_t} \tag{7.20}$$

where d is the diameter of the vessels and s is the center-to-center spacing between the paired artery and vein. The convective resistance per unit length, R_c, depends on the Nusselt number and blood thermal conductivity

$$R_c = \frac{1}{2\pi k_b \,\mathrm{Nu}} \tag{7.21}$$

Mitchell and Myers model the human arm as a cylinder with an 8-cm diameter embedded with a 0.5-cm diameter artery and vein spaced 1 cm apart. Assuming a minimum Nusselt number of 4.0 and $k_b \cong k_t =$ 0.67 W/m-°C, the conduction and convective resistances per unit length vessel are 0.63 and 0.06 °C-m/W, respectively. Under these conditions, the total resistance is 0.75 °C-m/W, corresponding to a $(UA')_c$ value of 1.33 W/m-°C. Mitchell and Myers neglect the convection resistances, essentially assuming an infinite Nusselt number. In this case $(UA')_c$ is 1.59 W/m-°C. For a blood mass flow rate of 2 g/s and specific heat 3.5 J/g-°C, the value of N_c for a 75-cm-long human arm according to Mitchell and Myers is 0.17. By including the maximum resistance provided by the convection effect, N_c will be slightly reduced to 0.14.

The total resistance $[(UA')_v]^{-1}$ between the vessel and the environment can be estimated by treating the vessel as an isolated tube surrounded by a tissue cylinder. This resistance is the sum of three resistances: convective resistance between the venous blood and the vein wall, conduction resistance through the tissue, and convective resistance from the cylinder surface to the surroundings. The conduction resistance per unit length vessel in this case is

$$R_{k2} = \frac{\ln(d_0/d)}{2\pi} \tag{7.22}$$

where d_0 is the cylinder diameter and d is the vessel diameter. The convective resistance inside the vessel is given by Eq. (7.21), while the convective resistance between the cylinder surface and the environment is

$$R_c = \frac{1}{2\pi k_t \, \mathrm{Bi}} \tag{7.23}$$

where Bi is the combined radiation/convection Biot number. For the geometry described above and assuming a combined Biot number of 2.0, the values of the three resistances per unit length listed above are 0.06, 0.66, and 0.12 °C-m/W, respectively. The total resistance per unit length vessel is 0.84 °C-m/W, corresponding to a $(UA')_v$ value of 1.19 W/m-°C. Using the physical constants listed above for the human extremity, the value of N_v in this case is 0.13. As in the evaluation of N_c, Mitchell and Myers neglect all but the conduction resistance through the tissue and calculate a slightly higher value of 0.16 for N_v.

According to these calculations, the ratio N_c/N_v in the human extremity is approximately unity. Considering the possible range of values for N_c and N_v, Mitchell and Myers show that this ratio is within the range 0.5 to 2 for the various mass flow rates possible in the human arm. Using the same range of mass flow rates, the range of the N_v values will be 0.08 to 0.4.

With N_c/N_v equal to unity and N_v ranging from 0.08 to 0.4, the model of Mitchell and Myers predicts that there is little countercurrent effect between the major artery and vein that supply the human arm. Under these conditions, the countercurrent heat transfer reduces heat loss from the arm only by about 5% compared to the case of zero countercurrent exchange. According to this model, essentially all the heat loss from the limb is controlled by the heat conductance between the vessels and the surroundings, and there is little conductance between the countercurrent artery and vein.

4. *Comparison with Experimental Data*

As a corroboration of their theory, Mitchell and Myers compare the predictions of their model to the experimental measurements of artery and vein temperatures in the human arm collected by Bazett *et al.* [6] with fair agreement. While the omission of metabolic heating from the model of Mitchell and Myers is not important relative to the heating effects of blood perfusion (only about 5%), their model is clearly insufficient in accounting for heat loss from the hand to the surroundings. Other features, such as the tapered geometry of the arm and the local heat transfer in the separate microcirculatory networks of the muscle and cutaneous layers of the limb, were ignored. These important heat transfer effects would eventually be incorporated into the much more detailed bioheat transfer model of the human arm by Song *et al.* about 20 years later [56].

Mitchell and Myers also estimate the N_v and N_c parameters for the sloth rete that was studied experimentally by Scholander and Krog [52]. In this case, N_c is quite high, on the order of 60, while N_v is on the order of unity. As with the human arm, Mitchell and Myers use these values in their first anatomical model ($N_a \cong N_v$). Due to the high value of N_c/N_v, this model predicts significant countercurrent rewarming of venous blood in the sloth rete, and the predictions are in fair agreement with the experimental temperature gradients measured by Scholander and Krog [52]. A third simulation of the countercurrent heat exchange in the porpoise fin, which is modeled by the second anatomical case ($N_a \cong 0$), predicts that there is not much countercurrent rewarming of the venous blood, but demonstrates the increased efficiency of the second anatomical configuration compared to the first arrangement. These results were not compared to any experimental data.

Despite the absence of several important heat transfer phenomena in their limb model, the theoretical study of Mitchell and Myers was significant as one of the first mathematical models which quantified the effect of countercurrent heat exchange in the circulation. By identifying the dimensionless heat transfer units N_v and N_c, the earlier experimental observations by Bazett *et al.* [6] and Scholander and colleagues [50–52] were explained analytically. For example, the inverse relationship between N_v and mass flow rate predicts that the countercurrent exchange mechanism will increase with decreasing flow rate. Under conditions of cold ambient temperature, Scholander and Krog observed this effect in their temperature measurements in the sloth rete. Thus by reducing blood flow to the extremity, less heat is lost to the environment not only due to the reduced time rate of thermal energy carried by the blood, but also by the more efficient rewarming of venous blood by the countercurrent exchange mechanism. The model of Mitchell and Myers was successful in explaining and predicting many of the earlier observations of experimental physiologists and represented a starting point for more sophisticated mathematical models of countercurrent heat exchange in the circulation.

C. Model of Keller and Seiler [36]

Three years after the publication of Mitchell and Myers's bioheat transfer model, Keller and Seiler presented a model of peripheral heat transfer that included the effect of countercurrent heat exchange as well as conduction, bulk convection with perfusion bleed-off, and metabolic heat production [36]. Keller and Seiler hypothesized that a countercurrent heat exchange mechanism would be important in the peripheral circulation near the body surface where the smaller arteries and veins were often positioned near each other. By combining the various heat transfer phenomena described

above, Keller and Seiler presented one of the earliest mathematical models of bioheat transfer in the microcirculation that considered heat transfer between separate tissue, artery, and vein compartments. This approach became the standard procedure in later formulations of more geometrically complex vascular bioheat transfer models by Weinbaum and colleagues [34, 55, 56, 59–63, 70], as well as Wissler [66, 68], Baish and colleagues [2, 4], and Charny and colleagues [18, 19].

Keller and Seiler [36] modeled bioheat transfer in the microcirculation of peripheral tissue according to the idealized one-dimensional schematic view shown in Fig. 9. The location $x = 0$ represents the boundary between the peripheral tissue and the core, which Keller and Seiler assume to be isothermal, while the location $x = \delta$ represents the boundary between the peripheral tissue and the ambient environment. According to the authors' interpretation, the value of δ depends on the heat transfer rate in the peripheral region as determined mainly by the rate of blood flow in the vessels and the thermal conductivity of the tissue. The single artery and vein shown in Fig. 10 are used to represent the system of many terminal arteries and veins that supply blood to and drain blood from the peripheral tissue, while capillaries are assumed to provide a continuous connection between the countercurrent terminal artery and vein. Using a continuity or mass balance relationship, the flow rates in the artery and vein shown in Fig. 10 can be determined as a function of x and the perfusion bleed-off rate per unit volume tissue. Similarly, energy balance equations can be utilized to compute the arterial, venous, and mean tissue temperatures as functions of x, the distance from the isothermal core hypothesized by Keller and Seiler.

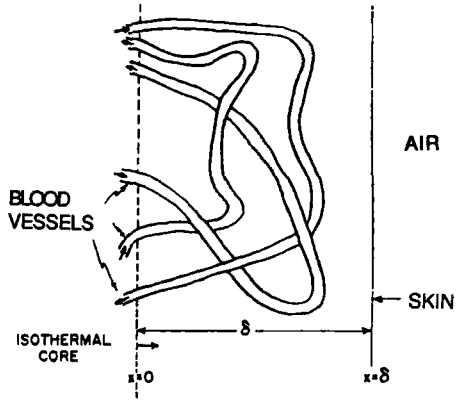

FIG. 9. A schematic view of the subcutaneous tissue region considered by Keller and Seiler. (Reproduced from [36], with permission.)

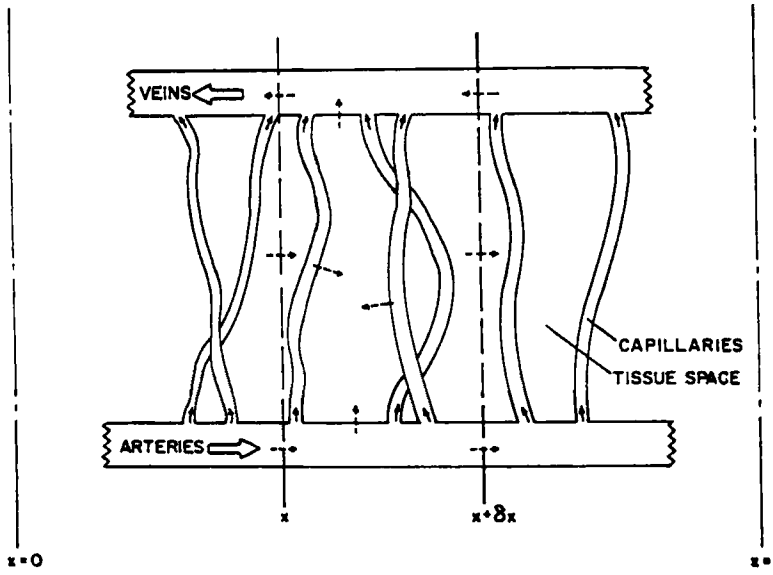

FIG. 10. A schematic diagram of an element, thickness dx, in the subcutaneous tissue region with heat flows indicated by dashed arrows and blood flow directions indicated with outlined arrows. The one-dimensional model of Keller and Seiler is derived from an energy balance across the vertical dashed lines. (Reproduced from [36], with permission.)

1. *Governing Equations*

The steady state energy balance equations are derived using a differential element of length dx, shown in Fig. 10. Assuming that δ was small relative to the curvature of the peripheral tissue region, Keller and Seiler model the peripheral tissue region as a one-dimensional slab, so that the cross-sectional area normal to the direction of heat flow, A_x, is considered constant. The energy balance for the artery element consists of four terms:

$$(m_a c_b T_a)_x = (m_a c_b T_a)_{x+dx} + c_b \omega \rho_b T_a A_x \, dx + (UA')_a \, dx(T_a - T_t) \quad (7.24)$$

where m_a and T_a are the arterial mass flow rate and temperature, respectively, ω is the spatially uniform perfusion bleed-off rate from the artery expressed as volume blood leaving the artery per time per volume tissue, $(UA')_a$ is the overall heat transfer coefficient–surface area product per unit length from the artery to the tissue, and T_t is the mean tissue temperature at position x. The temperature of the blood that leaves the artery as a result of bleed-off is clearly T_a, the local artery blood temperature. Note also that the Keller and Seiler neglect the effects of axial conduction along the length of the artery, which is reasonable for tube flow such as this with a significant

component of bulk convection heat transfer. Rearranging and solving for vanishing dx, Eq. (7.24) may be written as

$$\frac{d}{dx}\left(\frac{m_a c_b T_a}{A_x}\right) = \frac{(UA')_a}{A_x}(T_t - T_a) - c_b \omega \rho_b T_a \tag{7.25}$$

Similarly for the countercurrent flowing venous blood

$$(m_v c_b T_v)_{x+dx} + c_b \omega \rho_b T_{v0} A_x dx = (m_v c_b T_v)_x + (UA')_v dx(T_v - T_t) \tag{7.26}$$

where T_{v0} represents the temperature of the venous blood as it drains from the capillary in Fig. 10 into the terminal vein, and all other symbols are analogous to those that appear in Eq. (7.24). Note that for both the artery and vein, the mass flow rate m is considered a positive number regardless of the flow direction. The venous blood energy balance is thus

$$-\frac{d}{dx}\left(\frac{m_v c_b T_v}{A_x}\right) = \frac{(UA')_v}{A_x}(T_t - T_v) + c_b \omega \rho_b T_{v0} \tag{7.27}$$

The left-hand sides of Eqs. (7.25) and (7.27) both contain the derivative with respect to x of the product of blood mass flow rate and temperature. The relationship between the mass flow rate and x depending on the bleed-off rate from the vessel is

$$m_a = m_{a0} - \int_0^x \omega \rho_b A_x \, dx \tag{7.28}$$

where m_{a0} is the arterial mass flow rate at $x = 0$. In addition,

$$m_v = m_{v0} - \int_0^x \omega \rho_b A_x \, dx \tag{7.29}$$

where m_{v0} is the venous mass flow rate at $x = 0$. By essentially neglecting the effects of lymphatic circulation on the venous blood flow rate, Keller and Seiler also assume that

$$m_{v0} = m_{a0} \tag{7.30}$$

Based upon Eqs. (7.28)–(7.30), the magnitudes of the mass flow rates in the artery and vein must be equal at all x-locations. From Eqs. (7.28) and (7.29) it is also apparent that

$$\frac{dm_a}{dx} = -\omega \rho_b A_x = \frac{dm_v}{dx} \tag{7.31}$$

Keller and Seiler also simplify the convective heat transfer terms that appear on the right-hand sides of Eqs. (7.25) and (7.27) by assuming that

the surface area of the artery and vein is the same. This is reasonable in the peripheral region, where the paired terminal arteries and veins are equal-sized, and their number densities are also more or less the same. Under these conditions, the products $(UA')_a$ and $(UA')_v$ are equal to (UA'). Implementing the above simplifications, the artery and vein energy balance equations are reduced to

$$mc_b \frac{dT_a}{dx} = (UA')(T_t - T_a) \tag{7.32}$$

$$-mc_b \frac{dT_v}{dx} = (UA')(T_t - T_v) + c_b \omega \rho_b A_x (T_{v0} - T_v) \tag{7.33}$$

where m is the magnitude of the mass flow rate in the artery or vein.

Using the argument that blood in the capillaries will be in complete thermal equilibration with the tissue due to the large surface-to-area ratio in the capillary bed and the long residence time of blood in the capillaries, Keller and Seiler assume that T_{v0} is equal to T_t. This assumption, as was later demonstrated by the work of Chen and Holmes, is reasonable in the peripheral tissue, where the bleed-off vessels from the paired artery and vein are relatively small and consequently have a short thermal equilibration length relative to their own length. Therefore the energy balance equation for the vein becomes

$$-mc_b \frac{dT_v}{dx} = (UA')(T_t - T_v) + c_b \omega \rho_b A_x (T_t - T_v) \tag{7.34}$$

For deeper tissue, the assumption $T_{v0} = T_t$ is no longer valid since the bleed-off vessels are thermally significant due to their relatively large thermal equilibration lengths. It should be noted that the complete thermal equilibration between blood, the capillaries and the surrounding tissue that was assumed by Keller and Seiler is similar to the Pennes assumption (i.e., $k' = 0$ in the Pennes model). However, the Keller and Seiler model is otherwise quite different as it makes no assumptions regarding the arterial blood temperature, which varies in the x-direction. The effect of these differences can be seen in Keller and Seiler's derivation of the tissue energy balance equation below.

The effect of perfusion bleed-off on tissue temperature is assumed to be proportional to the product of ω and the local artery–tissue temperature difference. Note that Keller and Seiler use the local artery temperature rather than a central or core artery temperature that was employed in the Pennes formulation. This heat source is balanced by metabolic heating, conduction, and heat transfer with the adjacent artery and vein. Across the

differential tissue element of length dx:

$$\left(-k_t A_x \frac{dT_t}{dx}\right)_x + (UA')\,dx[(T_a - T_t) + (T_v - T_t)] + \omega\rho_b c_b(T_a - T_t)A_x\,dx + Q_m A_x\,dx = \left(-k_t A_x \frac{dT_t}{dx}\right)_{x+dx} \tag{7.35}$$

where Q_m is the spatially uniform metabolic heat source per volume tissue. For constant thermal conductivity k_t and vanishing dx, Eq. (7.35) may be written as

$$k_t \frac{d^2T_t}{dx^2} + \frac{(UA')}{A_x}[(T_a - T_t) + (T_v - T_t)] + \omega\rho_b c_b(T_a - T_t) + Q_m = 0 \tag{7.36}$$

In the tissue equation derived by Keller and Seiler, heat conduction is balanced by convective heat transfer with the artery and vein, a pefusion heat source whose strength is proportional to the local artery-tissue temperature, and the constant metabolic heat source. For the case where convective heat exchange with the artery and vein is neglected and $(UA') \cong 0$, Eq. (7.32) states that the arterial temperature is independent of x, and, as a result, the tissue energy balance reduces to the Pennes equation. For the case $(UA') \neq 0$, T_a varies with x, and the perfusion source term depends on the local artery temperature. Due to this dependence, the tissue equation (7.36) cannot be solved alone, but must be solved simultaneously with the artery and vein energy balances, Eqs. (7.32) and (7.34).

Keller and Seiler solve these coupled differential equations by assuming that the arterial blood enters the peripheral region at the isothermal core temperature

$$T_t(0) = T_a(0) = T_b \tag{7.37}$$

and that as a result of zero mass flow across the surface at $x = \delta$, the venous blood is completely equilibrated with the tissue at this location:

$$T_t(\delta) = T_v(\delta) = T_s \tag{7.38}$$

where T_b and T_s are specified temperatures.

2. *Analytical Solution*

As mentioned above, the solution to Eqs. (7.32), (7.34), and (7.36)-(7.38) are easily obtained when artery-tissue and vein-tissue interactions are neglected. With (UA') equal to zero, the artery temperature profile is simply

$$T_a(x) = T_b \tag{7.39}$$

Implementing this uniform artery temperature profile, the tissue energy balance equation reduces to the Pennes bioheat equation. The solution to this second order ordinary differential equation is

$$T_t = C_1 \cosh \lambda x + C_2 \sinh \lambda x + \frac{Q_m}{\omega \rho_b c_b} + T_b \tag{7.40}$$

where

$$\lambda = \sqrt{\frac{\omega \rho_b c_b}{k_t}}$$

The integration constants are evaluated using the fixed temperature boundary conditions in Eqs. (7.37) and (7.38). Note that this mathematical system is similar to that derived by Wulff in Eq. (4.9), except that Keller and Seiler do not neglect the metabolic heating source Q_m in the tissue heat balance equation. The boundary conditions, however, are identical. The dimensionless temperature profile can be written

$$\theta = \frac{T_t(x) - T_b}{T_s - T_b} = \Phi[\cosh \lambda x - 1] + [1 + \Phi(1 - \cosh \lambda \delta)] \frac{\sinh \lambda x}{\sinh \lambda \delta} \tag{7.41}$$

where

$$\Phi = \frac{Q_m}{\omega \rho_b c_b (T_b - T_s)}$$

Note that for zero metabolic heating ($\Phi = 0$) this result reduces to Wulff's solution to the Pennes bioheat equation for these fixed temperature boundary conditions as represented by Eq. (4.11).

3. *Derivation of Effective Thermal Conductivity*

In order to quantify the effect of blood flow on tissue heat transfer, Keller and Seiler introduce an effective thermal conductivity to describe the rate of heat transfer from the surface of this peripheral layer of tissue. According to their definition, for a thin flat slab of tissue with negligible curvature, the steady state surface heat flux, q_s, is the product of the effective thermal conductivity and the temperature gradient across the thickness of the entire slab; i.e., from $x = 0$ to $x = \delta$:

$$q_s \equiv \frac{k_{eff}(T_b - T_s)}{\delta} \tag{7.42}$$

Based upon Fourier's Law, the surface heat flux is also equal to the product of the negative value of the local tissue temperature gradient at the surface

and the tissue thermal conductivity. Therefore

$$\frac{k_{\text{eff}}}{k_t} = \frac{-\delta}{(T_b - T_s)} \left.\frac{dT_t}{dx}\right|_{x=\delta} \tag{7.43}$$

For the case of no artery–tissue and vein–tissue interactions, the effective thermal conductivity is determined from Eq. (7.41):

$$\frac{k_{\text{eff}}}{k_t} = \lambda\delta\left\{\Phi \sinh \lambda\delta + \frac{1 + \Phi(1 - \cosh \lambda\delta)}{\tanh \lambda\delta}\right\} \tag{7.44}$$

Keller and Seiler rewrite Eq. (7.44) in a manner that better illustrates the importance of the metabolic heat source on the effective thermal conductivity:

$$\frac{k_{\text{eff}}}{k_t} = \frac{\lambda\delta}{\tanh \lambda\delta} + \frac{Q_m\delta^2}{(T_b - T_s)} \frac{\tanh\left(\frac{\lambda\delta}{2}\right)}{k_t\lambda\delta} \tag{7.45}$$

The maximum value of the parametric group that appears as a coefficient for the second term on the right-hand side of Eq. (7.45) is estimated by Keller and Seiler by analyzing the maximum value of δ, the peripheral region thickness, for a given value of Q_m. As Q_m increases above zero, the temperature inside the peripheral layer increases and eventually surpasses the isothermal core temperature T_b, in which case a maximum exists inside the tissue layer. In this case, the heat flux from the tissue to the surroundings is proportional to the effective thermal conductivity and the difference between the maximum and surface temperatures. The region of interest, where the flow of heat is from the tissue to the surroundings, is between positions $x = x_m$ and $x = \delta$, where x_m is the location of the maximum temperature T_m inside the peripheral tissue layer. Defining the thickness of the tissue layer in which heat flows outwards towards the surroundings as $\delta_m = (\delta - x_m)$, the heat flux from the tissue to the surroundings is

$$q_s = -k_t \left.\frac{dT_t}{dx}\right|_{x=\delta} \equiv \frac{k_{\text{eff}}}{\delta_m}(T_m - T_s) \tag{7.46}$$

For a given metabolic heat source, the heat flow from the tissue to the surroundings is equal to the heat deposited in the tissue by the metabolic heat source under conditions of zero perfusion bleed-off. However, as the rate of bleed-off increases from zero, i.e., $\omega \neq 0$, the value of q_s is greater than the heat deposited in the tissue solely by the metabolic heat source due to the heating effect of warm blood perfusion on the tissue. Therefore

$$q_s \geq Q_m\delta_m \tag{7.47}$$

Substituting the condition in Eq. (7.47) into the definition in Eq. (7.46):

$$k_{\text{eff}} \geq \frac{Q_m \delta_m^2}{(T_m - T_s)} \tag{7.48}$$

By deriving the value of the minimum effective thermal conductivity, Keller and Seiler are able to define the maximum value of the parametric group on the right-hand side of Eq. (7.48), which also appears in Eq. (7.45). This situation occurs for the case of zero blood perfusion. In this case, it is easily shown that the effective conductivity is

$$k_{\text{eff}}(\omega = 0) = 2k_t \tag{7.49}$$

Thus Keller and Seiler conclude that the maximum value of the parametric group that appears in Eq. (7.45) is $2k_t$; i.e.,

$$\frac{Q_m \delta^2}{(T_b - T_s)} \leq 2k_t \tag{7.50}$$

Using a tissue conductivity of 0.5 W/m-°C, the estimated maximum value of the parametric group is 1.0 W/m-°C, while the minimum value is zero. Figure 11 shows the values of k_{eff} relative to k_t as a function of $(\lambda\delta)$ for this range of values. This product, $\lambda\delta$, can be physically interpreted as the ratio of perfusion bleed-off heat transfer to conduction heat transfer in the tissue. Keller and Seiler note that metabolic heating affects the effective conductivity most significantly at low values of $(\lambda\delta)$, while at higher $\lambda\delta$ values, metabolic heating has a negligible influence on k_{eff}. Keller and Seiler compare these predictions qualitatively to experimental measurements by others that demonstrated a difference between the tissue effective conductivity under conditions of rest and exercise. This difference between exercise and resting conditions was reduced significantly, however, as the peripheral layer blood flow was increased by vasodilation, thereby reducing the influence of metabolic heating as compared to perfusion bleed-off rate in the tissue.

When the metabolic heating rate is negligible compared to the bleed-off rate, the ratio k_{eff}/k_t approaches the product $(\lambda\delta)$ for large values of λ, i.e., large perfusion rates. In this case, the heat flux from the tissue to the surroundings from the nonisothermal peripheral layer is independent of the value of δ and the thickness of the peripheral layer approaches the length $1/\lambda$. As perfusion rates decrease, the ratio k_{eff}/k_t approaches unity.

Keller and Seiler also derive the tissue and blood temperature profiles for the case of significant blood vessel–tissue interactions, i.e., $(UA') \neq 0$. If the metabolic heat source term is neglected, the analytical solution to the

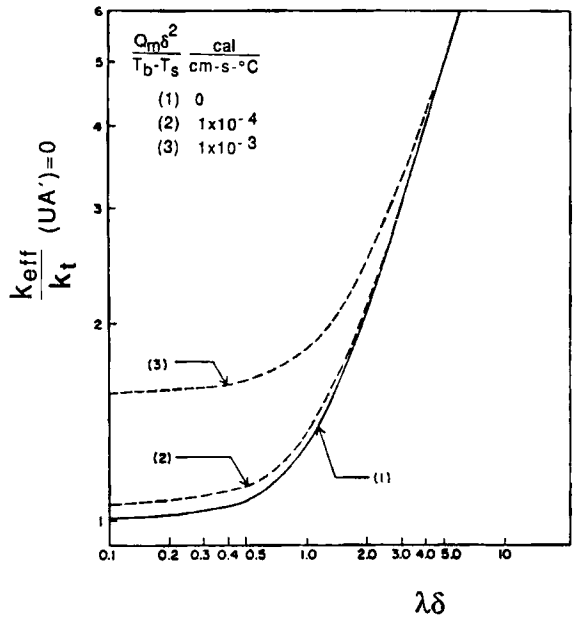

FIG. 11. Tissue effective thermal conductivity relative to the solid tissue conductivity as a function of the dimensionless product $\lambda\delta$, under conditions of zero blood-tissue convection heat transfer ($UA' = 0$). Each curve is based on a different value for the metabolic heat generation term $Q_m\delta^2/(T_b - T_s)$. Based on the bioheat transfer model of Keller and Seiler. (Reproduced from [36], with permission.)

tissue energy balance equation is

$$\theta = \frac{f(\zeta, \mu)}{f(\zeta_0, \mu)} \tag{7.51}$$

where the function f is defined by the integral equation

$$f(\zeta, \mu) = \int_0^{\zeta} \left\{ \sqrt{z'} I_\nu(z') \int_0^{z'} z^{-3/2} I_{-\nu}(z)\, dz - \sqrt{z'}\, I_{-\nu}(z') \int_0^{z'} z^{-3/2} I_\nu(z)\, dz + A\sqrt{z'}\, I_\nu(z') \right\} dz' \tag{7.52}$$

$$\nu = \mu + \tfrac{1}{2} \tag{7.53}$$

$$\zeta = \lambda\delta\sqrt{1 + 2\mu}\left(1 - \frac{x}{\delta}\right) \tag{7.54}$$

$$\mu = \frac{(UA')}{\omega\rho_b c_b A_x} \tag{7.55}$$

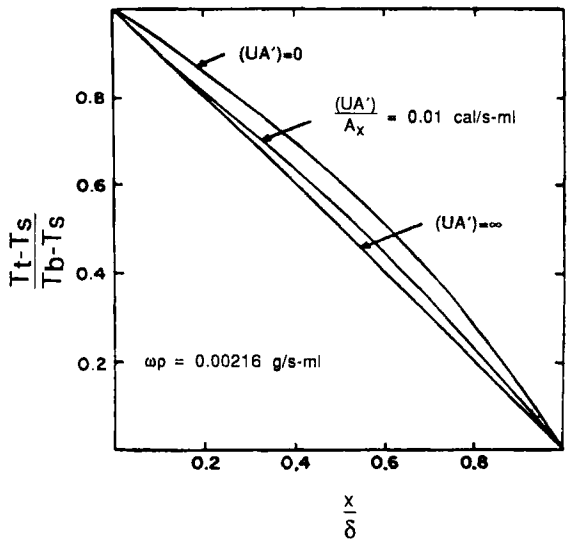

FIG. 12. Normalized tissue temperature profiles in the subcutaneous tissue region using a range of $(UA')/A_x$ values. The perfusion bleed-off rate is fixed at $\omega\rho_b = 2.16 \times 10^{-3}$ g blood/s-ml tissue. (Adapted from [36], with permission.)

and A is an integration constant. Keller and Seiler use the solution above along with Eq. (7.43) to solve for the effective conductivity in the tissue:

$$\frac{k_{\text{eff}}}{k_t} = \frac{-2 \sin \nu\pi}{\pi f(\zeta_0, \mu)} \frac{\lambda\delta\sqrt{1 + 2\mu}}{\mu(\mu + 1)} \tag{7.56}$$

Figure 12 shows the dimensionless tissue temperature profiles for the limiting cases of zero and infinite (UA'/A_x), as well as a representative intermediate value, using a constant bleed-off perfusion rate. As the heat transfer coefficient increases towards infinity, the enhancement of heat transfer by the perfusion bleed-off is canceled out by the convective heat transfer between the large vessels and the tissue. This results in an effective thermal conductivity equal to the tissue conductivity and the resulting temperature profile is linear, as expected for a pure conduction field. The dimensionless parameter μ represents ratio of the heat transfer between the large vessels and tissue to the heat transfer due to perfusion bleed-off. Figure 13 shows the relationship between the effective conductivity and μ. As μ increases and the large vessel interaction becomes more significant relative to the perfusion bleed-off, the effective conductivity approaches the tissue conductivity, a phenomenon Keller and Seiler describe as "arterial precooling." When the vessel-tissue conductance (UA') is significant

mean blood temperature $T_b(x)$ is

$$\frac{dT_b}{dx} + \frac{2h_e}{\rho_b U c_b R_1}(T_b - T_0) \tag{8.4}$$

Defining a dimensionless temperature θ and axial location $\bar{x}$:

$$\theta = \frac{T_b - T_0}{T_b(0) - T_0} \quad \text{and} \quad \bar{x} = \frac{x}{2R_1} \tag{8.5}$$

where L is the length of the blood vessel, the solution to this first order differential equation is readily obtained in terms of the dimensionless parameter λ, defined by Chato as $4\,\mathrm{Nu}_e/\mathrm{Pe}$. This term depends on the x-location as Nu_e will vary with axial position in the blood vessel.

2. *Solution—Effectiveness and Thermal Equilibrium Length*

The solution

$$\theta = \exp(-\lambda \bar{x}) \tag{8.6}$$

can be used to determine the dimensionless mean blood temperature at the blood vessel exit for the two limiting cases described above by substituting either Eq. (8.1) into Eq. (8.6) in the first case, or substituting $\mathrm{Nu}_e = 0.32$ for the second case. The concept of heat transfer effectiveness, ε, is implemented according to the definition

$$\varepsilon = \frac{T_{b,\mathrm{in}} - T_{b,\mathrm{out}}}{T_{b,\mathrm{in}} - T_0} \tag{8.7}$$

where $T_{b,\mathrm{in}}$ and $T_{b,\mathrm{out}}$ represent the blood temperatures at the blood vessel inlet and outlet, respectively. The values of heat transfer effectiveness are shown in Fig. 15 for the two limiting cases of vessel–tissue heat transfer. In addition, Chato computes a thermal equilibration length, similar in concept to that defined by Chen and Holmes. Chato determines the distance from the blood vessel inlet at which the mean blood temperature is 95% thermally equilibrated, i.e., where $\theta = 0.05$. For the case with $R_2 = R_1$, the thermal equilibration length according to this definition and the solution above is $0.34R_1$, while the case with $\mathrm{Nu}_e = 0.32$, the thermal equilibration length is $4.36R_1$.

Chato uses anatomical data from a dog to relate these theoretical results to heat transfer in the circulation. For the largest vessels, the heat transfer effectiveness is small due to the large Graetz numbers in these vessels (greater than 1000). Thus there is little heat transfer between these large blood vessels and the surrounding tissue. Conversely, in the smallest vessels,

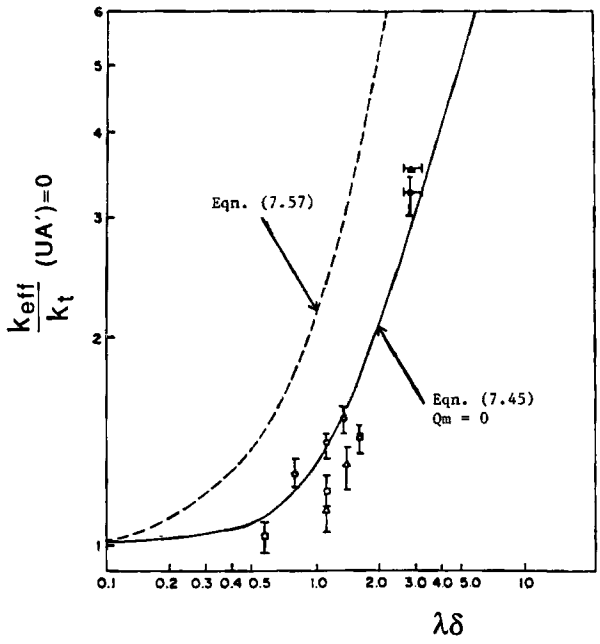

FIG. 14. Predictions of the Keller and Seiler model, represented by Eq. (7.45) (with $Q_m = 0$), compared with experimental data from the literature as compiled by Keller and Seiler. The dashed line indicates the predictions of a simple perfusion conductance model in Eq. (7.57). (Reproduced from [36], with permission.)

conductivity computed by the Keller and Seiler model was in good agreement with the experimental measurements [12]. A comparison between the measured and predicted effective conductivities is shown in Fig. 14.

In addition, Keller and Seiler show that earlier attempts to quantify the effect of perfusion on tissue conductivity as a linear addition to the thermal conductance resulted in a significant overestimation of the enhancement of tissue conductivity by blood perfusion. Substituting the definition of λ into Eq. (2.2):

$$\frac{k_{eff}}{k_t} = 1 + (\lambda\delta)^2 \tag{7.57}$$

This relationship was used in much of the earlier thermal physiological modeling work by Gagge and others [5, 11, 27, 30] and is plotted in Fig. 14.

Keller and Seiler also utilize their mathematical model to demonstrate that the effect of vasoconstriction on effective conductivity will be small at the low perfusion rates since k_{eff} cannot be less than k_t. At high perfusion rates,

the effect of added vasodilation on effective conductivity is also limited, in this case by the tissue thermal conductivity and the inlet arterial mass flow rate. Keller and Seiler conclude that while perfusion bleed-off can vary by two orders of magnitude, the effective conductivity, as predicted by their model and measured in the experiments of others, will vary by less than one order of magnitude in human peripheral tissue. The added effect of arterial precooling, based on this model, is to decrease the effective conductivity. An increase in the bleed-off perfusion rate, however, will tend to counteract arterial precooling and thus increase the effective conductivity.

4. *Parameter Estimation—Conductance Model*

Keller and Seiler also attempted to estimate the values of (UA') in peripheral tissue by modeling the supply artery and vein as cylinders with radius r_0, a total number density n, and a tortuosity τ (length of vessel per length of tissue). Assuming that the artery and vein are parallel and spaced a distance $2R$ apart from each other and that there are $n/2$ of each vessel, the conduction resistance between blood vessels is

$$U = \frac{k_t}{r_0 \ln(R/r_0)} \tag{7.58}$$

Note that in this formulation Keller and Seiler neglect the effect of any convection heat transfer resistance inside the two paired blood vessels. The total surface area of arteries or veins per unit length, A', depends on the number density–tissue cross-sectional area product and the surface area of the individual vessel:

$$A' = \frac{(n/2)A_x 2\pi r_0 \tau \delta}{\delta} \tag{7.59}$$

The total vessel density n can be approximated by considering four adjacent blood vessels in a periodic square arrangement of vessels. Because the total tissue area is $(2R)^2$, and the total number of blood vessels in this tissue space is $4 \times \frac{1}{4}$, Keller and Seiler approximate n as $\frac{1}{4}R^2$. Under these conditions, the parameter (UA') can be written as

$$\frac{(UA')}{A_x} = \frac{\pi \tau k_t}{4R^2 \ln(R/r_0)} \tag{7.60}$$

where the left-hand side of Eq. (7.60) represents the conductance between the artery or vein and adjacent tissue per unit volume of tissue. Substituting characteristic values of $R = 0.5$ cm and $r_0 = 0.05$ cm, Keller and Seiler use their model to demonstrate that under resting conditions arterial precooling

will result in a reduction in the effective conductivity from its maximum value (i.e., when there is no arterial precooling) by approximately 50%.

By applying separate energy balance equations to the separate artery, vein, and tissue components of perfused tissue, Keller and Seiler were able to analytically quantify several of the more important phenomena that affect bioheat transfer in tissue. These features include the presence of artery and venous supply vessels that are thermally significant, i.e., contain blood flowing at a significantly different temperature than the surroundings, the countercurrent blood flow arrangement, and the bleed-off of arterial blood at the local artery temperature (not a constant central or core temperature) into the tissue through vessels that eventually equilibrate with the surrounding tissue. While their model lacked detail concerning the different tissues of the peripheral layer, i.e., skin and fat as well as muscle tissue, this formulation was one of the first to implement a "three equation" approach to bioheat transfer modeling. This model also neglected the effect of the vascular architecture, which is actually a network of branching, tapered vessels, on the tissue heat transfer. The anatomical complexity of the microvascular network in both normal tissue and cancer tumors was known to be an important factor in bioheat transfer according to the observations of several experimental groups [33], but due to the computational difficulties associated with this type of geometry, only simplified models such as that of Keller and Seiler were derived.

VIII. Chato Vascular Heat Transfer Models [20]

A study by Chato [20] in 1980 examined heat transfer between tissue and blood vessels using the same basic approach as Keller and Seiler, i.e., a consideration of the governing differential energy balance equations for the separate blood and tissue media. Chato examined heat transfer between tissue and blood vessels for three different arrangements: a single vessel surrounded by tissue, a countercurrent pair of vessels surrounded by tissue, and a single vessel close to an isothermal surface such as the skin. In all three cases, the heat transfer effectiveness of the vascular configuration was considered.

A. ISOLATED VESSEL

The case of steady state heat transfer between a Casson fluid, e.g., blood, flowing in a round tube, e.g., blood vessel, with constant wall temperature was examined by Victor and Shah [58]. Under these conditions,

the tissue-blood heat transfer, as defined by a mean Nusselt number $\bar{h}D/k_b$, is

$$\overline{\mathrm{Nu}}_D = 4 + 0.155 \exp(1.58 \log \mathrm{Gz}_x) \tag{8.1}$$

which is valid for Gz_x, the local Graetz number, $\mathrm{Re\,Pr}D/x < 1000$. As shown, in the region of thermally fully developed flow, the mean Nusselt number is 4, which is close to the value of 3.66 for a Newtonian fluid.

1. *Governing Equations*

Chato considers the heat transfer between the blood vessel, with radius R_1 and bulk temperature T_b, and the surface of a tissue cylinder with radius R_2 that surrounds the blood vessel at temperature T_0. Under these conditions, the effective heat transfer between the single vessel and the cylinder surface is determined by summing the two heat transfer resistances from the blood to the cylinder surface in a manner that was employed by Chen and Holmes [22] as well as Keller and Seiler [36]. This results in a relationship

$$\frac{1}{\mathrm{Nu}_e} = \frac{1}{\overline{\mathrm{Nu}}_D} + \frac{k_b}{k_t} \ln \sqrt{\frac{R_2}{R_1}} \tag{8.2}$$

where the first and second terms on the right-hand side of Eq. (8.2) represent the convective and conduction resistances, respectively, while the left-hand side represents the overall resistance. Tissue metabolic heating and the effects of perfusion bleed-off are ignored in this formulation. If the layer of tissue around the blood vessel is thin compared to the vessel radius then the effective Nusselt number Nu_e is equivalent to the local Nusselt number, $\overline{\mathrm{Nu}}_D$. Equation (8.1) can thus be used in this case to predict the local heat transfer coefficient. The other limiting case for this isolated vessel occurs when the tissue cylinder is much larger than the blood vessel. Chato assumes that the ratio R_2/R_1 is less than 10 and the ratio k_b/k_t is between unity and 2.5. Using the thermally fully developed flow $\overline{\mathrm{Nu}}_D$ value of 4, Chato shows that the minimum effective Nusselt number in this region is

$$\mathrm{Nu}_{e,\min} = \{\tfrac{1}{4} + 2.5 \ln\sqrt{10}\}^{-1} = 0.32 \tag{8.3}$$

Using a differential energy balance analysis, the temperature profile along the length of the blood vessel can be determined under these limiting conditions. Chato writes an energy balance equation for blood flowing at a constant velocity, U, with an effective wall convection coefficient h_e based upon the effective Nusselt number Nu_e. If axial conduction along the length of the blood vessel is neglected, the governing equation for the

mean blood temperature $T_b(x)$ is

$$\frac{dT_b}{dx} + \frac{2h_e}{\rho_b U c_b R_1}(T_b - T_0) \tag{8.4}$$

Defining a dimensionless temperature θ and axial location $\bar{x}$:

$$\theta = \frac{T_b - T_0}{T_b(0) - T_0} \quad \text{and} \quad \bar{x} = \frac{x}{2R_1} \tag{8.5}$$

where L is the length of the blood vessel, the solution to this first order differential equation is readily obtained in terms of the dimensionless parameter λ, defined by Chato as $4\,\mathrm{Nu}_e/\mathrm{Pe}$. This term depends on the x-location as Nu_e will vary with axial position in the blood vessel.

2. *Solution—Effectiveness and Thermal Equilibrium Length*

The solution

$$\theta = \exp(-\lambda \bar{x}) \tag{8.6}$$

can be used to determine the dimensionless mean blood temperature at the blood vessel exit for the two limiting cases described above by substituting either Eq. (8.1) into Eq. (8.6) in the first case, or substituting $\mathrm{Nu}_e = 0.32$ for the second case. The concept of heat transfer effectiveness, ε, is implemented according to the definition

$$\varepsilon = \frac{T_{b,\mathrm{in}} - T_{b,\mathrm{out}}}{T_{b,\mathrm{in}} - T_0} \tag{8.7}$$

where $T_{b,\mathrm{in}}$ and $T_{b,\mathrm{out}}$ represent the blood temperatures at the blood vessel inlet and outlet, respectively. The values of heat transfer effectiveness are shown in Fig. 15 for the two limiting cases of vessel–tissue heat transfer. In addition, Chato computes a thermal equilibration length, similar in concept to that defined by Chen and Holmes. Chato determines the distance from the blood vessel inlet at which the mean blood temperature is 95% thermally equilibrated, i.e., where $\theta = 0.05$. For the case with $R_2 = R_1$, the thermal equilibration length according to this definition and the solution above is $0.34R_1$, while the case with $\mathrm{Nu}_e = 0.32$, the thermal equilibration length is $4.36R_1$.

Chato uses anatomical data from a dog to relate these theoretical results to heat transfer in the circulation. For the largest vessels, the heat transfer effectiveness is small due to the large Graetz numbers in these vessels (greater than 1000). Thus there is little heat transfer between these large blood vessels and the surrounding tissue. Conversely, in the smallest vessels,

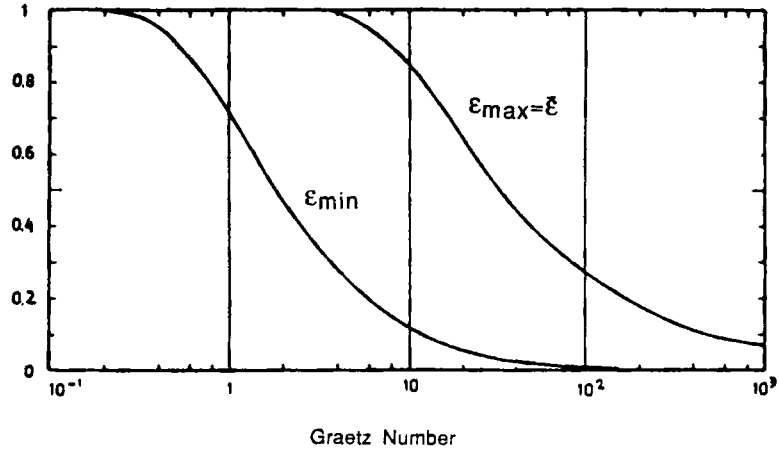

FIG. 15. Heat exchanger effectiveness of a single blood vessel based on the model of Chato. (Reproduced from [20], with permission from the American Society of Mechanical Engineers.)

i.e., in the microcirculation with vessels of diameter 300 μm or smaller, the Graetz numbers are small (less than 0.01) and there is complete thermal equilibrium between the vessels and surroundings over a very short distance, on the order of one vessel diameter. Finally, between the great vessels and the microcirculation lies a vascular region where the heat transfer effectiveness between the vessels and tissue varies from unity to zero. As observed in the analysis of Chen and Holmes, these vessels contain blood that is at a different temperature than the surroundings but becomes increasingly thermally equilibrated as the microcirculation is approached. Chato shows that the curve labeled "ε_{max}" is more representative of *in vivo* conditions since metabolic heating was neglected.

This same entrance problem was also analyzed numerically by Lagendijk [40], who determined the heat flow from the large vessel to the surrounding tissue during a simulation of hyperthermia. While Lagendijk neglected axial conduction in the blood vessel and assumed a uniform temperature profile and constant mass flow rate within the vessel, as did Chato, his results were useful in correlating large vessel blood flow with the efficacy of therapeutic hyperthermia treatments. As shown by Chato, blood inside vessels with large Peclet numbers will not be significantly heated relative to those with small Peclet numbers, thereby keeping the tissue near the vessel wall relatively cool. This is detrimental to the success of a hyperthermia treatment, which requires that all of the tissue is heated to a therapeutic level. The dimensionless temperature profile along the length of the vessel, where the tumor temperature is represented by T_0, is shown in Fig.16.

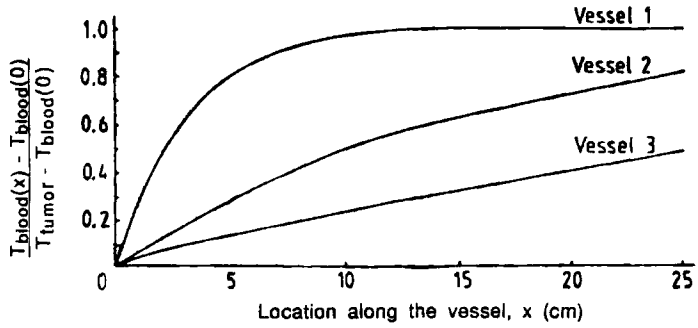

FIG. 16. Blood temperature profiles along the length of a vessel as computed by Lagendijk. The vessel characteristics are (1) $\bar{u} = 1\,\text{cm/s}$, $R = 500\,\mu\text{m}$; (2) $\bar{u} = 1.5\,\text{cm/s}$, $R = 1000\,\mu\text{m}$; (3) $\bar{u} = 2\,\text{cm/s}$, $R = 1500\,\mu\text{m}$. (Reproduced from [40], with permission.)

B. COUNTERCURRENT VESSEL PAIR

1. *Superposition Model*

The second blood vessel configuration examined by Chato was the countercurrent artery-vein pair. Using the superposition of a paired source and sink in an infinite tissue medium, the temperature difference between the isothermal walls of an artery with radius R_a and vein with radius R_v may be written as

$$T_a - T_v = \frac{Q'}{2\pi k_t} \ln[(b_a + \sqrt{b_a^2 - 1})(b_v + \sqrt{b_v^2 - 1})]$$

$$= \frac{Q'}{2\pi k_t} \ln B \tag{8.8}$$

where Q' is the heat transfer between blood vessels per unit length, b_a and b_v are vessel geometry parameters;

$$b_a = \frac{\left(\frac{s}{R_a}\right)^2 - \left(\frac{R_v}{R_a}\right)^2 + 1}{2\frac{s}{R_a}} \tag{8.9}$$

$$b_v = \frac{\left(\frac{s}{R_v}\right)^2 - \left(\frac{R_a}{R_v}\right)^2 + 1}{2\frac{s}{R_v}} \tag{8.10}$$

and s is the vessel spacing (center-to-center). In this formulation, as in the case of the isolated vessel, Chato neglects the effects of tissue heat metabolism and perfusion bleed-off on the tissue–blood heat transfer. If the paired artery and vein are assumed to have the same diameter, D, the temperature difference simplifies to

$$T_a - T_v = \frac{Q'}{\pi k_t} \ln\left[\frac{s}{D} + \sqrt{\left\{\frac{s}{D}\right\}^2 - 1}\right] \tag{8.11}$$

Chato shows that because the logarithmic term in Eq. (8.11) approaches the value ln[2b] for b values greater than 2.0, the artery-vein wall temperature difference may be written as

$$T_a - T_v = \frac{Q'}{2\pi k_t} \ln[4b_a b_v]$$

$$\cong \frac{Q'}{2\pi k_t} \ln B \tag{8.12}$$

as long as b_a and b_v are both greater than two.

Heat transfer between the paired artery and vein is quantified by Chato using the known solution for a countercurrent heat exchanger and the relationship in either Eq. (8.8) or (8.12). The overall heat transfer coefficient per unit length between the arterial and venous blood (UA') can be written in terms of three resistances in series: convective resistance between the arterial blood and arterial wall, conduction resistance from the arterial to venous wall, and convective resistance from the venous wall to the venous blood. Thus

$$\frac{1}{UA'} = \frac{1}{2\pi k_b}\left(\frac{2}{\mathrm{Nu}_a} + \frac{k_b}{k_t} \ln B + \frac{2}{\mathrm{Nu}_v}\right) \tag{8.13}$$

Chato uses the definitions of heat transfer units, N, and effectiveness, ε, to describe the heat transfer between the paired artery and vein. Defining

$$N = \frac{UA'}{m_{\min} c_b} \tag{8.14}$$

and assuming that both the artery and vein Nusselt numbers are four, the number of heat transfer units in this case is

$$N = \frac{2\pi k_b}{m_{\min} c_b\left(1 + \dfrac{k_b}{k_t} \ln B\right)} \tag{8.15}$$

The heat transfer effectiveness for this countercurrent arrangement is defined as

$$\varepsilon = \frac{m_a(T_{a,in} - T_{a,out})}{m_{min}(T_{a,in} - T_{v,in})} = \frac{m_v(T_{v,out} - T_{v,in})}{m_{min}(T_{a,in} - T_{v,in})} \tag{8.16}$$

and the relationship between N and ε for a countercurrent flow system has been shown to be

$$\varepsilon = \frac{1 - \exp[-N(1 - C)]}{1 - C\exp[-N(1 - C)]} \tag{8.17}$$

where $C = m_{min}/m_{max}$. The total heat transfer between the artery and vein is

$$Q = m_{min}c_b\varepsilon(T_{a,in} - T_{v,in}) \tag{8.18}$$

As in the bioheat transfer model of Mitchell and Myers [45], these countercurrent heat transfer equations are based on a constant mass flow rate in the artery and vein, i.e., m is independent of axial position x. This condition neglects the decrease in blood flow rate due to perfusion bleed-off from the arterial blood vessel to the surrounding tissue. In addition, while the model of Mitchell and Myers accounted for heat transfer between the blood vessels themselves and the blood vessels and the surroundings, the countercurrent model presented by Chato does not include the latter effect. The paired artery and vein are assumed to be in close enough proximity that the two vessels can be considered a "perfect" countercurrent heat exchange system. The differential energy balance equation for the arterial blood is

$$\frac{d}{dx}(T_a m_a c_b) + (UA')(T_a - T_v) - \frac{dm_a}{dz}c_b T_a = 0 \tag{8.19}$$

while the venous blood energy balance is

$$\frac{d}{dx}(T_v m_v c_b) + (UA')(T_a - T_v) - \frac{dm_a}{dz}c_b T_a = 0 \tag{8.20}$$

where (UA') is defined by Eq. (8.13). Equations (8.19) and (8.20) are similar to the energy balance equations (7.25) and (7.27) from the countercurrent model of Keller and Seiler [36], with the simplifying assumption that $(UA')_a$ and $(UA')_v$, the heat transfer coefficients between the vessels and the surrounding tissue, are both zero, and instead there is direct countercurrent heat transfer between the two vessels. Note that the axial gradient of m_a, the mass flow rate, is directly proportional to ω, the perfusion bleed-off rate utilized in the model of Keller and Seiler, which also considered the effects of perfusion bleed-off, while Mitchell and Myers did not. Chato's countercurrent model differs from that of Keller and Seiler in its neglect of heat transfer between the blood and surrounding tissue. In this manner,

only two energy balance equations must be solved simultaneously by the Chato model, as opposed to three in the model of Keller and Seiler. Finally, Chato also assumes that the overall heat transfer coefficient (UA') is not altered by the presence of bleed-off blood inside the solid tissue layer.

2. *Effect of Variable Vessel Flow Rate*

Variable mass flow rate due to perfusion bleed-off is modeled by Chato as a simple linear relationship. The arterial mass flow rate is assumed to decrease linearly with x-position, and all of the bleed-off fluid that leaves the artery at position x reenters the vein at the same position x. Thus the mass flow rates in the paired artery and vein are equal in magnitude at any x-location and in opposite directions. For the dimensionless axial position $\bar{x} = x/L$, where L is the length of the blood vessel (i.e., the axial location where $T_a = T_{a,out}$ and $T_v = T_{v,in}$), the expression for blood mass flow rate is

$$m_a = m_v = m_0(1 - E\bar{x}) \tag{8.21}$$

where E, with a value between zero and unity, is the constant of proportionality between the mass flow rate and axial position in the blood vessel. Using the linear relationship in Eq. (8.21), the coupled equations (8.19) and (8.20) can be written

$$\frac{dT_a}{d\bar{x}} + \frac{N_0}{1 - E\bar{x}} T_a = \frac{N_0}{1 - E\bar{x}} T_v \tag{8.22}$$

and

$$\frac{dT_v}{d\bar{x}} - \frac{N_0 + E}{1 - E\bar{x}} T_v = \frac{-N_0 - E}{1 - E\bar{x}} T_a \tag{8.23}$$

where N_0 is the reference number of heat transfer units based upon the inlet mass flow rate m_0 and overall heat transfer coefficient (UA'). Equations (8.22) and (8.23) are solved together with the boundary conditions $T_a(0) = T_{a,in}$ and $T_v(1) = T_{v,in}$. The solutions are

$$T_a = T_{a,in} + S_0 \frac{\bar{x}}{1 - E\bar{x}} \tag{8.24}$$

and

$$T_v = T_{v,in} + \frac{S_0}{N_0}\left(\frac{1 + N_0\bar{x}}{1 - E\bar{x}} - \frac{1 + N_0}{1 - E}\right) \tag{8.25}$$

where S_0 is defined

$$S_0 = -\left.\frac{dT_a}{d\bar{x}}\right|_{\bar{x}=0} = \frac{(T_{a,in} - T_{v,in})(1 - E)}{1/N_0 + 1} \tag{8.26}$$

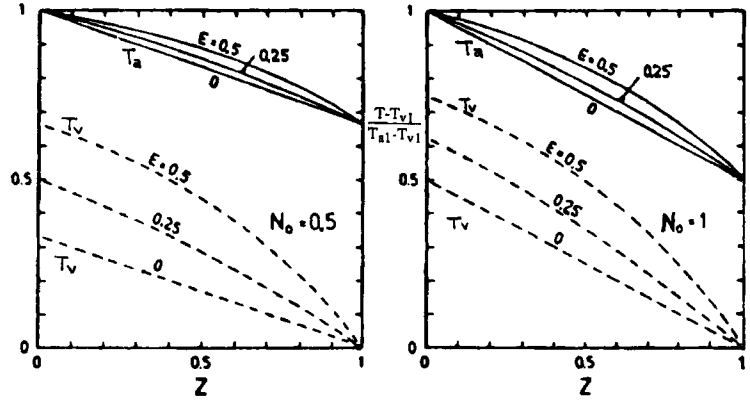

FIG. 17. Arterial and venous blood temperature profiles along the vessel axes according to the countercurrent model of Chato for a physiological range of E and N_0 values. (Reproduced from [20], with permission from the American Society of Mechanical Engineers.)

The total heat transfer between the paired artery and vein is

$$Q = m_0 c_b (T_{a,in} - T_{v,in}) \frac{E + N_0}{1 + N_0} \tag{8.27}$$

The arterial and venous temperature profiles along the length of the vessels with various E and N_0 values are shown in Fig. 17. Note that if $E = 0$, the mass flow rate is constant with x-position and the arterial and venous temperature profiles are linear and have the same slope. Using representative *in vivo* values of E, N_0, m_0, and other parameters in the bioheat model, Chato demonstrates that the effect of perfusion bleed-off is to increase the heat transfer between blood vessels relative to the case where the mass flow rates are constant on the order of 50–100%, depending on the chosen parameter values.

C. VESSEL NEAR SKIN SURFACE

1. *Superposition Model*

The third vessel geometry considered by Chato involves a blood vessel parallel to the surface of the skin. The environment, which is at a constant temperature T_0, exchanges heat convectively with the skin surface. The solution to this heat transfer problem can be found by representing the blood vessel as a line source, located at position $y = -a$ (where $y = 0$ is the location of the skin surface), superimposed on a pure conduction field. This is a form of the buried cable problem. The resulting temperature field

inside the tissue layer is

$$\frac{T - T_0}{Q'/\pi k_t} = \frac{Q'}{\pi k_t}\frac{1}{4}\ln\frac{x^2 + (y-a)^2}{x^2 + (y+a)^2} + \exp(H)\int_{-H}^{-\infty}\frac{\exp(u)\cos(\gamma x)\,du}{u} \tag{8.28}$$

where

$$H = \frac{ah}{k_t}\left(1 - \frac{y}{a}\right) \quad \text{and} \quad u = -\left(a\gamma + \frac{ah}{k_t}\right)\left(1 - \frac{y}{a}\right) \tag{8.29}$$

and h is the convective heat transfer coefficient between the environment and the tissue. The position $x = 0$ represents the inlet position of the blood vessel. At this axial position the temperature profile is

$$\frac{T(0,y) - T_0}{Q'/\pi k_t} = \frac{1}{2}\ln\frac{y-a}{y+1} + \exp(H)\int_{-H}^{-\infty}\frac{\exp(u)\,du}{u} \tag{8.30}$$

Chato shows that the integral term in Eq. (8.30) can be written as

$$\exp(H)\int_{-H}^{-\infty}\frac{\exp(u)\,du}{u} \cong \exp(H)\left(H - \frac{H^2}{4} - \ln H - 0.57716\right) \tag{8.31}$$

for H values smaller than 0.5. At the surface of the skin, $y = 0$, the function H has a value ah/k_t which is equivalent to $(R_1 h/k_t)\sqrt{b^2 - 1}$, where R_1 is the vessel radius and b is the ratio d_1/R_1. Note that d_1, the distance from the center of the vessel to the skin surface, is not the same as a, the distance from the line source to the skin surface, due to the nature of the line source superposition solution. The temperature of the blood at the blood vessel entrance is

$$\frac{T(0, R_1 - d_1) - T_0}{Q'/\pi k_t} = \frac{1}{2}\ln(b + \sqrt{b^2 - 1}) + \exp(H_b)\int_{-H_b}^{-\infty}\frac{\exp(u)\,du}{u} \tag{8.32}$$

where H_b is the constant $(R_1 h/k_t)(b - 1 + \sqrt{b^2 - 1})$. Using Eqs. (8.30) through (8.32), the surface and blood vessel temperatures at $x = 0$ depend on the dimensionless parameters $R_1 h/k_t$ (the Biot number) and b (the ratio of vessel depth from the surface to vessel radius). Typical Biot numbers range from 10^{-5} to 10^{-1}, resulting in a range of ratios of the skin and blood temperatures. Chato demonstrates that as either dimensionless parameter increases, the significance of the blood vessel as a source of heat flow towards the skin decreases and the temperature difference between the skin and the ambient air will decrease.

2. *Solution with Metabolic Heating*

Chato derives a similar model in which a uniform, constant metabolic heat generation term is included in the superposition solution. In addition, this model allows for a specified, uniform heat flux from the skin surface, G, which is due to all body heat dissipation not associated with the line source represented by the blood vessel. The governing energy balance equation is similar to that used in the surface model described above, except for the nonzero term on the right-hand side.

$$\frac{\partial^2 T}{\partial x^2} + \frac{\partial^2 T}{\partial y^2} = \frac{Q}{k_t} \tag{8.33}$$

As with the other surface heat transfer model, a convective heat transfer coefficient h is used to characterize heat transfer between the skin surface and the ambient air at temperature T_0. The superposition solution for this problem is

$$T - T_0 = \frac{Q'}{\pi k_t}\left(\frac{1}{4}\ln\left(\frac{x^2 + (y-a)^2}{x^2 + (y+a)^2}\right) + \exp(H)\int_{-H}^{-\infty}\frac{\exp(u)\cos(\gamma x)\,du}{u}\right) + \frac{G}{h} - \frac{Q}{2k_t}y^2 - \frac{G}{k_t}y \tag{8.34}$$

Note that Eq. (8.34) is similar to Eq. (8.28), with three additional terms due to the surface flux and internal heat generation. Chato notes that G is not independent of Q since at steady state the surface heat flux G must account for all heat generated by the tissue due to Q as well as the extra heat flux from the core of the body. While Q can be zero with a nonzero G, the converse is not true. G, surface flux due to tissue heating, cannot be zero if Q is nonzero. The heat flux G will be equivalent to the product QY, where Y is the thickness of the peripheral tissue layer which contains the blood vessel. In this manner, the parameter Q can be eliminated from the temperature profile in Eq. (8.34). Using this substitution, Chato shows that the skin surface temperature at $(x = 0, y = 0)$ is

$$\frac{T(0,0) - T_0}{Q'/\pi k_t} = \frac{G}{h}\frac{1}{Q'/\pi k_t} + \exp(H_s)\int_{-H_s}^{-\infty}\frac{\exp(u)\,du}{u} \tag{8.35}$$

where H_s is the value of H at $y = 0$, discussed previously. The blood temperature at $x = 0$ can be shown to be

$$\frac{T(0, R_1 - d_1) - T_0}{Q'/\pi k_t} = \frac{GR}{Q'/\pi}\left(\frac{k_t}{hR_1} + b - \frac{Rb^2}{2Y}\right) + \frac{1}{2}\ln(b + \sqrt{b^2 - 1}) + \exp(H_b)\int_{-H_b}^{-\infty}\frac{\exp(u)\,du}{u} \tag{8.36}$$

Chato estimates the parameter G by dividing the whole body metabolic heat rate by the whole body surface area under conditions of rest and intense exercise. Thus

$$G_{\min} = \frac{80\ \text{W}}{2\ \text{m}^2} = 40\ \text{W/m}^2 \tag{8.37}$$

$$G_{\max} = \frac{1000\ \text{W}}{2\ \text{m}^2} = 500\ \text{W/m}^2 \tag{8.38}$$

The parameter Q' is estimated by assuming a value for the axial temperature gradient in a peripheral blood vessel and using the relationship

$$Q' = \rho_b c_b v_b \pi R_1^2 \frac{\partial T_b}{\partial z} \tag{8.39}$$

For a capillary and main venous branch with $\partial T_b/\partial z = 0.1\ ^\circ\text{C/mm}$, the minimum and maximum values of Q', respectively, are

$$Q'_{\min} = 1.5 \times 10^{-5}\ \text{W/m} \quad \text{and} \quad Q'_{\max} = 30\ \text{W/m} \tag{8.40}$$

Using these values, Chato shows that

$$\left(\frac{GR_1}{Q'}\right)_{\max} = 133 = \bar{G}_{\max} \quad \text{and} \quad \left(\frac{GR_1}{Q'}\right)_{\max} = 0.001 = \bar{G}_{\min} \tag{8.41}$$

Chato calculates the ratio of the surface and blood temperatures at $x = 0$ under conditions of negligible heat flux from the line source that represents the blood vessel in the superposition solution. In this case

$$\frac{T(0, 0) - T_0}{T(0, R_1 - d_1) - T_0} = \frac{\dfrac{1}{\overline{Bi}}}{\dfrac{1}{\overline{Bi}} + b - \dfrac{Rb^2}{2Y}} \tag{8.42}$$

Equation (8.42) is valid if the integral terms in Eqs. (8.35) and (8.36), as well as the logarithmic term in Eq. (8.36), are small compared to the other heat transfer terms in these equations. Parametrically, this condition implies that the ratio of $\bar{G}$ to the Biot number is much greater than unity. The influence of the internal heat generation Q and the added heat from the core tissues included in parameter G on the skin surface temperature is to decrease the effect of the blood vessel line source.

Chato also demonstrates that the blood vessel has the greatest effect on skin temperature when it is of large diameter and positioned close to the skin surface. The influence of the blood on the skin temperature is independent of the linear metabolic heat generation and deep tissue heat flux terms. Evaluating Eq. (8.34) at position $y = 0$, the maximum

temperature increase on the skin surface imposed by the nearby blood vessel is

$$T_{s,\max} - T_{s,\min} = \frac{Q'}{\pi k_t} \exp(H_s) \int_{-H_s}^{-\infty} \frac{\exp(u)\cos(\gamma x)\, du}{u} \tag{8.43}$$

For a capillary with an axial temperature gradient of 0.1 °C/mm, this temperature difference is very small, on the order of 10^{-4} °C, while for a terminal vein with an axial temperature gradient of 10^{-3} °C/mm, the maximum increase in skin temperature due to the presence of the vessel is 0.33 °C.

The work of Chato was significant in isolating several of the important dimensionless parameters that influence heat transfer between vessels and tissue. The impact the Graetz, Nusselt, and Biot numbers along with countercurrent heat transfer units, heat exchanger effectiveness, and various dimensionless distances on tissue heat transfer was quantified for a variety of vascular arrangements. These vascular models can be readily adapted to model a wide range of bioheat transfer problems, especially those involved in the analysis of bioheat transfer during therapeutic hyperthermia.

At the same time that the bioheat transfer models of Chato were published, Weinbaum and Jiji presented a two phase mathematical model of vascular bioheat transfer that represented a different approach to analyzing the tissue-blood thermal interaction. A subsequent series of papers several years later expanded upon this initial formulation in order to model the effects of complex vascular structure on tissue heat transfer. Their development implements several phenomena that were previously studied by others whose work has been described above. The countercurrent phenomena first modeled by Mitchell and Myers, and later by Keller and Seiler and Chato; the thermal equilibration length characteristics of microvessels first quantified by Chen and Holmes, and later by Chato; the bulk convection term examined by Wulff and Klinger, in addition to Chen and Holmes; the three equation modeling approach of Keller and Seiler; the superposition solution in a conduction field between adjacent vessels utilized by Chato; an effective thermal conductivity due to blood flow; and finally the perfusion bleed-off originally presented by Pennes are all employed by Weinbaum and Jiji in their development of a "new" bioheat equation for perfused tissue.

IX. Weinbaum–Jiji Bioheat Transfer Models

Weinbaum and Jiji, along with several colleagues [34, 55, 56, 59–63, 70], have developed a mathematical model of bioheat transfer as an alternative to the Pennes bioheat equation. Their objections to the Pennes model

include the lack of directionality in the isotropic perfusion term and the neglect of the influence of larger blood vessels embedded in the perfused tissue on the tissue-blood heat transfer. In addition, Weinbaum and colleagues criticize the Pennes model for not accounting for the characteristic geometry of the blood vessel arrangement, i.e., the branching, tapered diameter ultrastructure of the paired, countercurrent arteries and veins as they gradually branch into arterioles, venules, and capillary beds. An early model of the heat transfer associated with this vascular architecture was presented by Weinbaum and Jiji in 1979 [59].

A. EARLY TWO PHASE FORMULATION

In this study, Weinbaum and Jiji [59] used a schematic view of the circulation, shown in Fig. 18, to analyze bioheat transfer between a paired countercurrent terminal artery and vein. Note that each artery-vein pair is

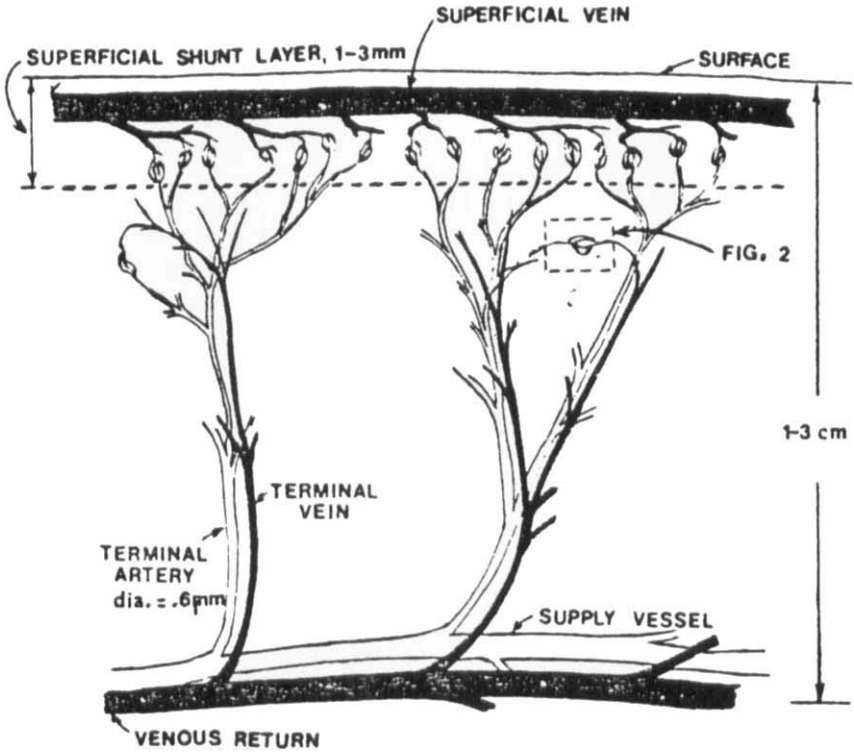

FIG. 18. Schematic view of the peripheral circulation used by Weinbaum and Jiji in 1979 [59]. (Reproduced from [59], with permission from the American Society of Mechanical Engineers.)

considered part of a periodic array of blood vessels in the tissue circulation. As blood flows along the length of the terminal artery towards the skin surface, the artery undergoes several, up to 10, generations of branching. Along with the continuous decrease in artery diameter from the deep tissue region to skin surface due to the tapered characteristics of the vessels, there is also a decrease in blood velocity due to the continuous flow of blood from the artery into capillary beds located in the plane normal to the paired artery–vein axes. Note that the circulation of blood in this plane, which Weinbaum and Jiji describe as "collateral" circulation, is not through a countercurrent system but can be considered unidirectional, from the artery to the paired vein in the radial direction. After the arterial blood passes through the capillary bed, it drains into the venous system, which is similarly tapered, and the blood velocity increases as the deep supply vein is approached due to the continuous drainage of blood from the capillary beds into the venous system.

1. *Blood Phase*

Weinbaum and Jiji argue that this vascular structure requires a mathematical model that can account for variations in vessel number density of roughly six orders of magnitude, velocity and vessel diameter variations of two orders of magnitude, and vessel Reynolds numbers that decrease by four orders of magnitude from the entrance of the flow system to the end of the vascular tree at the skin surface. The early two phase model of Weinbaum and Jiji considered an average artery and vein radius a_a and a_v, which both vary continuously in the direction normal to the skin surface, x. The periodicity of the vascular array yields a parameter l_s, which represents the distance between the paired countercurrent artery and vein and is also a function of x. Weinbaum and Jiji also define a radius of influence for each vessel pair, R, that decreases continuously from the deep tissue towards the skin surface. As shown in Fig. 19, the value of R depends on the amount of collateral circulation between the paired artery and vein.

Weinbaum and Jiji use a scaling law to describe the variation of R with x:

$$n(x)R(x)^2 = \text{constant} \tag{9.1}$$

where n is the number of arteries or veins crossing the plane normal to the vessel axes per unit area. If the function $n(x)$ is known from anatomical data, the radius of influence of the artery–vein pair can be determined. Another physical law that must be obeyed is mass conservation in the paired arteries and veins. For a constant, uniform capillary bleed-off rate g, the

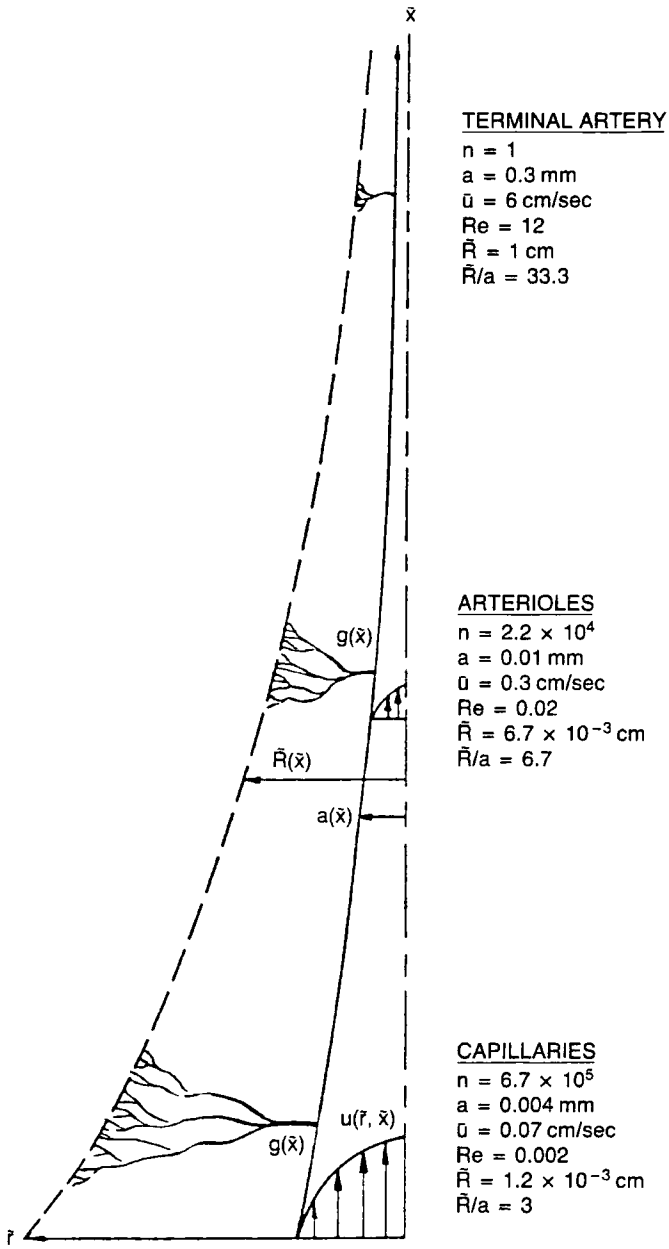

FIG. 19. Vascular parameters in the circulation as compiled from the literature [64] by Weinbaum and Jiji. (Reproduced from [59], with permission from the American Society of Mechanical Engineers.)

continuity relationship requires that

$$\frac{d}{dx}(n(x)a_a(x)^2\bar{u}_a(x)) = -2na_a g \tag{9.2}$$

$$\frac{d}{dx}(n(x)a_v(x)^2\bar{u}_v(x)) = +2na_v g \tag{9.3}$$

where $\bar{u}$ is the mean velocity in either the artery or vein and g is perfusion bleed-off (or collateral circulation rate) in volume blood per time per vessel surface area. These continuity relationships are similar to those used in the model of Keller and Seiler (see Eqs. (7.28)-(7.31)). Weinbaum and Jiji show that the energy balance equations for the artery and vein temperatures as a function of r, the radial distance from the vessel axis, are

$$\rho c_b u_a(x, r)\frac{\partial T_a(x, r)}{\partial r} = \frac{k_b}{r}\frac{\partial}{\partial r}\left(r\frac{\partial T_a(x, r)}{\partial r}\right) - \mu\left(\frac{\partial u_a}{\partial r}\right)^2 \tag{9.4}$$

$$\rho c_b u_v(x, r)\frac{\partial T_v(x, r)}{\partial r} = \frac{k_b}{r}\frac{\partial}{\partial r}\left(r\frac{\partial T_v(x, r)}{\partial r}\right) - \mu\left(\frac{\partial u_v}{\partial r}\right)^2 \tag{9.5}$$

where the second term on the right-hand sides represents the heat transfer associated with viscous dissipation in the blood vessels. Note that the algebraic sign of u_a is positive, while u_v is negative due to the countercurrent arrangement. These velocities may be assumed to have a parabolic profile inside the blood vessel since the Reynolds numbers in terminal arteries are on the order of unity or less. Thus

$$u_a(x, r) = 2\bar{u}_a(x)\left(1 - \left(\frac{r}{a_a}\right)^2\right) \tag{9.6}$$

$$u_v(x, r) = 2\bar{u}_v(x)\left(1 - \left(\frac{r}{a_v}\right)^2\right) \tag{9.7}$$

The mean velocities $\bar{u}_a$ and $\bar{u}_v$ are determined from the continuity relationships. It is important to note that neglecting fluid loss in the lymphatic system, the magnitudes of $\bar{u}_a$ and $\bar{u}_v$ are equal at any position x, but in opposite directions. This argument was also used in the model of Keller and Seiler [36]. By combining Eqs. (9.2) through (9.7), the energy balance equations for the arterial and venous blood streams are completely defined.

2. *Tissue Phase*

The second phase of Weinbaum and Jiji's two phase model involves the tissue medium that surrounds the artery-vein pair. As stated above, this earlier model of Weinbaum and Jiji proposed that collateral blood flow in

the plane normal to the artery-vein pair was unidirectional from the artery to the vein in the radial direction. In addition, these vessels are of small diameter and blood velocity so that their thermal equilibration lengths are very short. In this manner, the heat transfer characteristics of the collateral circulation can be modeled as fluid flow through a porous tissue medium, as was proposed earlier by Wulff. The form of the energy balance equation for the tissue medium is thus

$$\rho c_p v_p \nabla T = k \nabla^2 T + Q \tag{9.8}$$

where v_p is the perfusion velocity in the porous tissue medium and Q represents any heat sources in the solid tissue. Weinbaum and Jiji subdivide the tissue space into two regions which are represented by two temperatures θ_a and θ_v, as shown in Fig. 20. The energy balance equations for these two tissue regions are written based upon Eq. (9.8), where the perfusion velocity is inversely proportional to r-position in order to conserve mass in the collateral circulation:

$$c_b \frac{g a_a}{r} \frac{\partial \theta_a}{\partial r} = k_t \left(\frac{\partial^2 \theta_a}{\partial x^2} + \frac{1}{r} \frac{\partial}{\partial r} \left(r \frac{\partial \theta_a}{\partial r} \right) \right) + Q_m \tag{9.9}$$

$$-c_b \frac{g a_v}{r} \frac{\partial \theta_v}{\partial r} = k_t \left(\frac{\partial^2 \theta_v}{\partial x^2} + \frac{1}{r} \frac{\partial}{\partial r} \left(r \frac{\partial \theta_v}{\partial r} \right) \right) + Q_m \tag{9.10}$$

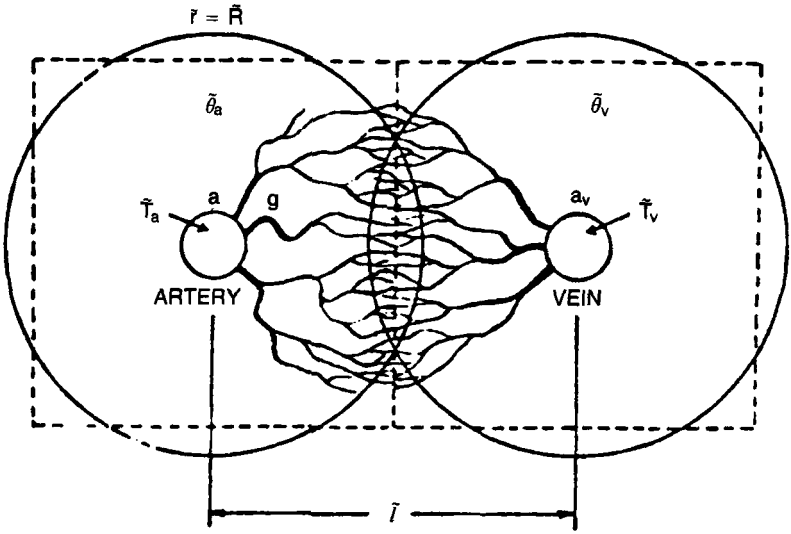

FIG. 20. Schematic view of a countercurrent vessel pair in the peripheral circulation and the collateral, or transverse, perfusion bleed-off circulation, as modeled by Weinbaum and Jiji. (Reproduced from [59], with permission from the American Society of Mechanical Engineers.)

Note that the minus sign on the left-hand side of Eq. (9.10) is necessary to account for the flow of venous blood in the terminal vein in the negative x-direction. The two tissue temperatures θ_a and θ_v proposed by Weinbaum and Jiji in this early model can be interpreted as the mean tissue temperatures within the radius of influence R from the paired countercurrent artery and vein, respectively.

3. *Skin Layer*

A model of heat transfer in the cutaneous circulation was also presented in this study. The tissue temperature in the thin skin layer was determined by considering the vascular architecture in this region. Based on anatomical observations, Weinbaum and Jiji argued that blood passes directly from arterioles to venules in the skin, as shown in Fig. 18, as part of the thermoregulatory control system. For example, under conditions of vasodilation, most of the arterial blood is directed into the superficial veins, which results in a highly perfused layer of tissue near the skin. In a later study by Weinbaum *et al.* [60], this view of the cutaneous circulation was modified based on experimental observations in the rabbit (see Section IX.B.1.c). In the 1979 study, however, Weinbaum and Jiji modeled the effect of blood flow in the skin tissue layer as one-dimensional heat transfer through a porous medium:

$$w_b(x)c_b\frac{d\theta_s}{dx} = k_t\frac{d^2\theta_s}{dx^2} \tag{9.11}$$

where w_b is the blood perfusion flux in the tissue layer beneath the skin, defined in the region $L \leq x \leq (L + \varepsilon)$. In this early study, Weinbaum and Jiji assumed the $w_b(x)$ would decrease linearly to zero from position $x = L$ to the skin surface at $x = L + \varepsilon$. Based upon continuity of flow, the value of w_b at $x = L$ was set equal to the value of $[\pi a^2 n\bar{u}]$ evaluated at $x = L$.

The coupled energy balance equations written above can be utilized to solve for blood temperatures T_a and T_v as functions of r and x, and tissue temperatures θ_a, θ_v, and θ_s as functions of r and x. A symmetry boundary condition must be enforced at $r = 0$, while a continuous temperature and heat flux is required at $r = a_a$ and $r = a_v$. In addition, the periodicity of the vascular array implies that there is no heat flux past the tissue cylinder surface at $r = R$. In terms of the axial x-direction, boundary values must be specified at $x = 0$ and $x = L + \varepsilon$, in addition to temperature and heat flux matching conditions at $x = L$. Weinbaum and Jiji did not present the results of these simulations, but illustrated the range of input parameters for their two phase model, which are shown in Fig. 19.

B. THREE LAYER MODEL OF PERIPHERAL TISSUE

1. *Physical Description*

The 1979 model by Weinbaum and Jiji represented one of the first attempts to model the effects of the circulation on tissue heat transfer on a vascular, rather than continuum basis, accounting for the complex geometry of the countercurrent artery–vein network. A more thorough investigation of this problem was presented in two companion papers published by Weinbaum, Jiji, and Lemons in 1984 [34, 60]. The first of these two papers presented the anatomical foundation for the Weinbaum–Jiji bioheat equation. In this aspect of their study, three different vascular structures were identified in rabbit limbs. Schematic views of these three layers are shown in Figs. 21 and 22. In the deep tissue layer the arteries and veins are paired, countercurrent, and are oriented oblique to the skin surface. Their number density, radii, inclination angle, center-to-center spacing, and radius of influence all vary along the length of the countercurrent network. The vessels branch as they approach the more peripheral tissue region and remain in a countercurrent arrangement for the first five

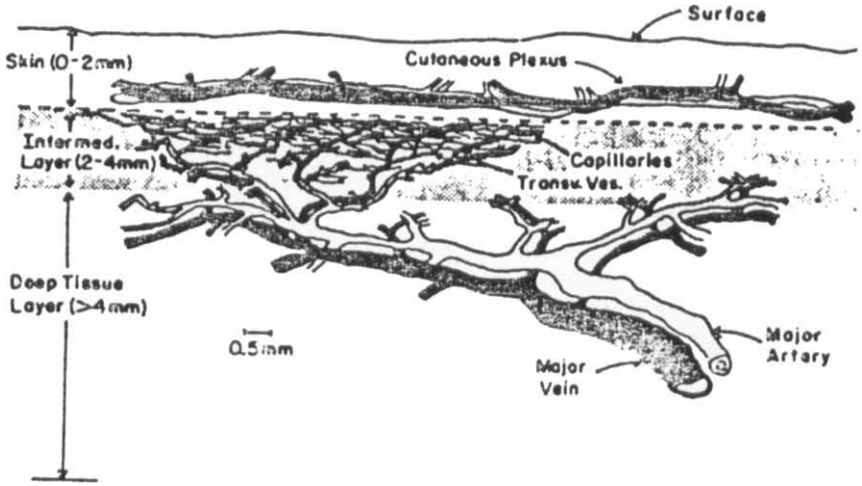

FIG. 21. A schematic view of the peripheral circulation with three tissue layers as modeled by Weinbaum *et al.* in 1984 [60]. The cutaneous layer is perfused with blood through a plexus which receives blood from vessels that are physically separate from muscle circulation (in contrast to that shown in Fig. 18). The intermediate layer contains thermally insignificant countercurrent vessels with transverse perfusion in the plane normal to the countercurrent vessel axes, as shown in Fig. 20. The deep tissue layer contains a branching network of thermally significant countercurrent blood vessels. (Reproduced from [60], with permission from the American Society of Mechanical Engineers.)

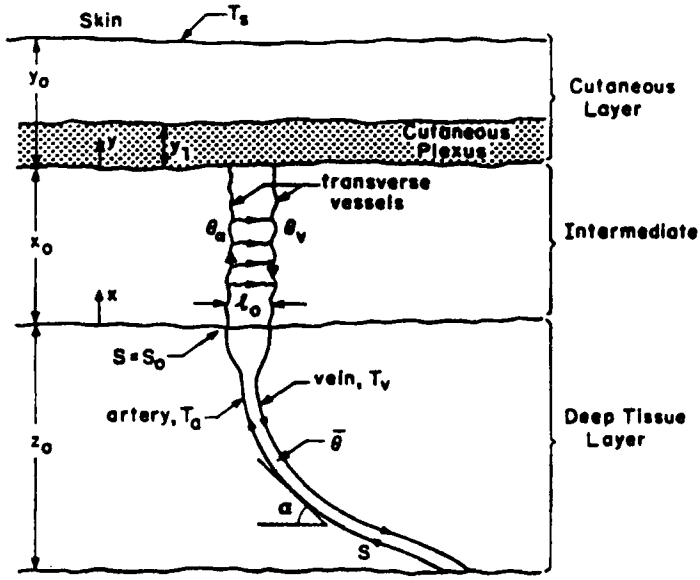

FIG. 22. A simplified view of the three layer model shown in Fig. 21.

or six branching generations. In addition to countercurrent heat transfer, there is heat exchange between the vessel pair in this layer by conduction into the tissue as well as by capillary bleed-off, since the arterial blood that perfuses the tissue via the collateral microcirculation is usually warmer than the local venous blood return temperature. As will be shown below, perfusion bleed-off has a significant effect on the artery-vein temperature difference ($T_a - T_v$) along the length of the countercurrent network. These complex effects are considered by Weinbaum and colleagues in the derivation of their bioheat equation.

As described in the initial 1979 study by Weinbaum and Jiji [59], after five or six generations of branching in the deep layer, an intermediate layer of tissue is approached, in which the vessel pairs are no longer as closely spaced as in the deep layer but rather are part of a periodic array of terminal vessels separated by a transverse, or collateral, microcirculation. This intermediate layer is discussed below after a presentation of the preliminary analysis used by Weinbaum *et al.* [60] to characterize the deep tissue layer countercurrent heat transfer.

a. *Deep Tissue Layer and Thermal Equilibration Lengths.* Based upon a thermal equilibration length model by Weinbaum *et al.* [60] that is similar to those proposed earlier by Chen and Holmes [22], as well as Chato [20], the deep tissue layer blood vessels are thermally significant; i.e., the blood

is at a temperature different than that of the surrounding tissue. Weinbaum *et al.* use a superposition technique similar to that employed by Chato [20] to model heat transfer between the paired artery and vein in the plane normal to their axes:

$$\nabla^2 T_t(x, y, z) = 0 \tag{9.12}$$

with the boundary conditions

$$T_t(x, y, z) = T_a(x) \qquad \text{along the artery surface} \tag{9.13}$$

$$T_t(x, y, z) = T_v(x) \qquad \text{along the vein surface} \tag{9.14}$$

where x is the direction normal to the skin surface and the y–z plane is the location of what Weinbaum and Jiji labeled the collateral circulation between the paired artery and vein due to perfusion bleed-off in the earlier 1979 paper [59]. The solution to this two-dimensional superposition problem is discussed in Section VIII.B.1.

This two-dimensional heat transfer solution is combined with the energy balance equations that describe heat transfer along the axes of the artery and vein (i.e., in the x-direction):

$$\rho_b c_b \pi a_a^2 u_a \frac{dT_a}{dx} = \int_0^{2\pi} k_t a_a \frac{\partial T_t(x, a_a, \gamma)}{\partial r} d\gamma \tag{9.15}$$

$$-\rho_b c_b \pi a_v^2 u_v \frac{dT_v}{dx} = \int_0^{2\pi} k_t a_v \frac{\partial T_t(x, a_v, \gamma)}{\partial r} d\gamma \tag{9.16}$$

where r is the radial position from either the center of the artery or vein. Thus the right-hand sides of Eqs. (9.15) and (9.16) represent the total heat flow into the artery and vein by conduction from the surrounding tissue. Note that a minus sign is needed in Eq. (9.16) to account for the countercurrent flow arrangement. This approach was also utilized by Chato [20] in his model of the heat transfer between parallel blood vessels described previously. In a simple preliminary formulation, Weinbaum *et al.* [60] assume that there is no net heat transfer into the tissue, and thus the system acts as a perfect countercurrent exchange system, where all of the heat lost from the artery to the tissue flows back into the vein. Under the conditions of zero perfusion bleed-off, the velocity is constant and of equal magnitude in both vessels, resulting in a constant $(T_a - T_v)$ difference along the vessel axes and a linear arterial, venous, and mean blood temperature profile $T_m \equiv ((T_a + T_v)/2)$ in the x-direction. As Weinbaum *et al.* [60] point out, these results are not to be expected *in vivo*, as they neglect the effects of variable vessel geometry in the x-direction, branching, capillary bleed-off, and heat loss to the tissue. These complicating phenomena are considered

in the derivation of the Weinbaum-Jiji bioheat transfer model described below. However, the predictions of the simple preliminary model in Eqs. (9.12)–(9.16) are convenient for defining a thermal equilibration length for a countercurrent vessel pair in the deep tissue layer.

The thermal equilibration length of the paired vessels is defined by Weinbaum *et al.* [60] as the distance required for the artery, vein, and mean blood temperatures to decrease by $[T_a(0) - T_v(0)]$, the artery–vein temperature difference at the entrance to the countercurrent network ($x = 0$). Using the solution to Eqs. (9.12) through (9.16), this length is

$$L_{eq,cc} = \frac{a}{2}\frac{k_b}{k_t}\,\mathrm{Pe}\cosh^{-1}\left(\frac{l_s}{a}\right) \tag{9.17}$$

where l_s represents the center-to-center spacing between the paired artery and vein and Pe is the flow Peclet number. According to the isolated vessel model presented by Chato [20], Chen and Holmes [22], as well as Weinbaum *et al.* in their 1984 paper [60], the thermal equilibration length of a single vessel (neglecting entrance effects) is

$$L_{eq,s} = \frac{a}{4}\mathrm{Pe}\left(\frac{3}{4} + \frac{k_b}{k_t}\ln(R/a)\right) \tag{9.18}$$

Using anatomical data from vascular casts in rabbit thigh muscle to evaluate the parameters in Eqs. (9.17) and (9.18), Weinbaum *et al.* calculate that under resting blood flow conditions all paired vessels larger than 50 μm in diameter have thermal equilibration lengths approximately three times shorter than the thermal equilibration length of the same single, isolated vessel. They conclude that countercurrent heat transfer is the dominant mechanism for blood–tissue interaction in this deep region that contains thermally significant countercurrent vessel pairs. The deep tissue layer ends at the x-location where the countercurrent vessels are no longer thermally significant. Under resting blood flow conditions, this corresponds to the 50-μm vessels in the fifth or sixth generation of branching.

The thermal equilibration analysis presented above is also used by Weinbaum *et al.* [60] to illustrate that vessels smaller than 50 μm are completely thermally equilibrated with the surroundings and thus a single temperature can be used to describe the blood and tissue that surrounds the blood vessel. Weinbaum *et al.* conclude that the basic assumption of the Pennes bioheat equation perfusion heat source term is physically impossible because arterial blood is thermally equilibrated with the surrounding tissue before it reaches the capillary beds. The temperature difference $(T_t - T_0)$ that appears in the Pennes perfusion heat source term is therefore zero due to this phenomenon of arterial precooling.

b. *Intermediate Tissue Layer.* In the intermediate tissue layer, the paired arterial and venous blood temperatures are slightly different, less than 0.2 °C based upon experimental measurements [41], due to their relatively larger spacing on the order of 0.5–1 mm. However, the vessels themselves are small enough so that there is nearly complete thermal equilibration between the blood and surrounding tissue near the vessel wall. As shown in Fig. 20, the tissue temperature associated with tissue near the artery, θ_a, will be different than the tissue temperature associated with tissue near the vein, θ_v. While the blood temperatures T_a and T_v will be equal to these two tissue temperatures θ_a and θ_v, respectively, there will be some heat transfer in the plane containing the transverse bleed-off vessels in the intermediate tissue layer. The two phase porous medium model presented in the 1979 study by Weinbaum and Jiji [59] can be applied in this region, since the unidirectional capillary bleed-off between periodically spaced vessel pairs acts to convect heat in the direction normal to the countercurrent vessel axes. Weinbaum *et al.* [60] describe the boundary region between the deep and intermediate tissue layers as a plane where small lateral (normal to the countercurrent vessel axes) temperature gradients coexist with large gradients normal to the skin surface. The intermediate tissue layer can be interpreted as a thin region, several millimeters thick, where temperature gradients due to the presence of thermally significant vessels in the deep and cutaneous layers are attenuated.

c. *Cutaneous Layer.* The outermost cutaneous layer is dominated by conduction heat transfer normal to the skin surface. Based upon experimental observations, Weinbaum *et al.* [60] report that arterial blood is supplied to the skin via a circulatory system that is physically separate from the muscle tissue blood supply. This is in contrast to the earlier model [59], which presumed that arterial blood was supplied to the skin via the last generation of branching in the muscle layer and that venous blood was drained from the skin either through the venous network in the muscle layer or through the superficial venous plexus. In the 1984 study, Weinbaum *et al.* [60] observe that arterial blood is supplied to the skin layer from major arteries that branch from the deep arteries and rise up to the skin surface where they bend and run parallel to the skin surface. Only a small fraction of the arterial feed blood is actually directed towards the cutaneous layer cells to provide nutrients and oxygen to the cells. Most of the blood in these thermally significant vessels flows directly from the large artery to the large vein through 20–40 μm anastomoses in the cutaneous plexus. Based upon this vascular structure, Weinbaum *et al.* [60] model the effect of blood flow in the cutaneous plexus as a distributed volumetric heat source. They note that the arterial supply vessels are quite large (200–500 μm in diameter)

and therefore have long thermal equilibration lengths. Under these conditions, the arterial blood will arrive in the cutaneous layer at a temperature that is different than the surroundings. Weinbaum *et al.* [60] propose that this effect can be mathematically modeled as a uniformly distributed heat source, similar in form to the Pennes perfusion heat source term, in the lower portion of the cutaneous layer. In the upper part of the cutaneous layer there is a small blood vessel plexus which perfuses blood to the skin cells via 20–40 μm vessels. Based on the arguments presented above, blood flow in this region is neglected, and Weinbaum *et al.* [60] model this most superficial portion of the skin layer as a pure conduction layer.

2. *Governing Equations*

a. *Deep Tissue Layer.* A mathematical description of each of these three tissue layers was presented by Jiji *et al.* [34] in the second part of their two-part paper. The governing equations for the deep tissue layer were derived by considering the vessel geometry and capillary bleed-off phenomena on a continuous basis. The continuity relationship that provides for mass conservation in the paired blood vessels is

$$\frac{d}{ds}(na^2\bar{u}) = -2nag \tag{9.19}$$

where s is the location along the length of the countercurrent network (different than x in the earlier 1979 study due to the inclination angle of the vessel pairs made with the axis normal to the skin surface), $\bar{u}$ is the bulk mean velocity in the blood vessel, and g is the perfusion bleed-off per unit vessel surface area. Note that Eq. (9.19) is similar to Eqs. (9.2) and (9.3). In their 1984 formulation, Jiji *et al.* [34] assume that the paired vessels are the same size and that there is no fluid loss to the lymphatic circulation. Under these conditions, the velocities $\bar{u}_a$ and $\bar{u}_v$ that appear in Eqs. (9.2) and (9.3) are identical in magnitude but opposite in direction due to the countercurrent flow arrangement.

As first applied by Keller and Seiler [36], three energy balance equations are used to describe the arterial, venous, and tissue temperatures in the deep tissue layer where the vessels are thermally significant. The governing equations for the countercurrent arterial and venous blood elements in the deep tissue layer are

$$\rho_b c_b \frac{d}{ds}(\pi a^2 \bar{u} T_a) = -q_a - \rho_b c_b [2\pi ag] T_a \tag{9.20}$$

$$\rho_b c_b \frac{d}{ds}(\pi a^2 \bar{u} T_v) = -q_v - \rho_b c_b [2\pi ag] T_v \tag{9.21}$$

where q_a is the heat loss from the artery by conduction through its wall per unit length and q_v is the heat gained by conduction through the vein wall into the vein per unit length. Note that the arterial blood flows in the positive s-direction, while the venous blood flows in the negative s-direction. The second terms on the right-hand sides of Eqs. (9.20) and (9.21) represent heat loss from the artery and heat gained by the vein due to capillary perfusion, respectively. The blood temperatures T_a and T_v are bulk mean temperatures inside the blood vessels. Note that Eqs. (9.20) and (9.21) are similar to the artery and vein energy balance equations in the models of Chato [20] and Keller and Seiler [36]. Using the continuity equation, the terms associated with heat loss from the arterial blood due to perfusion bleed-off and the heat gained by the venous blood from perfusion drainage can be eliminated, yielding the two energy balance equations

$$\rho_b c_b \pi a^2 \bar{u} \frac{dT_a}{ds} = -q_a \tag{9.22}$$

$$\rho_b c_b \pi a^2 \bar{u} \frac{dT_v}{ds} = -q_v \tag{9.23}$$

A third equation is required to solve for the temperature of the tissue that surrounds the countercurrent artery–vein pair. Assuming that each vessel pair is part of a periodic array of vessels at the location s, there will be no heat flow into the tissue cylinder of radius $R(s)$ (the radius of influence of the countercurrent vessel pair) that surrounds each vessel pair. In addition, there will be some energy deposited into the tissue due to the perfusion bleed-off as well as the conductive heat loss from the paired artery and vein. The corresponding tissue energy balance equation is

$$-(q_a - q_v) - \rho_b c_b 2\pi a g (T_a - T_v) = \frac{d}{ds}\left(k_t \pi R^2 \frac{dT_t}{ds}\right) \tag{9.24}$$

where the first term on the left-hand side is the net heat transfer by conduction from the tissue into the paired vessels, the second term on the left-hand side is the net heat deposited in the tissue due to perfusion bleed-off, and the last term is the net conduction gain in a tissue element of differential length ds. Note that q_v and q_a are not equal for an "imperfect" countercurrent heat exchange system, and T_a and T_v are not equal in the deep tissue layer proposed by Jili *et al.* [34] to describe heat transfer in the thermally significant vessels.

Combining Eqs. (9.22)–(9.24), the tissue energy balance equation is

$$\rho_c c_b a^2 \bar{u} \frac{d}{ds}(T_a - T_v) = 2\rho_b c_b a g (T_a - T_v) + \frac{d}{ds}\left(k_t R^2 \frac{dT_t}{ds}\right) \tag{9.25}$$

Equation (9.25) is a single equation with three unknown temperatures T_a, T_v, and T_t. In order to solve this equation, some approximations must be made. Based upon temperature measurements in the deep muscle layer of a rabbit reported by Weinbaum *et al.* [60], the tissue temperature T_t can be approximated by the mean value of the artery and vein temperatures, $(T_a + T_v)/2$. As shown in Fig. 23, the typical temperature profile in the vicinity of a countercurrent vessel pair is described by Jili *et al.* [34] as a perturbation on a mean tissue temperature profile over the length scale l_s, which is small relative to the macroscopic temperature measurement length scale. The tissue equation can thus be written

$$\rho_b c_b a^2 \bar{u} \frac{d}{ds}(T_a - T_v) = 2\rho_b c_b a g (T_a - T_v) + \frac{k_t}{2} \frac{d}{ds}\left(R^2 \frac{d}{ds}(T_a + T_v)\right) \tag{9.26}$$

Adding Eqs. (9.22) and (9.23) yields

$$q_a + q_v = -\rho_b c_b \pi a^2 \bar{u} \frac{d}{ds}(T_a + T_v) \tag{9.27}$$

At this point in their derivation, Jiji *et al.* [34] argue that the local tissue temperature gradient is large relative to the undisturbed temperature gradient and thus heat conduction normal to the countercurrent vessel pair is more significant than heat conduction in the tissue along the direction of the vessel axes. Based on this argument, the magnitudes of q_a and q_v are much larger than the difference $(q_a - q_v)$ and the value of $(q_a + q_v)$ can be approximated by the two-dimensional superposition of a line sink and source in a pure conduction field. This approach to solving the conduction

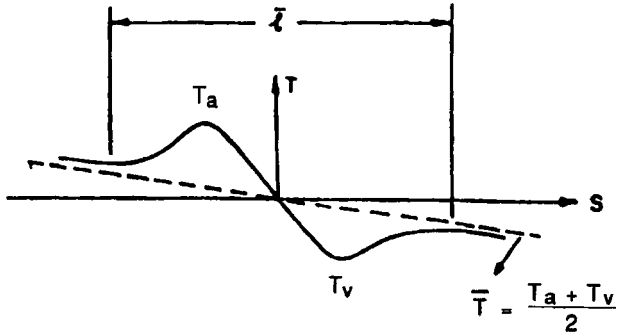

FIG. 23. The typical tissue temperature profile measured near a countercurrent vessel pair as measured in the rabbit thigh [60]. This observation served as a physical justification for the original form of the closure condition of the Weinbaum-Jiji bioheat equation. (Reproduced from [34], with permission from the American Society of Mechanical Engineers.)

problem between parallel vessels was described earlier in the presentation of Chato's bioheat transfer model [20]. Using this method, Jiji *et al.* [34] solve for the sum

$$(q_a + q_v) \cong 2q_0 \tag{9.28}$$

where

$$q_0 = \frac{2\pi k_t (T_a - T_v)}{\cosh^{-1}(l_s^2/2a^2 - 1)} \tag{9.29}$$

from the superposition solution. Substituting Eqs. (9.28) and (9.29) into Eq. (9.27)

$$-\rho_b c_b a^2 \bar{u} \frac{d}{ds}(T_a + T_v) = \frac{4k_t (T_a - T_v)}{\cosh^{-1}(l_s^2/2a^2 - 1)} \tag{9.30}$$

By applying the two-dimensional superposition solution, Jiji *et al.* [34] were able to eliminate the tissue temperature as an unknown in the system of energy balance equations and therefore Eqs. (9.30) and (9.26) can be used to solve for T_a and T_v as a function of s-position. The first order ordinary differential equations are solved with the two boundary conditions

$$T_a(0) = T_{a0} \tag{9.31}$$

$$T_v(0) = T_{vr} \tag{9.32}$$

where T_{vr} is the unknown venous return temperature at the entrance of the countercurrent network ($s = 0$), which is determined by a global heat balance across the three layer tissue model, described in Section IX.B.3.

Based upon a scaling law first proposed in the 1979 study, Jiji *et al.* [34] assume that the product nR^2 is constant with s-position. Since $n(0)$ is unity, the value of $R(s)$ can be determined based on $n(s)$ and $R(0)$. Jiji *et al.* [34] nondimensionalize the two governing equations in the deep tissue layer based on S_0, the total length of the countercurrent network in the deep layer, and Pe*(s), the flow Peclet number in the vessel at each s-location:

$$\tilde{a}\,\mathrm{Pe}^* \frac{d}{d\tilde{s}}(\tilde{T}_a - \tilde{T}_v) = 4\nu(\tilde{T}_a - \tilde{T}_v) + \frac{d}{d\tilde{s}}\left(\tilde{a}^2 \tilde{R}^2 \frac{d}{d\tilde{s}}(\tilde{T}_a + \tilde{T}_v)\right) \tag{9.33}$$

$$\tilde{a}\,\mathrm{Pe}^* \frac{d}{d\tilde{s}}(\tilde{T}_a + \tilde{T}_v) = \frac{-8(\tilde{T}_a - \tilde{T}_v)}{\cosh^{-1}(\tilde{l}_s^2/2 - 1)} \tag{9.34}$$

where the dimensionless distances $\tilde{a}$, $\tilde{s}$, $\tilde{l}_s$, and $\tilde{R}$ are the parameters a, s, l_s, and R normalized by the distance S_0, respectively. The dimensionless temperatures $\tilde{T}_a$ and $\tilde{T}_v$ are ratios of the difference between T_a and T_v and T_s (the skin surface temperature) relative to the difference $(T_0 - T_s)$, respectively. The dimensionless perfusion parameter ν is equal to $\rho_b c_b a g / k_t$ and Pe* is the flow Peclet number times the ratio k_b/k_t. Note that Pe*

varies with s-position along the deep layer vascular network. The dimensionless boundary conditions are $\tilde{T}_a(0) = 1$ and $\tilde{T}_v(0) = \tilde{T}_r$, the dimensionless venous return temperature at the entrance of the countercurrent network.

b. *Intermediate Tissue Layer*

The mathematical model in the intermediate tissue layer is based on the schematic view of the transverse terminal vessels shown in Fig. 22. The spacing l_0 between the paired artery and vein in this layer is assumed to be constant with s-position and equal to the diameter of the tissue cylinder that surrounds the artery-vein pair at position $s = S_0$, the location of the deep-intermediate tissue layer boundary. Applying the condition that the product nR^2 is constant with s-position, the length l_0, which is the diameter of influence around either the artery or the paired vein in this intermediate layer, is

$$l_0 = \sqrt{\frac{2n(0)}{n(S_0)}} R(0) \tag{9.35}$$

since the combined area of influence of the artery and vein, $2((\pi/4)l_0^2)$, must be equal to the cross-sectional area of the tissue cylinder surrounding the deep layer vessel pair at the layer interface, $\pi r(S_0)^2$.

Based upon the physical intepretation of the intermediate transverse bleed-off vessels that connect the paired artery and vein as unidirectional conduits in a porous tissue medium, the two phase model developed in the 1979 study by Weinbaum and Jiji is applied to describe the heat transfer in the intermediate layer. Equations (9.9) and (9.10) are nondimensionalized using $\tilde{x} = x/x_0$, where x_0 is the thickness of the intermediate layer, $\tilde{r} = 2r/l_0$, and $\tilde{\theta}_a$ and $\tilde{\theta}_v$ are the dimensionless temperatures of the tissue surrounding the paired artery and vein in this layer and are defined in the same manner as $\tilde{T}_a$ and $\tilde{T}_v$ in the deep tissue layer. The radial position r indicates the distance from the axis of either the artery or the vein, depending on the equation. The dimensioness forms of Eqs. (9.9) and (9.10) are

$$\beta^2 \frac{\partial^2 \tilde{\theta}_a}{\partial \tilde{x}^2} + \frac{\partial^2 \tilde{\theta}_a}{\partial \tilde{r}^2} + (1 - \nu)\frac{1}{\tilde{r}} \frac{\partial \tilde{\theta}_a}{\partial \tilde{r}} = -\lambda \tag{9.36}$$

$$\beta^2 \frac{\partial^2 \tilde{\theta}_v}{\partial \tilde{x}^2} + \frac{\partial^2 \tilde{\theta}_v}{\partial \tilde{r}^2} + (1 + \nu)\frac{1}{\tilde{r}} \frac{\partial \tilde{\theta}_v}{\partial \tilde{r}} = -\lambda \tag{9.37}$$

where β is the ratio $l_0/2x_0$ and λ is the dimensionless metabolic heat source $Q_m l_0^2/(4k_t(T_0 - T_s))$. Equations (9.36) and (9.37) are subject to the

following boundary conditions:

$$\frac{\partial \tilde{\theta}_a}{\partial \tilde{r}} = \frac{\partial \tilde{\theta}_v}{\partial \tilde{r}} = 0, \qquad \text{at } \tilde{r} = 0 \tag{9.38}$$

$$\tilde{\theta}_a = F(\tilde{r}) \quad \text{and} \quad \tilde{\theta}_v = G(\tilde{r}), \qquad \text{at } \tilde{x} = 0 \tag{9.39}$$

$$\tilde{\theta}_a = \tilde{\theta}_v = \tilde{\phi}_0, \qquad \text{at } \tilde{x} = 1 \tag{9.40}$$

$$\tilde{\theta}_a = \tilde{\theta}_v, \qquad \text{at } \tilde{r} = 1 \tag{9.41}$$

$$\frac{\partial \tilde{\theta}_a}{\partial \tilde{r}} = \frac{\partial \tilde{\theta}_v}{\partial \tilde{r}}, \qquad \text{at } \tilde{r} = 1 \tag{9.42}$$

The first boundary condition accounts for symmetry inside the artery and vein, the second and third boundary conditions describe the temperatures at the upper and lower boundary of the intermediate layer, while the last two boundary conditions are needed to match the temperature and heat flux at the boundary between the two tissue cylinders that surround the artery and vein. As with the venous return temperature T_{r0} in the deep tissue layer, the functions $F(\tilde{r})$, $G(\tilde{r})$, and $\tilde{\phi}_0$ are unknown and are determined by matching solutions with the other two layers of this three-layer model.

c. *Cutaneous Layer.* Based on the physical description of the cutaneous layer, this superficial region is divided into two sections, an inner layer where the large cutaneous vessels are located, and an outer layer where the thermally insignificant bleed-off vessels supply blood to the skin cells. In the inner region, the effect of blood flow in the cutaneous plexus is modeled by Jiji *et al.* [34] as an isotropic heat source. Arterial blood arrives in this region at a temperature ϕ_b which is between T_0, the temperature of arterial blood at the entrance to the deep tissue layer countercurrent network, and $\phi_1(y)$, the local tissue temperature in the inner region of the cutaneous layer, due to heat transfer with surrounding tissue along the route to the surface layer. As blood flows through the small (20–40 μm) anastomoses that connect the large superficial artery and vein, there is complete thermal equilibration between the arterial blood and the surrounding tissue, based upon the very short thermal equilibration lengths associated with these small vessels. In this case, blood perfusion can be modeled by a perfusion heat source that is similar in form to the Pennes perfusion term

$$Q_c = 2\pi \rho_b c_b a_c n_c g_c (\phi_b - \phi_1) \tag{9.43}$$

where a_c, n_c, and g_c are the radius, number density, and perfusion bleed-off rate associated with the small bleed-off vessels in this region, respectively. Jiji *et al.* [34] nondimensionalize the distance from the intermediate layer interface y by the thickness of the cutaneous layer y_0. As before, the

temperatures $\phi_1(y)$ and ϕ_b are normalized by the ratio of their difference with temperature T_s relative to the maximum temperature difference across the three tissue layers, $T_0 - T_s$. The dimensionless energy balance equation in the inner region of the cutaneous layer is

$$\frac{d^2\tilde{\phi}_1}{d\tilde{y}^2} + W_b^2(\tilde{\phi}_b - \tilde{\phi}_1) = 0, \qquad 0 < \tilde{y} < \tilde{y}_1 \tag{9.44}$$

where W_b^2 is a dimensionless cutaneous perfusion parameter

$$2\pi\rho_b c_b a_c n_c g_c y_0^2/k_c$$

and y_1 is the thickness of the inner region of the cutaneous tissue layer. Jiji *et al.* [34] point out that the governing equation for heat transfer in this region has exactly the same form as the Pennes bioheat equation, with the temperature $\tilde{\phi}_b$ and perfusion rate W_b analogous to the temperature T_0 and perfusion rate ω in the Pennes equation, respectively.

The outer region of the cutaneous layer is simply a one-dimensional conduction layer so that

$$\frac{d^2\tilde{\phi}_2}{d\tilde{y}^2} = 0, \qquad \tilde{y}_1 < \tilde{y} < 1 \tag{9.45}$$

Note that the governing equations in both regions of the cutaneous layer neglect any metabolic heating in the tissue. The two equations are subject to the boundary conditions

$$\tilde{\phi}_1(0) = \tilde{\phi}_0 \tag{9.46}$$

$$\int_0^1 \frac{\partial\tilde{\theta}_a(\tilde{r}, 1)}{\partial\tilde{x}}\tilde{r}\,d\tilde{r} + \int_0^1 \frac{\partial\tilde{\theta}_v(\tilde{r}, 1)}{\partial\tilde{x}}\tilde{r}\,d\tilde{r} = \frac{x_0}{y_0}\frac{\partial\tilde{\phi}_1(0)}{\partial\tilde{y}} \tag{9.47}$$

$$\tilde{\phi}_1 = \tilde{\phi}_2, \qquad \text{at } \tilde{y} = \tilde{y}_1 \tag{9.48}$$

$$\frac{\partial\tilde{\phi}_1}{\partial\tilde{y}} = \frac{\partial\tilde{\phi}_2}{\partial\tilde{y}}, \qquad \text{at } \tilde{y} = \tilde{y}_1 \tag{9.49}$$

$$\tilde{\phi}_2(1) = 0 \tag{9.50}$$

The first two boundary conditions enforce a continuous temperature and heat flux across the interface between the intermediate and cutaneous layers, while the third and fourth boundary conditions similarly satisfy continuity relationships at the interface between the inner and outer cutaneous regions. The fifth boundary condition is a result of the nondimensionalization of the temperatures based on the skin surface temperature T_s.

3. *Analytical Solution*

The solution to this three layer tissue model involves the determination of $\tilde{T}_a$, $\tilde{T}_v$, $\tilde{\theta}_a$, $\tilde{\theta}_v$, $\tilde{\phi}_1$, and $\tilde{\phi}_2$ as functions of position along the vascular

network. In the deep tissue layer, the solution for the local temperature difference is

$$\tilde{T}_a - \tilde{T}_v = (1 - \tilde{T}_r)\{\exp[I_1(\tilde{s}) - I_2(\tilde{s})]\} \tag{9.51}$$

where the functions I_1 and I_2 are the integral functions

$$I_1 = \int_0^{\tilde{s}} \frac{\nu \, d\tilde{s}}{\dfrac{8\tilde{a}\tilde{R}^2}{\text{Pe}^* \cosh^{-1}(\tilde{l}_s^2/2 - 1)} + \tilde{a}\,\text{Pe}^*} \tag{9.52}$$

$$I_2 = \int_0^{\tilde{s}} \frac{\dfrac{d}{d\tilde{s}}\left(\dfrac{a\tilde{R}^2/S_0}{\text{Pe}^* \cosh^{-1}(\tilde{l}_s^2/2 - 1)}\right) d\tilde{s}}{\dfrac{\tilde{a}\tilde{R}^2}{\text{Pe}^* \cosh^{-1}(\tilde{l}_s^2/2 - 1)} + \dfrac{a\,\text{Pe}^*}{8}} \tag{9.53}$$

and $\tilde{T}_r$ is the unknown venous return temperature in the deep tissue layer, which is determined using the global energy balance requirement described below. The function I_1 represents heat transfer due to capillary bleed-off from the warm artery to the surrounding tissue. Since capillary bleed-off increases tissue temperature near the artery and decreases tissue temperature near the vein, the net effect of function I_1 is to increase the deep tissue countercurrent artery-vein temperature difference. The I_2 function is associated with the direct conduction between the vessels and surrounding tissue and is related to the local geometry of the countercurrent pair. As shown in Eq. (9.51), this integral term acts to decrease the local artery-vein temperature difference. A third integral function is derived by Jiji *et al.* to describe the mean blood temperature $((\tilde{T}_a + \tilde{T}_v)/2)$:

$$I_3 = \int_0^{\tilde{s}} \frac{8 \exp[I_1 - I_2]\, d\tilde{s}}{\tilde{a}\,\text{Pe}^* \cosh^{-1}(\tilde{l}_s^2/2 - 1)} \tag{9.54}$$

where

$$I_3 = 1 - \frac{\tilde{T}_a + \tilde{T}_v}{1 + \tilde{T}_r} \tag{9.55}$$

The blood temperatures $\tilde{\theta}_a$ and $\tilde{\theta}_v$ in the intermediate tissue layer are solved by a superposition method. The solution is decomposed into homogeneous and particular parts. Two sets of homogeneous solutions must be utilized for both $\tilde{\theta}_a$ and $\tilde{\theta}_v$ in order to yield a continuous temperature and heat flux at $\tilde{r} = 1$, the boundary between the two adjacent tissue cylinders:

$$\tilde{\theta}_a = \tilde{\theta}_{a1} + \tilde{\theta}_{a2} - \frac{\lambda \tilde{x}^2}{2\beta} \tag{9.56}$$

$$\tilde{\theta}_v = \tilde{\theta}_{v1} + \tilde{\theta}_{v2} - \frac{\lambda \tilde{x}^2}{2\beta} \tag{9.57}$$

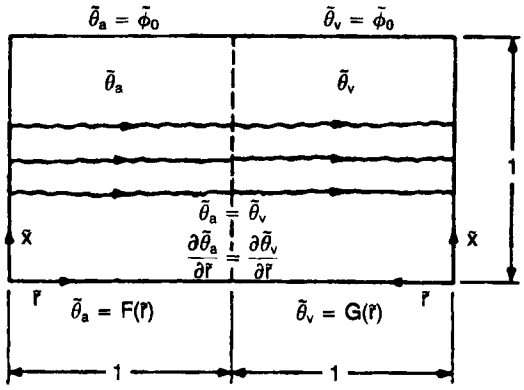

FIG. 24. The boundary value problem for the intermediate tissue layer. (Reproduced from [34], with permission from the American Society of Mechanical Engineers.)

where the first two terms on the right-hand sides of Eqs. (9.56) and (9.57) are the homogeneous solutions, while the last terms are the particular solutions associated with metabolic heating in the tissue. The superposition problem, with all necessary temperature and heat flux boundary conditions, is shown schematically in Fig. 24.

Jiji *et al.* [34] obtain the solution to this boundary value problem by assuming that ν, the perfusion term, is spatially uniform. Under these conditions, the solution to the superposition problem is

$$\tilde{\theta}_{a1} = \sum_{n=1}^{\infty} A_n \tilde{r}^{-\nu/2} I_{-\nu/2}(\gamma_n \tilde{r}) \sin \frac{\gamma_n \tilde{x}}{\beta} \tag{9.58}$$

$$\tilde{\theta}_{a2} = \sum_{k=1}^{\infty} B_k \tilde{r}^{\nu/2} J_{-\nu/2}(\sigma_k \tilde{r}) \left(\cosh \frac{\sigma_k \tilde{x}}{\beta} - \cosh \frac{\sigma_k}{\beta} \sinh \frac{\sigma_k \tilde{x}}{\beta} \right) + b_0 + b_1 \tilde{x} \tag{9.59}$$

$$\tilde{\theta}_{v1} = \sum_{n=1}^{\infty} A_n \tilde{r}^{-\nu/2} \frac{I_{1-\nu/2}(\gamma_n)}{I_{1+\nu/2}(\gamma_n)} I_{\nu/2}(\gamma_n \tilde{r}) \sin \frac{\gamma_n \tilde{x}}{\beta} \tag{9.60}$$

$$\tilde{\theta}_{v2} = \sum_{i=1}^{\infty} C_i \tilde{r}^{-\nu/2} J_{\nu/2}(\Gamma_i \tilde{r}) \left(\cosh \frac{\Gamma_i \tilde{x}}{\beta} - \coth \frac{\Gamma_i}{\beta} \sinh \frac{\Gamma_i \tilde{x}}{\beta} \right) + c_0 + c_1 \tilde{x} \tag{9.61}$$

where the eigenvalues are

$$\gamma_n = n\pi\beta, \qquad n = 1, 2, 3, \ldots \tag{9.62}$$

$$J_{1-\nu/2}(\sigma_k) = 0 \tag{9.63}$$

$$J_{1+\nu/2}(\Gamma_i) = 0 \tag{9.64}$$

The coefficients A_n, B_k, C_i, b_0, b_1, c_0, and c_1 are found via matching conditions at the boundaries. The difference between functions $g(\tilde{x})$ and $f(\tilde{x})$, the artery-vein temperature difference at position $\tilde{r} = 1$, is evaluated using the solutions above for the differences $\tilde{\theta}_{a1} - \tilde{\theta}_{v1}$ and $\tilde{\theta}_{a2} - \tilde{\theta}_{v2}$. Matching conditions at the boundary between the intermediate and deep tissue layers are used to evaluate the functions $F(\tilde{r})$ and $G(\tilde{r})$ in Fig. 24. Jiji *et al.* [34] assume that these two functions are linear and that their value at $\tilde{r} = 1$ is equal to the mean of the arterial and venous blood temperatures at $s = S_0$. Thus

$$F(\tilde{r}) = \tilde{T}_a(1) - \tfrac{1}{2}[\tilde{T}_a(1) - \tilde{T}_v(1)]\tilde{r} \tag{9.65}$$

$$G(\tilde{r}) = \tilde{T}_v(1) + \tfrac{1}{2}[\tilde{T}_a(1) - \tilde{T}_v(1)]\tilde{r} \tag{9.66}$$

where the boundary values $\tilde{T}_a(1)$ and $\tilde{T}_v(1)$ are evaluated using the artery and vein temperature solutions in the deep tissue layer shown previously.

The tissue temperature profiles in the two cutaneous layers are found by integrating Eqs. (9.44) and (9.45) twice with respect to spatial coordinate $\tilde{y}$, respectively, to yield

$$\tilde{\phi}_1 = C_1 \sinh W_b\tilde{y} + C_2 \cosh W_b\tilde{y} + \tilde{\phi}_b \tag{9.67}$$

$$\tilde{\phi}_2 = C_3\tilde{y} + C_4 \tag{9.68}$$

Note that the shape of the temperature profile in the inner cutaneous layer is a Pennes-like hyperbolic function of the blood perfusion rate-spatial location product. Temperature and heat flux matching conditions at the intermediate-inner cutaneous and inner-outer cutaneous tissue boundaries are utilized to evaluate the four integration constants in Eqns. (9.67) and (9.68).

In the determination of these integration constants, the parameter $\tilde{\phi}_0$, the temperature at the intermediate-inner cutaneous tissue interface, is introduced into the solution (see Eq. (9.46)). The complete solution to the three layer model thus contains two unknown temperatures $\tilde{\phi}_0$ and $\tilde{T}_r$, the temperature of the venous blood at the position $s = 0$ in the deep tissue layer. The flux continuity condition in Eq. (9.47) and a global energy balance are subsequently used by Jiji *et al.* [34] to relate $\tilde{\phi}_0$ to $\tilde{T}_r$. The global heat balance across the entire three layer model, from $s = 0$ in the deep tissue layer to the skin surface at $y = 0$, requires that the temperature difference $(\tilde{T}_a - \tilde{T}_v)$ at $s = 0$ in the deep tissue layer, which represents the heat lost from the blood to the tissue, is equal to net heat lost from the tissue layer to the surroundings. Jiji *et al.* assume that the inner surface at $s = 0$ is insulated. Thus the total energy lost from the blood during its flow through the vascular network shown in Fig. 22, proportional to the product $[\mathrm{Pe}^*(0)(\tilde{T}_a(0) - \tilde{T}_v(0))]$, is equal to the heat conduction loss from the outer

cutaneous layer to the surroundings at $y = 0$. Combining the appropriate terms, the resulting relationship between $\tilde{\phi}_0$ and $\tilde{T}_r$ that satisfies the global energy balance is

$$\tilde{T}_r = 1 + \frac{2\tilde{I}_s(1)}{\mathrm{Pe}^*(0)} \frac{\tilde{a}(1)n(1)}{\tilde{a}(0)n(0)} \left\{ \frac{k_c}{k_t} \frac{x_0}{y_0} C_1 \beta W_b + \frac{\lambda}{\beta} \right\} \tag{9.69}$$

The integration constant C_1 is readily available from the cutaneous layer solution:

$$C_1 = \frac{1}{W_b \cosh W_b \tilde{y}_1} \left\{ \frac{\tilde{\phi}_b(1 - \cosh W_b \tilde{y}_1) - \tilde{\phi}_0}{(1 - \tilde{y}_1) \cosh W_b \tilde{y}_1 + (1/W_b) \sinh W_b \tilde{y}_1} - (\tilde{\phi}_0 - \tilde{\phi}_b) W_b \sinh W_b \tilde{y}_1 \right\} \tag{9.70}$$

Equations (9.69) and (9.70) provide the necessary relationship between the unknowns $\tilde{T}_r$ and $\tilde{\phi}_0$. The three layer mathematical model presented by Jiji *et al.* is now complete and can be solved without a trial-and-error guessing procedure.

4. *Parameter Evaluation*

Solutions to the Weinbaum–Jiji three layer tissue model involve the evaluation of numerous parameter values. For convenience, variations in the vessel number density, vessel radius, and the vessel spacing with position along the vascular network are all modeled using a continuous function, even though the *in vivo* variations are discrete. In addition, the inclination angle between the countercurrent vessels and the axis parallel to the skin surface is chosen to be a constant 22°, which represents a simplification since this angle should increase monotonically to 90° at the deep–intermediate tissue interface. The vessel spacing function is chosen to be

$$n(\tilde{s}) = (1 - k\tilde{s})^{-b} \tag{9.71}$$

Using $b = 2$, Jiji *et al.* [34] compute k such that the number density is 32 at $\tilde{s} = 1$, corresponding to a total of six branching generations of vessels in the deep tissue layer with a single artery–vein pair at $\tilde{s} = 0$. In this case, $k = 0.823$, Jiji *et al.* [34] point out that the functional form of Eq. (9.71), along with $b = 2$ and $k = 0.823$, yields several physiologically realistic results: (1) the first two vessel generations penetrate over half of the deep tissue layer, (2) the length of each vessel generation is shorter than the previous one, and (3) the final vessel generation has a length on the same order as the transverse vessels in the intermediate tissue layer.

Jiji *et al.* [34] model the tapering size of the countercurrent vessels in a similar manner. A function is chosen so that a fictitious velocity, which would exist under conditions of zero perfusion bleed-off from the artery, will decrease according to the relationship

$$u^*(\tilde{s}) = u(0)(1 - c\tilde{s})^d \tag{9.72}$$

where $u^*(\tilde{s})$ is the blood velocity in the absence of perfusion bleed-off and c and d are constants. Under conditions of zero bleed-off, continuity of mass requires that

$$n(0)a^2(0)u(0) = na^2u^* \tag{9.73}$$

Thus

$$a(\tilde{s}) = a(0)(1 - k\tilde{s})^{b/2}(1 - c\tilde{s})^{-d/2} \tag{9.74}$$

The constants c and d are chosen so that u^* decreases from 10 cm/s at the entrance to the countercurrent network ($\tilde{s} = 0$) to 5 cm/s at the exit ($\tilde{s} = 1$). Under these conditions, $d = 3$ and $c = 0.206$.

Experimental observations reported by Weinbaum *et al.* [60] reveal that the countercurrent vessel spacing is very small in the first two generations, then increases rapidly towards the intermediate tissue layer. The countercurrent vessel spacing in the deep tissue layer, $\tilde{l}_s$, is therefore chosen by Jiji *et al.* [34] to fit the function

$$\tilde{l}_s = \tilde{l}_s(0) + e\tilde{s}^f \tag{9.75}$$

where constants e and f are evaluated such that $\tilde{l}_s$ matches the spacing of the transverse vessels in the intermediate tissue layer. For $f = 16$, the constant e is 9.618, corresponding to a 0.47-mm separation at the deep-intermediate tissue interface when $\tilde{l}_s(0) = 2.1$ and $a(0) = 160\,\mu$m.

The perfusion parameter v could not be matched with any experimental data, as none were available to Jiji *et al.* [34]. Consequently, a range of values for g, the perfusion velocity, was used in the solution of the three layer model. Values of 6.2×10^{-4}, 3.1×10^{-3}, and 4.6×10^{-3} cm/s correspond to a total perfusion bleed-off in the deep tissue layer equal to 10, 50, and 75% of the blood entering the countercurrent network at $\tilde{s} = 0$, respectively, assuming a value of 4 cm for S_0 and a constant inclination angle of 22°. The blood that remains in the countercurrent vessels at $\tilde{s} = 1$ enters the transverse vessels of the intermediate tissue layer. In this manner a bleed-off fraction G, the ratio of blood perfused into the deep tissue layer to the total blood that enters the countercurrent network at $\tilde{s} = 0$, can be defined as

$$G = 1 - \frac{n(1)u^*(1)a^2(1)}{u^*(0)a^2(0)} \tag{9.76}$$

In the other two tissue layers, several more parameters had to be specified. Jiji *et al.* [34] assumed a value of 0.5 for ϕ_b. The thermal conductivities k_t and k_c were assumed to be equal at 0.5 W/m-°C. The metabolic heating parameter, λ, was set to zero so that the effect of perfusion, characterized by v in the deep and intermediate tissue layers and W_b in the cutaneous layer, could be easily observed. The results of the simulations for a range of G and W_b values are shown in Figs. 25 through 27.

5. *Simulation Results*

Figure 25 shows the mean tissue temperature, assumed equal to $((\tilde{T}_a + \tilde{T}_v)/2)$ in the development of this model, as a function of position in the three tissue layers for G fixed at 0.33 and a range of W_b values for the cutaneous blood perfusion rate. As the cutaneous perfusion rate increases, the warm blood tends to increase the tissue temperature in all three tissue layers. As with models that utilize the Pennes bioheat equation, the temperature gradient at the surface of the skin increases with increasing perfusion rate due to the increased magnitude of the source term that represents perfusion heating. Figure 27 illustrates this effect at different values of bleed-off fraction G. Note that at high skin perfusion rates, the surface heat flux is independent of G since blood perfusion in the deep tissue layer

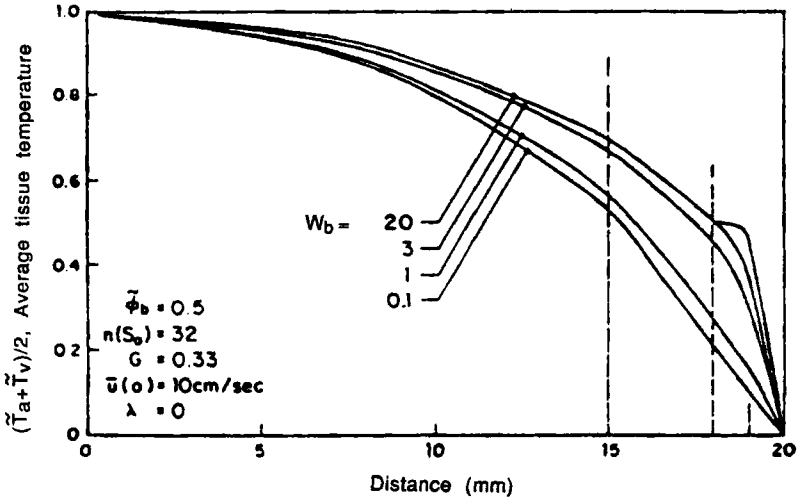

FIG. 25. Mean artery-vein blood temperature profiles, equivalent to the mean tissue temperature profiles, across the three layer model of Jiji *et al.* for a range of cutaneous blood perfusion rates. (Reproduced from [34], with permission from the American Society of Mechanical Engineers.)

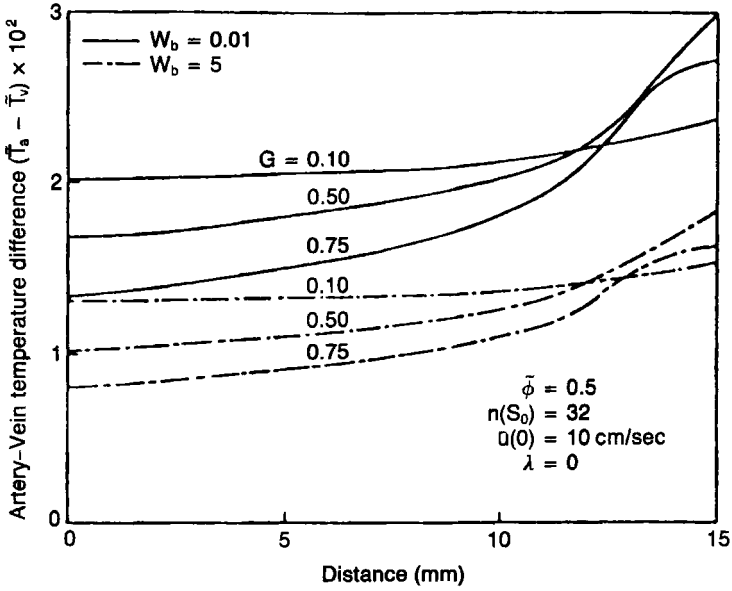

FIG. 26. The artery-vein temperature difference across the three layer model of Jiji *et al.* at different muscle bleed-off rates and cutaneous blood perfusion rates. (Reproduced from [34], with permission from the American Society of Mechanical Engineers.)

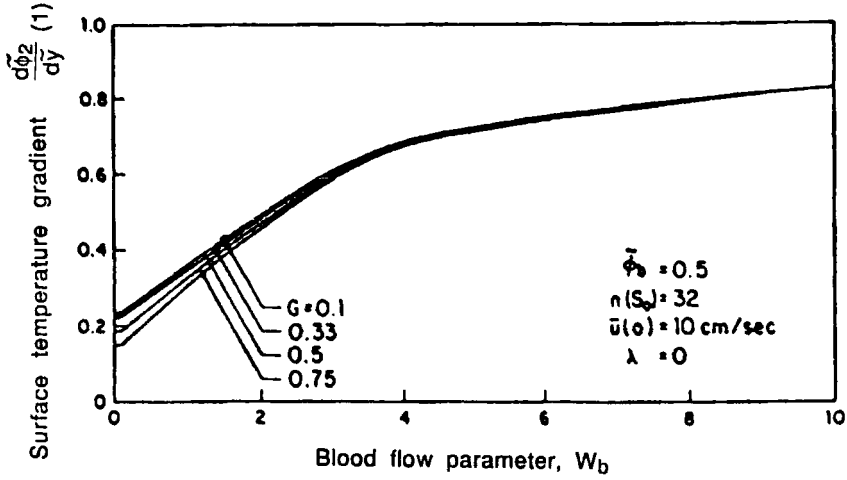

FIG. 27. The surface temperature gradient as a function of cutaneous blood perfusion rate. (Reproduced from [34], with permission from the American Society of Mechanical Engineers.)

has relatively little influence on surface heat transfer. According to these results, surface heat transfer can be increased by a factor of 3 during vasodilation, which facilitates heat removal from the body during periods of thermal stress.

The artery–vein temperature difference as a function of spatial position in the tissue is shown in Fig. 26 for a range of G values with $W_b = 5$ and $W_b = 0.01$. These results indicate that the local artery–vein temperature difference is fairly uniform within the first two-thirds of the deep tissue layer, despite order of magnitude changes in vessel diameter and velocity. While this dimensionless temperature difference is quite small, on the order of 0.01–0.02, it is sensitive to variations in the perfusion rate g in the deep tissue layer $0 < s < 15$ mm, but not in the intermediate layer (not shown). In terms of dimensional quantities, for a range of 5–10 °C temperature difference between the arterial blood entering the deep tissue and the skin, this corresponds to a local artery–vein temperature difference in the range of only 0.1–0.2 °C between these thermally significant countercurrent vessels. This temperature difference is almost negligible, yet its effect on the tissue temperature is significant. This prediction agrees closely to the experimental measurements made by Lemons *et al.* [41] in their experimental study of blood and tissue temperatures in the rabbit thigh. It is important to note that if the countercurrent exchange is perfect, there is no net heat transfer between the paired vessels and the surrounding tissue, resulting in a constant $T_a - T_v$ temperature difference along the vascular network as long as the mass flows are equal at any given spatial location inside the vessels. This result was seen earlier in the countercurrent model of Chato [20], as well as in the simplified thermal equilibration length studies of Weinbaum *et al.* [60] described previously in this chapter (see Eqs. (9.12) through (9.17).

Another feature of this model is its prediction of a significant change in the slope of the temperature profile at the interface of the deep and intermediate tissue layers. In addition, at high cutaneous perfusion rates, there is a region with a flat temperature profile in the inner cutaneous layer. Both of these characteristics were also observed in the experimental measurements of Lemons *et al.* [41]. The three layer model therefore is successful in characterizing several important aspects of tissue–blood heat transfer. While blood perfusion has some effect on the local arterial–venous blood temperature difference, arterial bleed-off does not substantially increase the tissue temperature due to the complete thermal equilibration that occurs between the bleed-off blood and the surrounding tissue in these microcirculatory beds.

A follow-up paper by Dagan *et al.* [24] examined the tissue and blood temperatures predicted by this three layer model using a range of values for

the Reynolds number at the inlet to the countercurrent network, the fraction of blood supplied to the cutaneous layer, the number of countercurrent branching generations, and the intensity of the metabolic heat source. As before, the difference between the arterial and venous blood in the deep tissue layer was calculated to be uniformly small under the range of parameter values examined.

The main conclusion from these important combined experimental and theoretical studies by Weinbaum and colleagues [34, 41, 59, 60] was that the main component of heat transfer between tissue and blood in the deep tissue layer is the imperfect countercurrent heat exchange between paired arteries and veins. Temperature differences on the order of $(T_t - T_0)$ used to model the effects of blood flow on tissue heat transfer in the Pennes bioheat formulation are essentially nonexistent. Using both a simple preliminary model that ignored perfusion bleed-off and only examined thermal equilibration lengths, and the complex three layer model described above, Weinbaum and colleagues showed that heat flow between the countercurrent pairs and the tissue that surrounds these vessels will dominate the heat transfer in vascularized tissue of the type modeled previously in this chapter, typically skeletal muscle. The influence of countercurrent blood flow on tissue temperature was next investigated by Weinbaum and Jiji [61] in a paper published 1 year later that presented the derivation of a "new" bioheat equation.

C. NEW SIMPLIFIED BIOHEAT EQUATION

The mathematical and practical advantage of the new bioheat equation of Weinbaum and Jiji [61] is that it includes the imperfect countercurrent heat exchange phenomenon in a single equation, derived from the initial three heat transfer equations for the artery, vein, and tissue, that contains only the tissue temperature and its spatial derivatives. Predictions of local artery and venous temperatures along the countercurrent network cannot be determined from this one equation model. A more complicated three equation model, such as that presented in the 1984 study [34, 60], is necessary for this determination. Weinbaum and Jiji use what is essentially a simplified version of their three layer model to derive their bioheat equation, which contains an effective thermal conductivity that takes into account the effect of imperfect countercurrent heat exchange between arteries and veins on tissue–blood heat transfer. This effective thermal conductivity is a function solely of the vascular geometry and blood flow rate. The main advantage of this one-equation model is its relative ease of implementation compared to the three layer, three equation model presented in 1984 [34, 60].

As shown in the 1984 study [34, 60], the imperfect countercurrent heat transfer between paired arteries and veins yields a net energy transfer to the tissue when there is a temperature gradient in the same direction as the blood flow. Under these conditions, the arterial and venous blood flow from tissue regions with different temperatures, thus delivering or removing some energy to or from the tissue. Weinbaum and Jiji [61] argue that the countercurrent effect acts like a source or sink of heat in the tissue, which will subsequently appear in the new bioheat equation. In addition to the countercurrent heat source, the effect of unidirectional capillary bleed-off normal to the axes of the paired countercurrent vessels is also included in the tissue energy balance equation.

1. *Preliminary Calculations of Perfusion Bleed-off*

As part of a preliminary study, Weinbaum and Jiji [61] show that while the heat transfer associated with capillary blood perfusion is negligible when modeled as a volumetric heat source, as is done in the Pennes bioheat equation, it is important relative to conduction in the same direction when modeled as a unidirectional convective term. Conduction and directed capillary perfusion heat transfer normal to the countercurrent vessel axes can be characterized by two terms, $k_t(d^2T_t/dx^2)$ and $\rho_b c_b A_b u_p(dT_t/dx)$, respectively, where A_b is the area of the bleed-off vessels relative to the total cross-sectional area normal to conductive heat flow and u_p is the velocity of blood in the perfusion bleed-off vessels. Note that the blood temperature is equivalent to the tissue temperature in these thermally insignificant vessels that comprise the microcirculation. Weinbaum and Jiji [61] estimate these two heat transfer terms using a range of A_b values of 0.02–0.1, and u_p values from 1–2 mm/s, and a tissue thermal conductivity value of 0.54 W/m-°C. Using these parameters, directed perfusion heat transfer relative to conduction heat flow ranges from 0.04 to 0.60. Weinbaum and Jiji [61] conclude that directed perfusion cannot be neglected when considering heat transfer normal to paired countercurrent vessels and therefore must be included in a bioheat transfer model, as was the case in their earlier three layer, three equation model.

2. *Derivation of the Weinbaum–Jiji Bioheat Equation*

a. *Energy Balance Equations.* Starting from the three equation model that describes the deep tissue layer of the three layer model, Weinbaum and Jiji [61] derive the one bioheat equation that includes an effective thermal conductivity tensor. A tissue control volume is chosen that includes the capillary beds, which are thermally insignificant and contain blood fully equilibrated with the surrounding tissue, while countercurrent blood

vessels are omitted from the tissue control volume. The orientation of the control volume relative to the vessel axes is arbitrary and characterized by an inclination angle α. Thermally significant countercurrent vessels with number density n, radius a, center-to-center spacing l_s, and blood velocity u cross the tissue control volume. As shown in the earlier studies by Weinbaum and colleagues [34, 59, 60], continuity requires that m_a, the mass flow rate in the artery, is equal to m_v, the mass flow rate in the countercurrent vein, when lymphatic fluid losses are neglected. The velocities u_a and u_v are therefore equal in magnitude and opposite in sign.

The tissue and blood energy balances are derived by modeling the effects of imperfect countercurrent heat exchange on tissue heat transfer as was done in the earlier 1984 formulation [34, 60]. The artery and vein energy balances above, Eqs. (9.20) and (9.21), must be modified in order to account for variations in the countercurrent vessel number density with s-position. This modification yields

$$\rho_b c_b \frac{d}{ds}(\pi a^2 n \bar{u} T_a) = -n q_a - \rho_b c_b [2\pi a n g] T_a \tag{9.77}$$

$$\rho_b c_b \frac{d}{ds}(\pi a^2 n \bar{u} T_v) = -n q_v - \rho_b c_b [2\pi a n g] T_v \tag{9.78}$$

for an equal size artery–vein pair. Subtracting Eq. (9.78) from (9.77) yields

$$\rho_b c_b \left\{ \frac{d}{ds}(\pi a^2 n \bar{u} T_a) - \frac{d}{ds}(\pi a^2 n \bar{u} T_v) \right\} = -n(q_a - q_v) - \rho_b c_b [2\pi a n g](T_a - T_v) \tag{9.79}$$

Weinbaum and Jiji [61] use an integrated tissue control volume analysis to show that the term on the left-hand side of Eq. (9.79) is the total heat exchange between blood in the countercurrent vessels and the surrounding tissue. It can be viewed as a heat source or sink per unit volume tissue due to the opposite flow of two blood vessels, both with a nonzero thermal equilibration length, along the same axis as one component of the tissue temperature gradient. This term is balanced by conduction losses and metabolic heating within the tissue control volume

$$\rho_b c_b \left\{ \frac{d}{ds}(\pi a^2 n \bar{u} T_a) - \frac{d}{ds}(\pi a^2 n \bar{u} T_v) \right\} = \nabla k_t \nabla T_t + Q_m \tag{9.80}$$

where Q_m is the metabolic heat source per unit volume tissue. Combining Eqs. (9.79) and (9.80)

$$-n(q_a - q_v) - 2\pi \rho_b c_b a n g (T_a - T_v) = \nabla k_t \nabla T_t + Q_m \tag{9.81}$$

The first term on the right-hand side of Eq. (9.81) is the imperfect countercurrent exchange heat source term, while the second term is the perfusion bleed-off heat source term. Equation (9.81), the tissue energy balance equation, is essentially a more general version of Eq. (9.24), where the effect of vessel number density is included in the blood flow source terms on the left-hand side, and a metabolic heat source term is added. It is interesting to note that the tissue heat balance equation derived by Weinbaum and Jiji [61] does indeed contain a perfusion bleed-off term that superficially resembles the Pennes isotropic perfusion term. However, this perfusion term is proportional to a $(T_a - T_v)$ temperature difference, rather than $(T_a - T_t)$. In addition, of course, the countercurrent heat source term in Eq. (9.81) is completely absent from the Pennes formulation.

Equations (9.22) and (9.23) can be used to quantify the rate of energy entering and leaving the tissue control volume per unit length of blood vessel–tissue control due to imperfect countercurrent exchange:

$$q_a - q_v = \pi \rho_b c_b a^2 u \frac{d}{ds}[T_v - T_a] \tag{9.82}$$

Implementing the vessel number density parameter, the total strength of the countercurrent heat source per unit volume tissue is

$$-n(q_a - q_v) = \pi \rho_b c_b a^2 n u \frac{d}{ds}[T_a - T_v] \tag{9.83}$$

Equation (9.81) can now be written as

$$\pi \rho_b c_b a^2 n u \frac{d}{ds}[T_a - T_v] - 2\pi \rho_b c_b a n g (T_a - T_v) = \nabla k_t \nabla T_t + Q_m \tag{9.84}$$

b. *Closure Condition.* Equation (9.84), as written, cannot be solved for T_t, since both T_a and T_v are unknowns that vary with s-position. In the 1984 study [34, 60], the two energy balances for the artery and vein were solved simultaneously along with the tissue energy balance in the deep tissue layer after several simplifying assumptions were made based on physical arguments. The objective of the 1985 study by Weinbaum and Jiji [61] was to derive a simplified, single equation model to describe tissue temperature variations with spatial position that accounted for the important heat transfer effects associated with blood flow: perfusion bleed-off and imperfect countercurrent exchange. Based upon physical arguments presented in the 1984 study [34, 60], Weinbaum and Jiji propose that the mean tissue temperature around an artery–vein pair can be approximated as

$$T_t \cong \frac{T_a + T_v}{2} \tag{9.85}$$

and that the magnitude of the difference $(q_a - q_v)$ is much smaller than the magnitude of either q_a or q_v. As discussed above, the second condition implies that q_a and q_v can be obtained from the superposition of a paired line source and line sink within a pure conduction field. By assuming that the tissue field around the vessel pair is a pure conduction region, Weinbaum and Jiji essentially neglected the effects of capillary bleed-off on the temperature distribution around a countercurrent vessel pair. The validity of this assumption was examined several years later in an experimental study presented in Zhu *et al.* [70], which is described in Section IX.C.5.c. In addition, a numerical study by Charny and Levin [17] indicated that the neglect of perfusion in the two-dimensional tissue region between the paired vessels was reasonable for a range of blood flow conditions and that the superposition solution was a very good approximation of the two-dimensional heat transfer between the paired vessels.

The result of the symmetric boundary value problem for heat transfer normal to a pair of tubes with equal radii and uniform wall temperatures is

$$q_a \cong q_v = \sigma k_t (T_a - T_v) \tag{9.86}$$

where σ is a geometrical factor

$$\sigma = \frac{\pi}{\cosh^{-1}(l_s/2a)} \tag{9.87}$$

produced from the superposition solution. The ratio $l_s/2a$ indicates the ratio of the vessel spacing to vessel diameter. Note that Eq. (9.86) is identical to Eq. (9.29) since

$$\cosh^{-1}\left(\frac{l_s^2}{2a^2} - 1\right) = 2\cosh^{-1}(l_s/2a) \tag{9.88}$$

Equations (9.22), (9.23), (9.85), and (9.86) are combined to yield the needed relationship between the artery–vein temperature difference and the tissue temperature gradient:

$$T_a - T_v = -\frac{\pi \rho_b c_b a^2 u}{\sigma k_t} \frac{dT_t}{ds} \tag{9.89}$$

Substituting Eq. (9.89) into the tissue energy balance Eq. (9.84) results in a single equation that contains only the tissue temperature, its spatial gradients, and vascular parameters:

$$\frac{\pi^2 \rho_b^2 c_b^2 a^2 nu}{k_t} \frac{d}{ds}\left\{\frac{a^2 u}{\sigma} \frac{dT_t}{ds}\right\} - \frac{2\pi^2 \rho_b^2 c_b^2 a^3 ung}{\sigma k_t} \frac{dT_t}{ds} = -\nabla k_t \nabla T_t - Q_m \tag{9.90}$$

Some of the constants in Eq. (9.90) can be grouped together in Pe, the flow Peclet number, equal to $2a\rho_b c_b u/k_b$:

$$\frac{\pi^2 a n k_b^2}{4k_t}\,\mathrm{Pe}\left(\frac{d}{ds}\left\{\frac{a\,\mathrm{Pe}}{\sigma}\frac{dT_t}{ds}\right\} - \frac{2g\,\mathrm{Pe}}{\sigma u}\frac{dT_t}{ds}\right) = -\nabla k_t \nabla T_t - Q_m \quad (9.91)$$

Equation (9.91), the new bioheat equation proposed by Weinbaum and Jiji [61], can be rewritten in terms of an effective thermal conductivity that symbolizes the effect of blood flow on tissue heat transfer.

c. *Effective Thermal Conductivity.* Based on Fourier's Law of Conduction, q_k, the total conductive energy transport in a three-dimensional medium is

$$q_k = -\frac{d}{dx_i}\left(k_{ij}\frac{dT_t}{dx_j}\right) \quad (9.92)$$

where k_{ij} is a thermal conductivity tensor with i as the direction of the heat flux and j as the direction of the temperature gradient. Note that according to this general expression, temperature gradients in all three principal directions influence the heat flux in any one principal direction. For the bioheat problem examined by Weinbaum and Jiji [61], derivatives in the s-direction can be related to those in x_j:

$$\frac{dT_t}{ds} = \cos\theta_j \frac{dT_t}{dx_j} \quad (9.93)$$

where θ_j is the angle between coordinate axes s and x_j. Similarly

$$\frac{d^2T_t}{ds^2} = l_i \frac{d}{dx_i}\left(l_j \frac{dT_t}{dx_j}\right) \quad (9.94)$$

where l_j is equivalent to $\cos\theta_j$. Rearranging Eq. (9.94) results in the expression

$$\frac{d^2T_t}{ds^2} = \frac{d}{dx_i}\left(l_i l_j \frac{dT_t}{dx_j}\right) - l_j \frac{dl_i}{dx_i}\frac{dT_t}{dx_j} \quad (9.95)$$

Equations (9.93) and (9.95) are used by Weinbaum and Jiji to rewrite the tissue energy balance Eq. (9.91) and isolate an effective thermal conductivity tensor:

$$\frac{d}{dx_i}\left\{\frac{\pi^2 k_b^2}{4k_t\sigma} a^2 n l_i l_j \,\mathrm{Pe}^2 \frac{dT_t}{dx_j}\right\} - \frac{\pi^2 k_b^2}{4k_t\sigma} a\,\mathrm{Pe}\left(\frac{d}{dx_i}(n a l_i\,\mathrm{Pe}) + \frac{2}{u} n g\,\mathrm{Pe}\right)\frac{dT_t}{dx_j}$$
$$= -\frac{d}{dx_i}\left(k_t \delta_{ij}\frac{dT_j}{dx_j}\right) - Q_m \quad (9.96)$$

Note that the term $k_t \delta_{ij}$ is used to represent the solid tissue thermal conductivity as an isotropic medium. The first terms on the left- and right-hand sides of Eq. (9.96) can be combined into one effective conductivity term:

$$-\frac{\pi^2 k_b^2}{4k_t\sigma} a \,\mathrm{Pe}\left(\frac{d}{dx_i}(nal_i\,\mathrm{Pe}) + \frac{2}{u} ng\,\mathrm{Pe}\right) l_i \frac{dT_t}{dx_j} = -\frac{d}{dx_i}\left(k_{ij,\mathrm{eff}} \frac{dT_t}{dx_j}\right) - Q_m \tag{9.97}$$

where

$$k_{ij,\mathrm{eff}} = k_t\left(\delta_{ij} + \frac{\pi^2 k_b^2}{4k_t^2\sigma} \mathrm{Pe}^2 a^2 n l_i l_j\right) \tag{9.98}$$

The left-hand side of Eq. (9.97) contains two convective terms that both utilize a blood velocity-temperature gradient product. The first term characterizes the heat transfer effect of the tapered geometry of the countercurrent network, while the second term accounts for the convective effect of perfusion bleed-off from the countercurrent artery to its paired vein. For convenience, the continuity relationship, Eq. (9.19), is substituted into Eq. (9.97), resulting in the relationship

$$\frac{\pi^2 k_b^2}{4k_t\sigma} na^2 \,\mathrm{Pe}^2 l_j \frac{dl_i}{dx_i}\frac{dT_t}{dx_j} = \frac{d}{dx_i}\left(k_{ij,\mathrm{eff}} \frac{dT_t}{dx_j}\right) + Q_m \tag{9.99}$$

If the inclination angle of the vessels is assumed constant with spatial position, as was done in the earlier 1984 study of Weinbaum and colleagues [34, 60], the left-hand side of Eq. (9.99) is zero.

The effective thermal conductivity described by Eq. (9.98) can be more easily interpreted for the case where the vessels are in the same direction as the temperature gradient. Under these conditions, the direction cosines l_i and l_j are both unity and

$$k_{\mathrm{eff}} = k_t\left\{1 + \frac{n}{\sigma}\left(\frac{k_b}{k_t}\right)^2\left(\frac{\pi a\,\mathrm{Pe}}{2}\right)^2\right\} \tag{9.100}$$

This equation can be written in terms of the thermal equilibration length of the blood vessel, derived above and shown in Eq. (9.17). This substitution, along with the definition of σ in Eq. (9.87), yields

$$k_{\mathrm{eff}} = k_t\{1 + \sigma L_{\mathrm{eq}}^2 n\} \tag{9.101}$$

for a thermal equilibration length defined as

$$L_{\mathrm{eq}} = \frac{\pi a\,\mathrm{Pe}}{2\sigma}\frac{k_b}{k_t} \tag{9.102}$$

Based on vascular geometrical data in the literature, Eqn. (9.100) indicates that the ratio k_{eff}/k_t is 3.5, 1.7, 1.2, and 1.05 in blood vessels with 300-, 200-, 100-, and 50-μm diameters, respectively, assuming that blood and tissue thermal conductivities are equivalent. It is important to note that these calculations were made by assuming resting blood flow conditions. During intense exercise, blood velocity can increase by several orders of magnitude, resulting in much larger values of k_{eff}/k_t. The importance of this effect is discussed in Section IX.C.5.a. The resting calculations indicate that the countercurrent heat transfer between the blood and the tissue dominates heat transfer in vessels larger than 200 μm in diameter, while for vessels smaller than 50 μm in diameter the countercurrent mechanism does not significantly heat the tissue. In the latter case, there is a small, almost negligible, enhancement of tissue conductivity due to the directed perfusion of blood from the artery to the paired vein. For vessels with diameters between 50 and 200 μm, directed perfusion and countercurrent heat transfer are of comparable, but small, importance in the enhancement of the tissue heat conductivity.

3. *Experimental Observations*

Experimental measurements made in the rabbit thigh by Lemons *et al.* [41] validate several features of the Weinbaum–Jiji bioheat equation. First, the temperature distribution in the plane normal to paired countercurrent artery and vein is observed to be essentially a pure conduction field. The convective effect of the thermally insignificant perfusion bleed-off vessels on tissue temperature is not noticeable in the tissue surrounding the thermally significant countercurrent vessels. This acts to support the implementation by Weinbaum *et al.* [34, 60] of the solution to the superposition of a line source and sink in a pure conduction field to model the countercurrent heat transfer between the artery–vein pair. Lemons *et al.* [41] also confirm that the tissue temperature gradient along the axes of the countercurrent vessels is essentially the same as the mean tissue temperature gradient away from the countercurrent vessels, in the far field. Based on these measurements, the application of the superposition theory to quantify heat transfer near a pair of countercurrent vessels appears reasonable.

4. *Implementation in the Three Layer Tissue Model*

The new bioheat equation of Weinbaum and Jiji [61], Eq. (9.99), is a mathematically simple single equation description of the effects of blood flow on peripheral tissue heat transfer. Given a known vascular architecture, the parameters n, a, l, and u can be estimated or measured in order to evaluate the spatially varying effective thermal conductivity of the tissue.

In a study by Song *et al.* [55], the Weinbaum–Jiji bioheat equation was solved in peripheral tissue. As with the three layer model developed by Weinbaum *et al.* [34, 60] and subsequently examined numerically by Dagan *et al.* [24], the peripheral tissue layer was subdivided into three separate regions: deep, intermediate, and cutaneous layers. Radial curvature was neglected so that the expression for the one-dimensional effective thermal conductivity shown in Eq. (9.101) could be applied. A schematic view of the three layer, one-dimensional model is shown in Fig. 28.

The bioheat equation of Weinbaum and Jiji, Eq. (9.99), can be expressed in a one-dimensional Cartesian coordinate system as

$$\frac{\pi^2 k_b^2}{4k_t\sigma} na^2 \mathrm{Pe}^2 / \frac{dl}{dz_l}\frac{dT_t}{dz_l} = \frac{d}{dz_l}\left(k_{\mathrm{eff}}\frac{dT_t}{dz_l}\right) + Q_{ml} \tag{9.103}$$

where z_l is the deep tissue layer coordinate axis measured from the entrance to the artery-vein countercurrent network and k_{eff}, the effective thermal conductivity, is described by Eq. (9.101). This equation can be

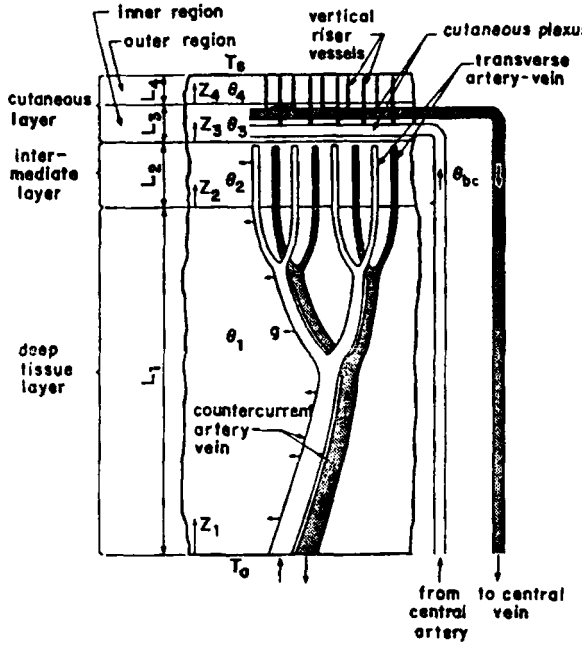

FIG. 28. A schematic view of the three layer model of Song *et al.* Note that only thermally significant vessels are shown. All capillary beds are omitted. (Reproduced from [55], with permission from the American Society of Mechanical Engineers.)

nondimensionalized using the transformations

$$\tilde{z}_1 = \frac{z_1}{L_1} \qquad \text{and} \qquad \tilde{T}_1 = \frac{T_t - T_s}{T_0 - T_s},$$

where T_0 and T_s are the arterial inlet and skin surface temperatures, respectively. For tissue with a uniform capillary bleed-off rate per unit volume tissue, the product $2nag$ in the continuity equation is constant with z_1-position, and the resulting dimensionless version of the one-dimensional Weinbaum–Jiji equation is

$$\frac{k_{\text{eff}}}{k_t}\frac{d^2\tilde{T}_1}{d\tilde{z}_1^2} + \text{Pe}_0^2\left(\frac{dA}{d\tilde{z}_1} - B\right)\frac{d\tilde{T}_1}{d\tilde{z}_1} + \frac{Q_{m1}L_1^2}{k_t(T_0 - T_s)} = 0 \tag{9.104}$$

where

$$\frac{k_{\text{eff}}}{k_t}(\tilde{z}) = 1 + \text{Pe}_0^2 A(\tilde{z}) \tag{9.105}$$

$$A(\tilde{z}) = \left(\frac{\pi k_b}{2k_t}\right)^2 \frac{na^4 l_1^2}{\sigma a_0^2}\left(\frac{n_0 a_0^2}{na^2}\right)^2\left(1 - \frac{s}{S_D}\right)^2 \tag{9.106}$$

$$B(\tilde{z}) = \frac{1}{2}\left(\frac{\pi k_b}{2k_t}\right)^2 \frac{na^4}{\sigma a_0^2}\left(\frac{n_0 a_0^2}{na^2}\right)^2\left(1 - \frac{s}{S_D}\right)^2 \frac{dl_1^2}{d\tilde{z}_1} \tag{9.107}$$

$$\text{Pe}_0 = \frac{2a_0\rho_b c_b u_0}{k_b} \tag{9.108}$$

The "0" subscripts indicate parameters evaluated at the entrance to the countercurrent network at $\tilde{z}_1 = 0$; s is the distance in the countercurrent network relative to the entrance (not equal to z_1 due to variable inclination angles along the countercurrent network), and S_D is the combined length of the vascular network in the three tissue layers.

a. *Deep Tissue Layer.* The functions A and B were evaluated by Song *et al.* [55] for the deep tissue layer based on vascular anatomical data presented in earlier experimental and theoretical studies by Weinbaum and colleagues [34, 41, 60]. Continuous variations in vessel density n and radius a with spatial position z_1 were given from functions presented in Jiji and colleagues [34] and Dagan *et al.* [24] (see Eqs. (9.71) and (9.74)). The conduction coupling factor σ was evaluated based on Eq. (9.87), where the spacing to diameter ratio $l_s/2a$ was assumed to fit the function

$$l_s/2a = C_1(1 + C_2\tilde{z}_1^{C_3}) \tag{9.109}$$

Similarly, the cosine of the inclination angle between the deep layer vessel and the axis normal to the skin surface, l_1, was assumed to vary with $\tilde{z}_1$

according to the function

$$I_1 = \cos[C_4(1 - \tilde{z}_1)] \tag{9.110}$$

The values of the constants contained within these four functions are presented in Song *et al.* [55]. As expected, evaluation of the function A with these four functions indicates that the ratio k_{eff}/k_t decreases towards unity along the countercurrent network in the deep tissue layer, with the most significant augmentation of tissue conductivity in vessels between 300-μm diameter (at the entrance) and 100-μm diameter (approximately the fourth branching generation). It is important to realize that these calculations were made assuming a range of arterial inflow Peclet numbers at $z_1 = 0$ from 60 to 240, which represents the resting state and moderate exercise.

b. *Intermediate Tissue Layer.* In the intermediate tissue layer, the countercurrent vessels are oriented normal to the skin surface throughout, implying that the derivative $dI_2^2/d\tilde{z}_2$ is zero throughout this layer. Consequently, the vascular geometrical function B is zero in the intermediate layer. In addition, these countercurrent vessels are very small, with diameters on the order of 50 μm. Under these conditions the function A is essentially zero throughout the layer for the range of inflow Peclet numbers considered in this numerical study. For functions A and B equal to zero everywhere in the intermediate layer, the energy balance equation is

$$\frac{d^2\tilde{T}_2}{d\tilde{z}_2^2} + \frac{Q_{m2}L_2^2}{k_t(T_0 - T_s)} = 0 \tag{9.111}$$

c. *Cutaneous layer.* The governing energy balance equation in the inner and outer portions of the cutaneous layer of the three layer model is also simplified. Based on the 1984 study by Jiji *et al.* [34], Song *et al.* [55] model the effect of blood flow in the inner cutaneous layer as a distributed heat source whose strength is proportional to the local tissue–arterial blood temperature difference and the perfusion rate (see Eqs. (9.43) and (9.44)). The outer cutaneous layer is a pure conduction layer with no thermally significant blood vessels (see Eq. (9.45)). Assuming there is no significant metabolic heating in the absence of muscle cells, the nondimensional heat equations in these tissue layers are

$$\frac{d^2\tilde{T}_3}{d\tilde{z}_3^2} + \text{Pe}_0 R \frac{\pi n_0 a_0 L_3 k_b}{2k_t}(\tilde{T}_3 - \tilde{T}_{bc}) = 0 \tag{9.112}$$

and

$$\frac{d^2\tilde{T}_4}{d\tilde{z}_4^2} = 0 \tag{9.113}$$

where R is the ratio of blood supplied to the inner cutaneous layer relative to the intermediate and deep tissue layers. This parameter is physiologically significant as it represents the degree to which blood is shunted from the core to the cutaneous region by the body's thermoregulatory system during periods of thermal stress. While this vasomodulatory effect is not included in the study by Song *et al.* [55], it has been examined mathematically in the whole body thermal models of Wissler [65], Jain [33], Huckaba *et al.* [31, 32], Stolwijk and Hardy [57], and Charny and Levin [16].

In the three layer model of peripheral heat transfer developed by Weinbaum and colleagues [34, 60], blood from the core is fed to the inner cutaneous layer through a circulatory system that is physically separate from the countercurrent system that supplies and drains blood from the two muscle layers. The temperature of the blood as it arrives in the cutaneous layer is nondimensionalized as $\tilde{T}_{bc}$. Song *et al.* [55] argue that this temperature depends on the volume flow rate of blood into the cutaneous layer. When the cutaneous blood flow rate is very low, e.g., under low temperature ambient conditions, blood will be thermally equilibrated with the inner cutaneous tissue at position $z_3 = 0$, and therefore $\tilde{T}_{bc} = \tilde{T}_3(0)$. On the other hand, if the body is under high thermal stress, the flow rate of blood in the skin is high and there is little thermal equilibration between the vessels that supply the cutaneous layer and the surrounding tissue. In this case $\tilde{T}_{bc} = 1$ (i.e., $T_{bc} = T_0$, the inlet arterial temperature). Based upon the linear relationship between the integrated heat loss from a tube with constant cross section and the Peclet number, Song *et al.* [55] propose that $\tilde{T}_{bc}$ can be approximated by a linear function of the product $\mathrm{Pe}_0 R$, the cutaneous blood flow rate.

The metabolic heating terms that appear in Eqs. (9.103) and (9.111) are also assumed to be functions of the flow Peclet number. The metabolic rate is proportional to the rate at which oxygen is consumed by tissue, which Song *et al.* assume depends on the rate at which blood flows through the tissue. Song *et al.* [55] choose a linear relationship between both Q_{m1} and Pe_0, and Q_{m2} and Pe_0. The constants associated with variations in $\tilde{T}_{bc}$, Q_{m1}, and Q_{m2} with Pe_0 are given in Song *et al.* [55].

d. *Three Layer Model Results.* The three layer model of Song *et al.* [55] which implements the Weinbaum-Jiji bioheat equation to solve for the mean temperature in peripheral tissue as a function of depth is solved analytically for a range of parameter values. The boundary conditions needed to solve are the same as those used to solve for the blood temperatures in the 1984 study by Weinbaum and colleagues [34, 60], namely, matching temperature and heat flux at each tissue layer interface. Inflow Peclet numbers range from 60, the resting state, to 240, moderate exercise.

The cutaneous blood flow fraction R varies from a basal, vasoconstricted value of 0.01 to a maximum vasodilation value of 3.0. During the moderate exercise conditions simulated in this study, an intermediate value of 1.0 is used to account for the simultaneous increase in cutaneous and muscle blood flow rates. Figures 29 through 31 show the effect of arterial inflow Peclet number and blood flow fraction on the dimensionless tissue temperature profile across the three layer model and heat loss from the surface of the peripheral tissue.

The results of these calculations by Song *et al.* [55] reveal that blood flow in the regions of the deep tissue layer that contain vessels smaller than approximately 200 μm in diameter does not significantly enhance tissue conductivity. At low Peclet numbers the temperature profile is basically linear in all three tissue layers. As the inflow Peclet number increases, the heating effect of the thermally significant countercurrent vessels in the deep tissue layer increases. At the same time, there is greater metabolic heating in the muscle layers due to the linear relationship prescribed by Song *et al.* [55]

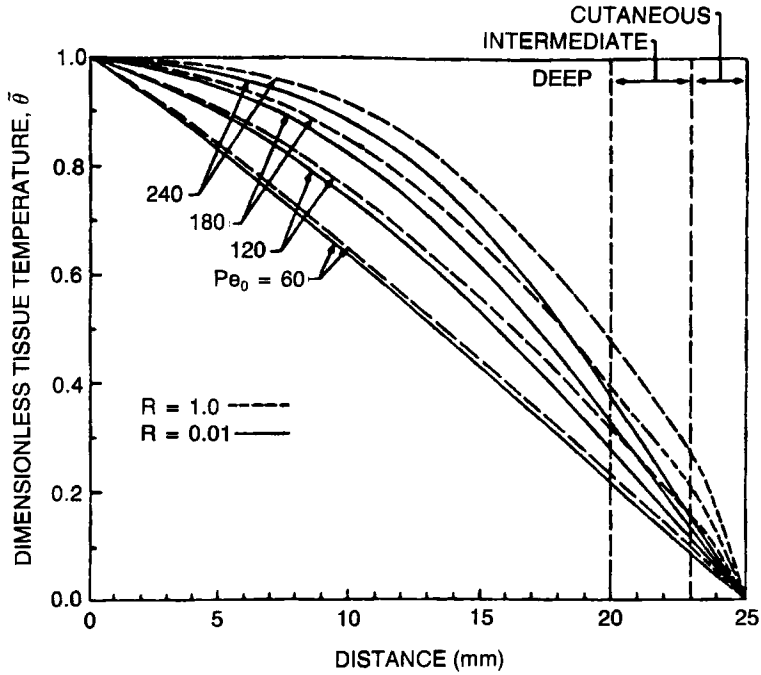

FIG. 29. Tissue temperature profiles across the three layer model of Song *et al.* for a range of inflow Peclet numbers Pe_0. (Reproduced from [55], with permission from the American Society of Mechanical Engineers.)

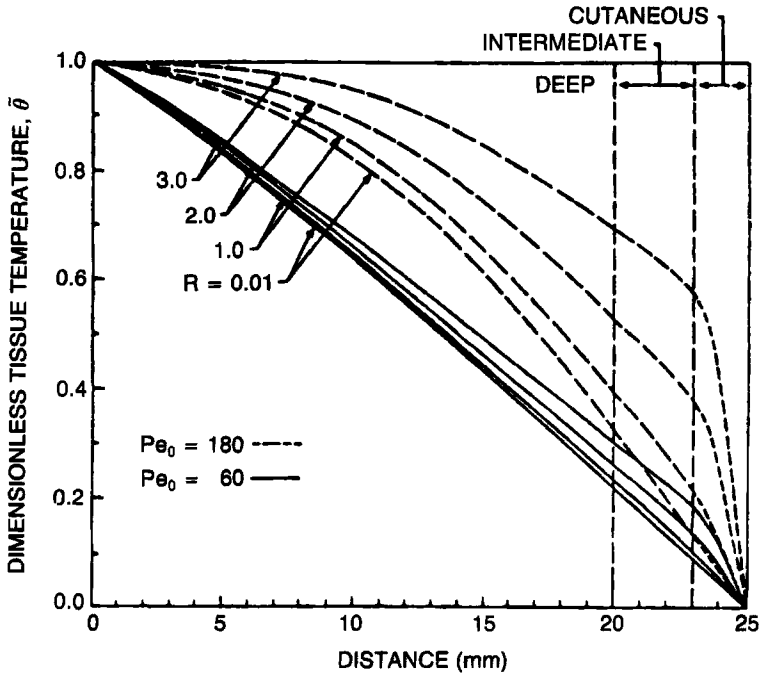

FIG. 30. Tissue temperature profiles across the three layer model of Song *et al.* for a range of values of R, the ratio of blood flow to the cutaneous to blood flow to the muscle layers. (Reproduced from [55], with permission from the American Society of Mechanical Engineers.)

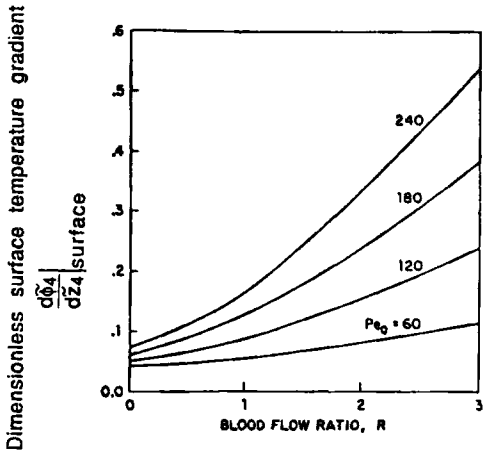

FIG. 31. Surface heat flux according to the three layer model of Song *et al.* for a range of R values and inflow Peclet numbers. (Reproduced from [55], with permission from the American Society of Mechanical Engineers.)

between the metabolic rate and the Peclet number. This combination yields a heating of the tissue above the level of the linear profile. In the region of the deep tissue layer that contains the thermally insignificant vessels, this temperature rise is due solely to the increased metabolic heat deposition. The effect of increased blood flow to the cutaneous layer is to increase the amount of heat delivered to the skin due to the increase in both the blood temperature T_{bc} as well as the flow fraction F. These increases act to intensify the magnitude of the perfusion heat source in the inner cutaneous layer, and consequently the temperatures in the cutaneous layer and the heat flux from the surface are greater than the case of resting flow rate and vasoconstriction.

The parametric study by Song *et al.* [55] was useful in demonstrating the applicability of the Weinbaum–Jiji bioheat equation to the analysis of peripheral tissue heat transfer and relating the predictions to several aspects of thermal physiology. The countercurrent arrangement of blood vessels in the deep muscle tissue layer was demonstrated to be a very efficient mechanism for heat conservation, while the transverse orientation of the thermally insignificant countercurrent vessels in the intermediate layer was shown to conduct heat towards the surface during periods of heavy metabolic activity, such as exercise. Finally, the cutaneous circulation was capable of removing a large amount of the metabolic heat generated during exercise from the body as long as the blood that was supplied to the cutaneous plexus from the core did not undergo significant precooling before it arrived in the skin layer.

5. *Applicability of the Weinbaum–Jiji Bioheat equation*

A very important characteristic of the Weinbaum–Jiji bioheat equation is that it was derived to describe heat transfer in peripheral tissue only, where its fundamental assumptions are most applicable. One of these assumptions, that the mean tissue temperature surrounding a countercurrent vessel pair is approximately equal to the mean blood temperature, $(T_a + T_v)/2$, was questioned in a series of papers by Wissler [66, 67]. In response, Weinbaum and colleagues published several studies [62, 63] that examined the basic assumptions of the Weinbaum–Jiji bioheat equation in greater detail.

a. *First Order Analysis with* ε. In the first response, published in 1987, Weinbaum and J'ji [62] used the superposition model of Baish *et al.* [2] to demonstrate the validity of their model. As shown in Fig. 32, the Baish *et al.* [2] superposition problem involves the separation of imperfect countercurrent heat transfer into two separate radial conduction problems. The first problem involves heat loss from a countercurrent vessel pair to the tissue

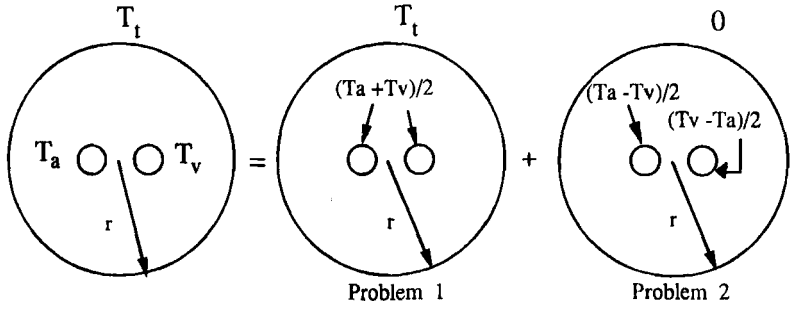

FIG. 32. Superposition of two boundary value problems in the plane normal to the countercurrent vessel pair axes. Problem 1 represents heat loss to the tissue from the countercurrent pair with no heat transfer between the vessels themselves. Problem 2 describes heat exchange between the vessels with no heat loss to the far field. (Adapted from [20], with permission from the American Society of Mechanical Engineers.)

with no heat exchange between the two vessels, while the second describes so-called perfect countercurrent heat exchange between the paired vessels with no energy transfer to the surrounding tissue. Variations in the artery and vein blood temperatures with axial position, neglecting perfusion bleed-off from the artery to the vein, can be modeled by the following two equations:

$$m_a c_b \frac{dT_a}{dx} = -k\sigma_c(T_a - T_v) - \frac{k_t\sigma_t}{2}(T_m - T_t) \tag{9.114}$$

$$m_v c_b \frac{dT_v}{dx} = -k\sigma_c(T_a - T_v) + \frac{k_t\sigma_t}{2}(T_m - T_t) \tag{9.115}$$

where T_m is the mean artery–vein temperature, $(T_a - T_v)/2$, and σ_t and σ_c are two conduction coupling parameters, defined by Baish *et al.* in their 1986 paper [2]. In this study, analytical expressions for these two factors as functions of vessel size, spacing, and Nusselt number are derived [2].

Equations (9.114) and (9.115) are similar to those in the simple countercurrent model of Mitchell and Myers [45], where the rate at which energy convected away by blood is balanced by the rate at which energy enters the blood from the surrounding tissue. The first terms on the right-hand sides of Eqs. (9.114) and (9.115) represent heat transfer described by the second superposition problem presented by Baish [2], where there is perfect countercurrent exchange, while the second terms describe heat transfer from the artery–vein pair to the surrounding tissue. Note that the total heat flow from the vessel pair to the surrounding tissue in the first problem is assumed to come equally from the artery and vein, resulting in the factor of $\frac{1}{2}$. This assumption is relaxed in a later study by Zhu *et al.* [70] (see Section IX.C.5.b).

Equations (9.114) and (9.115) can be manipulated into the following two equations by first taking their difference, then their sum, and finally substituting the differenced equation into the first derivative of the summed equation. Similarly, the summed equation can be substituted into the first derivative of the differenced equation to yield a second independent equation. In this derivation, as in all others described above, the arterial blood mass flow rate m_a is assumed equal to the venous mass flow rate m_v at any position x:

$$\left(\frac{mc_b}{k_t}\right)^2 \frac{d^2T_m}{dx^2} = \sigma_c\sigma_t(T_m - T_t) \tag{9.116}$$

$$\left(\frac{mc_b}{k_t}\right)^2 \frac{d^2}{dx^2}(T_a - T_v) = \sigma_c\sigma_t(T_a - T_v) + \frac{mc_b\sigma_t}{k_t}\frac{dT_t}{dx} \tag{9.117}$$

Weinbaum and Jiji [62] nondimensionalize these two energy balance equations with the spatial coordinate $\eta = x/L$, where L is the characteristic length of the macroscopic temperature gradient, an approach also utilized in the model of Chen and Holmes [22]. In this manner, Eqs. (9.116) and (9.117) are transformed to

$$\varepsilon^2 \frac{d^2T_m}{d\eta^2} = \frac{\sigma_t}{\sigma_c}(T_m - T_t) \tag{9.118}$$

$$\varepsilon^2 \frac{d^2}{d\eta^2}(T_a - T_v) = \frac{\sigma_t}{\sigma_c}(T_a - T_v) + \varepsilon\frac{\sigma_t}{\sigma_c}\frac{dT_t}{d\eta} \tag{9.119}$$

where

$$\varepsilon = \frac{mc_b}{k_t L\sigma_c} = \frac{\pi a\,\mathrm{Pe}}{2L\sigma_c} = \frac{L_{eq}}{L} \tag{9.120}$$

using the definition of thermal equilibrium length in Eq. (9.102) and assuming the ratio k_b/k_t is equal to unity.

As shown by Baish *et al.* [2], the ratio of the two conduction coupling factors σ_t/σ_c is of the order unity, while the values of these two parameters are in the range 2–5. The dimensionless parameter ε, however, is quite different from unity in many cases. Under normal physiological conditions of resting blood flow rate, Weinbaum *et al.* [60], as well as Chato [20] and Chen and Holmes [22], demonstrate that the thermal equilibration length of vessels smaller than 300 μm in diameter is much smaller than the length scale of macroscopic temperature gradients. Under resting conditions ε is 0.112, 0.024, and 0.003 in a 300-, 200-, and 100-μm-diameter vessel, respectively, assuming a value of 5 cm for L in the arm. Therefore ε is a parameter that is much smaller than unity and can be used in a perturbation analysis to evaluate the solutions to Eqs. (9.118) and (9.119). Under

conditions of elevated blood flow, however, it is important to realize that ε will increase in proportion to the mass flow rate, which can be evaluated by up to two orders of magnitude during intense exercise. In this case, clearly, even the 100-μm-diameter vessel may be thermally significant, and the values of ε are no longer small compared to unity in these microvessels. An analogous situation exists during local hyperthermia, where the characteristic length L may be significantly reduced relative to the normothermic value.

Weinbaum and Jiji [62] use an asymptotic expansion with the parameter ε to evaluate the solution to Eqs. (9.118) and (9.119). For the first order solution, the terms on the left-hand side of both of these equations are zero, yielding

$$T_m = T_t \tag{9.121}$$

$$T_a - T_v = -\varepsilon \frac{dT_t}{d\eta} \tag{9.122}$$

Equation (9.121) states that the tissue temperature, to order ε, is equal to the mean of the artery-vein temperatures, while Eq. (9.122) predicts that the tissue temperature gradient is proportional to the local artery-vein temperature difference and that the artery-vein temperature difference is zero in the absence of a tissue temperature gradient. Both of these results were used in the derivation of the Weinbaum-Jiji bioheat equation in 1985 [61]. Weinbaum and Jiji [62] point out that there will be regions of thickness on the order ε, analogous to boundary layers, where large differences between T_m and T_t will exist. However, they argue, these deviations will be eliminated over a short distance from the boundary.

Again, it should be emphasized that this normalized distance ε depends not only on the size and spacing of the paired vessels but also on the blood flow rate. During the elevated blood flow conditions associated with intense exercise, ε can be on the order of 10 in a 300-μm-diameter vessel. Under resting conditions, this same blood vessel may have a normalized thermal equilibration length of 0.1. Hence, both Wissler [67] and Weinbaum and Jiji [62] have convincingly demonstrated that the Weinbaum-Jiji bioheat equation cannot be universally applied to describe heat transfer in all vascular networks. Originally intended for use in peripheral tissue where the countercurrent vessels are smaller than 300 μm in diameter, the Weinbaum-Jiji formulation must be carefully applied so that its fundamental assumptions are not violated by the physical circumstances.

b. *Countercurrent Pairs with Different Radii.* The Weinbaum-Jiji bioheat equation was extended to describe countercurrent heat transfer in a vascular network with paired arteries and veins of different size in a 1988 paper

by Zhu *et al.* [70]. Lemons *et al.* [41] had observed experimentally that the countercurrent arteries, which are typically one-half to one-third the diameter of the veins with which they are paired, produced significantly more measurable temperature fluctuations than their paired vein. Similarly, the countercurrent veins had to be at least 300 μm in diameter in order to be thermally significant under resting conditions, while arteries as small as 100 μm in diameter caused perturbations in the tissue temperature field. In order to account for the *in vivo* condition of paired arteries and veins of unequal size, the two-dimensional superposition solution used to describe heat transfer in the plane normal to the countercurrent vessel axes in the original Weinbaum–Jiji formulation was modified by Zhu *et al.* [70]. In the same study, an asymptotic analysis of the equations used to derive the Weinbaum–Jiji bioheat equation was performed in order to rigorously derive a relationship between the mean temperature of the unequal size artery–vein pair, $(T_a + T_v)/2$, and the mean tissue temperature of the tissue surrounding the vessel pair.

The governing energy balance equations for the paired artery and vein surrounded by tissue are shown in Eqs. (9.77)–(9.79), where the net heat flow from the paired artery and vein to the surrounding tissue per unit length vessel, the so-called imperfect countercurrent heat transfer, is

$$q_a - q_v = mc_b\left(\frac{dT_v}{ds} - \frac{dT_a}{ds}\right) \tag{9.123}$$

Note that q_a is the heat loss from the artery to the surrounding tissue per unit length, and q_v is the heat transfer from the surrounding tissue to the venous blood per unit length vessel. The original version of the Weinbaum–Jiji bioheat equation assumed, for mathematical convenience, that the paired artery and vein were of equal size. In this case, the two-dimensional heat transfer problem of determining the magnitudes of q_a and q_v (assumed approximately equal) was solved by the superposition of two heat transfer problems shown in Fig. 32. The resulting Eqs. (9.86) and (9.87) were used to describe the net heat transfer from the vessel pair to the surrounding tissue due to imperfect countercurrent exchange.

Equations (9.114) and (9.115) can be modified in order to relate these heat flow terms q_a and q_v to the tissue and blood temperatures for equal or unequal size vessels:

$$mc_b\frac{dT_a}{ds} = -k\sigma_c(T_a - T_v) - pk_t\sigma_t(T_m - T_t) = -q_a \tag{9.124}$$

$$mc_b\frac{dT_v}{ds} = -k\sigma_c(T_a - T_v) + (1 - p)k_t\sigma_t(T_m - T_t) = -q_v \tag{9.125}$$

Note that the spatial coordinate s represents the location along the length of the countercurrent network, while the parameter p indicates the fraction of heat loss from the countercurrent artery to the far field in the tissue, with the remainder lost from the countercurrent vein. As shown by Zhu *et al.* [70], p is a function solely of the vessel geometry, i.e., spacing and diameter. For countercurrent paired vessels of equal size, p is exactly one-half, yielding Eqs. (9.114) and (9.115). Summing and differencing these relationships gives

$$q_a - q_v = k_t \sigma_t (T_m - T_t) = -mc_b \frac{d}{ds}(T_a - T_v) \tag{9.126}$$

$$q_a + q_v = 2k_t \sigma_c (T_a - T_v) + (2p - 1)k_t \sigma_t (T_m - T_t) = -2mc_b \frac{dT_m}{ds} \tag{9.127}$$

In the derivation of the original Weinbaum–Jiji equation [61], the imperfect heat loss from the equal size vessel pair to the surrounding tissue, $q_a - q_v$, was assumed to be much smaller than the countercurrent exchange between the vessels themselves, $q_a + q_v$, based upon physical arguments. It is important to note, however, that although $q_a - q_v$ is small, it is not exactly zero. Clearly, tissue is not thermally affected by countercurrent vessels if all of the heat conducted from the artery to the surrounding tissue is transported from the tissue back into the vein. The first order asymptotic analysis presented above in Section IX.C.5.a demonstrated that for vessel pairs of equal size, the assumption that $q_a - q_v$ is small is correct to order ε, the normalized thermal equilibration length of the countercurrent vessel.

Equations (9.126) and (9.127) can be manipulated in the same manner that Eqs. (9.114) and (9.115) in the previous section were transformed into Eqs. (9.118) and (9.119) in order to isolate the parameter ε in the governing equations for heat transfer normal to the unequal countercurrent vessel pairs. The final expressions are based on the normalized spatial coordinate $\eta = s/L$:

$$\varepsilon^2 \frac{d^2 T_m}{d\eta^2} = \frac{\sigma_t}{\sigma_c}(T_m - T_t) + \varepsilon P \frac{\sigma_t}{\sigma_c} \frac{d}{d\eta}(T_m - T_t) \tag{9.128}$$

$$\varepsilon^2 \frac{d^2}{d\eta^2}(T_a - T_v) = \frac{\sigma_t}{\sigma_c}(T_a - T_v) + \varepsilon \frac{\sigma_t}{\sigma_c} \frac{dT_t}{d\eta} - P\left(\frac{\sigma_t}{\sigma_c}\right)^2 (T_m - T_t) \tag{9.129}$$

where ε, the normalized thermal equilibration length, is defined by Eq. (9.120) and P is a vascular geometrical function that depends on the unequal size countercurrent artery and vein radii a_a and a_v and their

center-to-center spacing l_s:

$$P = \frac{1 + \gamma}{2} - p \tag{9.130}$$

$$p = -\frac{\ln b}{\ln R_a} \tag{9.131}$$

$$b = \frac{l_s^2 + a_v^2 - a_a^2 - \sqrt{[(l_s + a_a)^2 - a_v^2][(l_s - a_v)^2 - a_v^2]}}{2a_v l_s} \tag{9.132}$$

$$R_a = \frac{l_s^2 - a_a^2 - a_v^2 - \sqrt{[(l_s + a_a)^2 - a_v^2][(l_s - a_a)^2 - a_v^2]}}{2a_a a_v} \tag{9.133}$$

$$\gamma = \frac{\cosh^{-1}(B_a) - \cosh^{-1}(B_v)}{\cosh^{-1}(B_a) + \cosh^{-1}(B_v)} \tag{9.134}$$

$$\sigma_c = \frac{2\pi}{\cosh^{-1} B_a + \cosh^{-1} B_v} \tag{9.135}$$

$$B_a = \frac{(l_s/a_a)^2 - (a_v/a_a)^2 + 1}{2(l_s/a_a)} \tag{9.136}$$

$$B_v = \frac{(l_s/a_v)^2 - (a_a/a_v)^2 + 1}{2(l_s/a_v)} \tag{9.137}$$

The relationships in Eqs. (9.130) through (9.137) were derived by Zhu *et al.* using a superposition technique to solve the asymmetric boundary value problem described by the two-dimensional heat transfer between two unequal size tubes with different wall temperatures. For an equal size artery-vein pair, $R_a = 1/b^2$, $p = 1/2$, and $\gamma = 0$. The superposition solution by Zhu *et al.* utilizes the parameter γ in the definition

$$T_m \equiv \tfrac{1}{2}((1 - \gamma)T_a + (1 + \gamma)T_v) \tag{9.138}$$

Equations (9.128) and (9.129) reduce to Eqs. (9.118) and (9.119) for the case of vessel pairs with equal radii, since $P = 0$. Under these conditions the mean tissue temperature is equal to the artery-vein mean temperature to order ε as long as the parameter ε is small. Under normal resting conditions, ε is less than 0.1 in vessels smaller than 300 μm in diameter, but ε increases significantly under conditions of heavy exercise due to order of magnitude changes in blood flow rate. The parameter ε may also increase under conditions of local hyperthermia, where the length scale of the tissue temperature gradients is significantly reduced due to intense local heating.

For countercurrent vessels with unequal radii, P is not zero, and consequently the asymptotic analysis must be modified due to the presence of the third term on the right-hand-side of Eq. (9.129). Equation (9.128) can be integrated to solve for the local $T_m - T_t$ temperature difference as a function of ε and P:

$$(T_m - T_t)|_{\eta=\eta^*} = (T_m - T_t)|_{\eta=0} \exp(-\eta^*/\varepsilon P) + \varepsilon \frac{\sigma_c}{\sigma_t P} \int_0^{\eta^*} \frac{d^2 T_m}{d\eta^2} \exp(-\eta/\varepsilon P)\, d\eta \qquad (9.139)$$

Zhu *et al.* [70] apply the mean value theorem in order to interpret the integral term in Eq. (9.139):

$$\int_0^{\eta^*} \frac{d^2 T_m}{d\eta^2} \exp(-\eta/\varepsilon P)\, d\eta = \left.\frac{d^2 T_m}{d\eta^2}\right|_{\eta=\xi\eta^*} \eta^* \exp(-\xi\eta^*/\varepsilon P) \qquad (9.140)$$

where ξ is a dimensionless parameter between zero and unity.

The first term on the right-hand side of Eq. (9.139) represents the difference between the average blood and tissue temperatures due to a temperature difference at the entrance location. Based on the form of this exponential term, any difference between T_m and T_t at the entrance to the vessel pair will be eliminated over a distance εPL. The second term relates differences in the average blood and tissue temperatures caused by any gradient in the mean blood temperature along the vessel axis. Based upon this model, for vessels of unequal radii with small ε, Eqs. (9.128) and (9.129) reduce to

$$T_m(\eta) = T_t(\eta) + O(e^{-\xi\eta/\varepsilon P}) \qquad (9.141)$$

$$T_a(\eta) - T_v(\eta) = -\varepsilon \frac{dT_t}{d\eta} + O(\varepsilon^2) \qquad (9.142)$$

A very important result of this analysis is that Eqs. (9.141) and (9.142) are identical to those for an equal size vessel pair with the exception that σ_c in the definition of ε is based on the superposition solution for an unequal size vessel pair as described by Eq. (9.135). Therefore the effective thermal conductivity defined by the Weinbaum-Jiji bioheat equation (see Eq. (9.99)) is affected by the presence of countercurrent pairs of different size only in the evaluation of σ_c. A later study by Weinbaum and Jiji [63], published in 1989, performed the same perturbation analysis to a higher order in order to evaluate the differences between T_m and T_t to greater accuracy. The results and implications of this analysis are discussed in Section IX.C.5.d.

c. *Experimental Verification.* The 1988 paper by Zhu *et al.* [70] also presents the results of a significant experiment in which the applicability of the superposition solution to describe heat transfer normal to the axes of an unequal size countercurrent artery-vein vessel pair was examined. The temperature distribution around an experimental apparatus that modeled the perfect countercurrent heat transfer between two tubes with approximately constant, but different, wall temperatures and different radii was compared to the predictions of the theory derived by Zhu *et al.* [70] to describe this two-dimensional heat transfer. This comparison, shown in Fig. 33, reveals that the solution to one part of the superposition theory utilized in the derivation of the Weinbaum-Jiji equation for unequal size vessels—the perfect countercurrent exchange boundary value problem (see Fig. 32— second circle on right-hand side)—was in excellent agreement with experimental measurements. Differences betwen the predictions of the theory and the experimental measurements were explained by

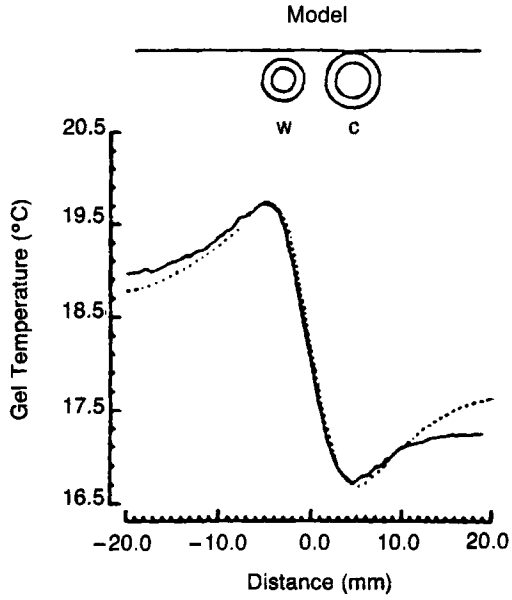

FIG. 33. Temperature profile for a thermocouple passed transverse through a gelatin block in which two tubes with different size and flowing water temperature are embedded. The centerline temperatures of the two tubes are 20.8 and 16 °C. The solid curve is experimentally measured, while the dashed curve is theoretical and based on the solution to superposition Problem 2 shown in Fig. 32. The outer surface of the gelatin block is insulated so that there is little heat exchange between the vessels and the surroundings. (Reproduced from [70], with permission from the American Society of Mechanical Engineers.)

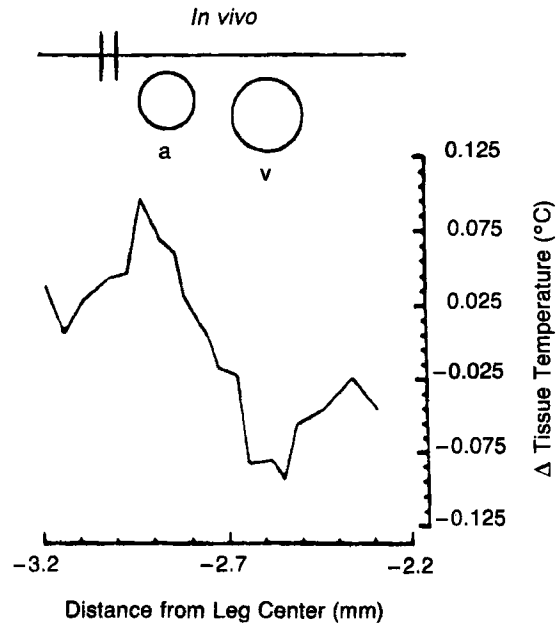

FIG. 34. Temperature profile for a thermocouple passed transverse to a countercurrent artery–vein pair *in vivo*. (Reproduced from [70], with permission from the American Society of Mechanical Engineers.)

Zhu *et al.* [70] to be due to actual nonuniformities in wall temperatures of the tubes in the experimental apparatus. In addition, there was most likely some heat transfer between the apparatus and the ambient surroundings, which was not accounted for by the part of the theory examined in this comparative study.

The predictions of the superposition theory derived by Zhu *et al.* [70] were also compared to *in vivo* measurements of temperatures near an artery–vein pair of unequal size in the rabbit thigh. These data, shown in Fig. 34, are in good qualitative agreement with the theoretical predictions in Fig. 33. Zhu *et al.* [70] conclude that it is valid to apply their superposition theory to the two-dimensional heat transfer between countercurrent vessels of different size. Consequently it is reasonable to neglect the heat transfer effect of the small, thermally insignificant microvessels that perfuse the tissue in this two-dimensional plane on the heat transfer normal to countercurrent artery–vein pairs.

d. *Second Order Analysis with* ε. A recent study by Weinbaum and Jiji [63] considers the relationship between T_m and T_t to a greater accuracy than earlier studies. The two steady state artery and vein energy balances that

define the effect of blood flow on tissue heat transfer are

$$\varepsilon \frac{d}{d\eta}(T_a - T_v) = -\frac{\sigma_t}{\sigma_c}(T_m - T_t) \tag{9.143}$$

$$\varepsilon \frac{dT_m}{d\eta} = -(T_a - T_v) + \frac{(2p-1)}{2}\frac{\sigma_t}{\sigma_c}(T_m - T_t) \tag{9.144}$$

Equations (9.143) and (9.144) are simply nondimensional versions of Eqs. (9.126) and (9.127), the combined artery and venous blood equations for unequal size artery-vein pairs. These two equations can be combined into the following single equation for the temperature difference between the tissue and the artery-vein pair by differentiating Eq. (9.144) and substituting Eq. (9.143) and its derivative:

$$T_m - T_t = \frac{\varepsilon^2}{\sigma_t/\sigma_c}\left(\frac{d^2T_m}{d\eta^2} + \frac{2p-1}{2}\frac{d^2}{d\eta^2}(T_a - T_v)\right) \tag{9.145}$$

Equation (9.145), as Weinbaum and Jiji [63] point out, is a demonstration that the temperature difference $T_m - T_t$ is of the order ε^2, even when the artery-vein temperature difference $T_a - T_v$ is significant, e.g., of order unity.

The steady state tissue energy balance, Eq. (9.81), can be written for the case of zero perfusion bleed-off as

$$nmc_b \frac{d}{ds}(T_a - T_v) = \nabla k_t \nabla T_t + Q_m \tag{9.146}$$

where $q_a - q_v$, the net heat transfer from the countercurrent vessels to the tissue, has been replaced by substitution with Eq. (9.126). Weinbaum and Jiji [63] choose to neglect the perfusion bleed-off term that appears in Eq. (9.81) in order to focus their analysis on the relationship between the perturbation parameter ε, the temperature gradients, and the countercurrent heat transfer term. Equation (9.146) is similarly nondimensionalized in terms of the spatial coordinate s:

$$n\sigma_c L^2 \varepsilon \frac{d}{d\eta}(T_a - T_v) = \tilde{\nabla}^2 T_t + \frac{Q_m L^2}{k_t} \tag{9.147}$$

Weinbaum and Jiji [63] write asymptotic expansions for T_t, T_m, and $T_a - T_v$ based on the perturbation parameter ε, the normalized vessel thermal equilibration length:

$$T_t = T_{t0} + \varepsilon T_{t1} + \varepsilon^2 T_{t2} + \cdots \tag{9.148}$$

$$T_m = T_{m0} + \varepsilon T_{m1} + \varepsilon^2 T_{m2} + \cdots \tag{9.149}$$

$$T_a - T_v = (T_a - T_v)_0 + \varepsilon(T_a - T_v)_1 + \varepsilon^2(T_a - T_v)_2 + \cdots \tag{9.150}$$

The three governing equations (9.143), (9.144), and (9.147) are next examined for each order of the asymptotic expansion. The order unity equations are

$$0 = \tilde{\nabla}^2 T_{t0} + \frac{Q_m L^2}{k_t} \tag{9.151}$$

$$0 = -\frac{\sigma_t}{\sigma_c}(T_{m0} - T_{t0}) \tag{9.152}$$

$$0 = -(T_a - T_v)_0 + \frac{(2p-1)}{2}\frac{\sigma_t}{\sigma_c}(T_{m0} - T_{t0}) \tag{9.153}$$

Thus to the lowest order of the expansion, $T_{m0} = T_{t0}$ and $(T_a - T_v)_0 = 0$. Based on this solution, the next order ε equations are simplified to

$$0 = \tilde{\nabla}^2 T_{t1} \tag{9.154}$$

$$0 = -\frac{\sigma_t}{\sigma_c}(T_{m1} - T_{t1}) \tag{9.155}$$

$$\frac{dT_{m0}}{d\eta} = -(T_a - T_v)_1 + \frac{(2p-1)}{2}\frac{\sigma_t}{\sigma_c}(T_{m1} - T_{t1}) \tag{9.156}$$

The order ε solution also indicates that T_m and T_t are equal. Equation (9.156) can be combined with Eq. (9.142) to relate tissue and blood temperature gradients:

$$\frac{dT_{m0}}{d\eta} = -(T_a - T_v)_1 = \frac{dT_{t0}}{d\eta} \tag{9.157}$$

Equation (9.157), which states that to order ε, the gradient of the mean tissue temperature is equal to the gradient of the mean blood temperature, can be viewed as the actual closure condition used in the derivation of the Weinbaum–Jiji bioheat equation. This substitution facilitates the reduction of the system of three coupled energy balance equations into a single energy balance equation that contains only the mean tissue temperature and its gradients. The resulting equation, the Weinbaum–Jiji bioheat equation shown in Eq. (9.99), is a linear, ordinary differential equation that is easily solved once the appropriate boundary conditions are specified.

Earlier derivations of the new bioheat equation by Weinbaum and colleagues relied on physical arguments to justify that $T_t \cong T_m$, and $(q_a - q_v) \ll q_a$, while the asymptotic analyses presented here and in Section IX.C.5.a show rigorously that the actual closure condition for the Weinbaum–Jiji equation is that $dT_t/d\eta = dT_m/d\eta$. The equality between T_t and T_m is essentially a result of this closure condition. It is important to note again that these relationships are valid only for cases where ε,

the normalized thermal equilibration length of the blood vessels, is much smaller than unity. Tissue regions heated by localized hyperthermia will have a characteristic temperature gradient length that is much smaller than the normothermic case, thereby increasing ε by orders of magnitude. Another exceptional case is that of heavy exercise, during which the blood flow rates in all vessels of the countercurrent network can increase by several orders of magnitude. These two examples dramatically illustrate that the applicability of the Weinbaum-Jiji bioheat heat equation depends not only on the vessel size but also on the blood flow rate as well as on the physical conditions that are being simulated.

An interesting new bioheat transfer model by Baish [4] has been developed which does not require that the mean blood temperature gradient be oriented in the same direction as the mean tissue temperature gradient. Baish shows that the enhancement in tissue thermal conductivity by convection in the vasculature can be modeled using highly conductive fibers with characteristic radii and thermal conductivities [4]. Baish also demonstrates that the effects of blood flow on tissue heat transfer in this composite model can be quantified with an effective conductance based on the number density of these conductive vessel fibers only under the condition that the mean blood temperature gradient is proportional to the mean tissue temperature gradient. This condition is the closure condition of the Weinbaum-Jiji bioheat equation.

The order ε^2 equations are

$$n\sigma_c L^2 \frac{d}{d\eta}(T_a - T_v)_1 = \tilde{\nabla}^2 T_{t2} \tag{9.158}$$

$$\frac{d}{d\eta}(T_a - T_v)_1 = -\frac{\sigma_t}{\sigma_c}(T_{m2} - T_{t2}) \tag{9.159}$$

$$\frac{dT_{m1}}{d\eta} = -(T_a - T_v)_2 + \frac{(2p-1)}{2}\frac{\sigma_t}{\sigma_c}(T_{m2} - T_{t2}) \tag{9.160}$$

Equations (9.158)-(9.160) can be combined with Eqs. (9.150), (9.155), and (9.157):

$$\tilde{\nabla}^2 T_{t2} = -n\sigma_c L^2 \frac{d^2 T_{t0}}{d\eta^2} \tag{9.161}$$

$$(T_a - T_v) = -\varepsilon \frac{dT_{t0}}{d\eta} + \varepsilon^2 \left(\frac{2p-1}{2} \frac{d^2 T_{t0}}{d\eta^2} - \frac{dT_{m1}}{d\eta} \right) + O(\varepsilon^3) \tag{9.162}$$

$$T_m - T_t = \varepsilon^2 \frac{\sigma_c}{\sigma_t} \frac{d^2 T_{t0}}{d\eta^2} + O(\varepsilon^3) \tag{9.163}$$

Equations (9.151), (9.154), and (9.161), the first three tissue energy balance equations that describe the asymptotic expansion for T_t, demonstrate that the thermal effect of the countercurrent vascular network on the tissue does not enter the solution until the order ε^2 term. Based on Eq. (9.161), the magnitude of tissue temperature T_{t2} is of order $n\sigma_c L^2$, which corresponds to a correction in the expansion for tissue temperature of $\varepsilon^2 n\sigma_c L^2$ or $n\sigma_c L_{eq}^2$. Weinbaum and Jiji [63] note that this is exactly the correction term that appears in their definition of effective thermal conductivity for the case of $k_b = k_t$ in a one-dimensional geometry (see Eq. (9.102)). The authors also emphasize that depending upon the vessel generation, this correction term may be significant. For example, under resting conditions in muscle tissue with a characteristic length $L = 5$ cm, the product $n\sigma_c L_{eq}^2$ is approximately 1.25 in the 300-μm vessels that are located in the third generation of network branching, while the parameter ε^2 is on the order of 0.01 in these same thermally insignificant vessels. For these vessel pairs the $(T_m - T_t)$ temperature difference is negligible but the net heat transfer between the vessel pair and the tissue, the so-called imperfect countercurrent exchange, is quite significant due to a large vessel density in this region.

The blood temperature equation (9.162) shows that for equal size vessels, where $p = \frac{1}{2}$, the closure approximation used to derive the Weinbaum–Jiji bioheat equation, represented by Eq. (9.157), is valid to order ε^2. For unequal vessel pairs, *in vivo* measurements of vessel spacing and radii indicate that the parameter p is nearly one-half when the ratio of the vein to artery radii is less than two. Thus the closure condition appears to be applicable to unequal size countercurrent vessel pairs as well. As noted previously in this chapter and presented in Eq. (9.163), the $(T_m - T_t)$ temperature difference is of order ε^2. Note that if the vessel pair is embedded in tissue with a linear temperature gradient, the correction term on the right-hand side of Eq. (9.163) is zero and consequently $(T_m - T_t)$ is zero, which corresponds to a perfect countercurrent exchange system where the artery, vein, and tissue temperature profiles are linear and parallel.

X. Concluding Remarks

Despite its inherent inconsistencies, certain characteristics of the original Pennes theory are considered valid in the study and application of bioheat transfer. The concept of a perfusion heat source can be a reasonable approximation of the thermal effect of blood flow on tissue under some conditions, e.g., where blood flow in large vessels is perpendicular to the tissue temperature gradient, as suggested by Wissler [67]. Regions of tissue

that contain the thermally significant blood vessels appear, in some cases, to be well described by the traditional Pennes bioheat equation. Baish *et al.* [1] measured temperatures in a laboratory model of tissue that contained an array of thermally significant tubes with high fluid flow rates. At these flow rates, there was little thermal equilibration between the tubes and the tissue matrix. Under conditions of externally applied hyperthermia, the temperatures measured in the tissue matrix were in excellent agreement with the predictions of the Pennes equation. Baish *et al.* [1] suggested that the thermally significant vessels that were examined in their laboratory behaved like line sources or sinks in the tissue, regardless of orientation, thereby corresponding to the isotropic Pennes perfusion heat source–sink formulation. A theoretical study by Charny *et al.* [19] also reported that in tissue regions that contained the thermally significant vessels, there was good agreement between the predictions of the Pennes model and a more complex vascular model that accounted for countercurrent exchange. The effect of capillary bleed-off from the large vessels in these tissue regions appeared to result in a heat source type of behavior that matched the Pennes equation. The fundamental mechanisms that explain agreement between the Pennes model and experimental measurements in these tissue regions need to be investigated on both a theoretical and experimental basis.

Since its first complete presentation in 1984, the Weinbaum–Jiji thermal model has been a major topic of analysis and discussion among members of the bioheat transfer community. Similar to the work of Wulff, Chen and Holmes, and others presented in this review, several fundamental inconsistencies of the Pennes formulation served as a motivation for the derivation of this new bioheat equation. This energy balance equation has been implemented in several peripheral tissue [24, 55] and a whole organ, macroscopic tissue model [56] to serve as a predictor of tissue temperatures during thermal stress. In their derivation and subsequent asymptotic examination of the behavior of their heat transfer model, Weinbaum and Jiji have quantified several important phenomena that have been observed *in vivo*, namely countercurrent heat transfer and perfusion bleed-off from this vascular network.

There are significant limitations to the Weinbaum–Jiji bioheat equation, however, that must be understood in order to apply the equation to a given bioheat transfer problem. The main condition for applicability is that the thermal equilibrium lengths of the blood vessels in the countercurrent network are small compared to the length scale of the macroscopic temperature gradients in the tissue. Recent comparative theoretical studies by Charny *et al.* [19] indicate that under normothermic conditions the assumptions and subsequent predictions of the Weinbaum–Jiji equation

in the tissue regions where the parameter ε is much less than unity are reasonable compared to more exact theory that solves the three blood and tissue energy balances simultaneously. More theoretical and experimental studies of the Weinbaum–Jiji equation, especially in relation to the clinical applications such as therapeutic hyperthermia and surgical rewarming, are needed to evaluate its applicability.

As suggested by Wissler [67], no single equation can be used to model bioheat transfer with a wide range of vessel sizes, and perhaps a combination of governing equations is most appropriate. The recent study by Charny *et al.* [19], which proposes a hybrid model of both the Pennes and Weinbaum–Jiji equations to be applied in different tissue regions, seems to support this suggestion. The effectiveness of these hybrid models in describing bioheat transfer in tissue is another topic for future study.

Finally, the anatomical observations and measurements of temperature fields around paired vessels by Lemons *et al.* [41] have been very useful in terms of understanding the geometry of the system being modeled and subsequently testing the predictions of the model. More of these detailed anatomical studies are needed in a variety of tissues, for instance tumors being treated with hyperthermia, so that the mathematical models of bioheat transfer will represent the actual *in vivo* physiological situations.

References

1. J. W. Baish, K. R. Foster, and P. S. Ayyaswamy, Perfused phantom models of microwave irradiated tissue. *ASME J. Biomech. Eng.* **108**, 239 (1986).
2. J. W. Baish, P. S. Ayyaswamy, and K. R. Foster, Small-scale temperature fluctuations in perfused tissue during local hyperthermia. *ASME J. Biomech. Eng.* **108**, 246 (1986).
3. J. W. Baish, P. S. Ayyaswamy, and K. R. Foster, Heat transport mechanisms in vascular tissues: A model comparison. *ASME J. Biomech. Eng.* **108**, 324 (1986).
4. J. W. Baish, Heat transport by countercurrent blood vessels in the presence of an arbitrary temperature gradient. *ASME J. Biomech. Eng.* **112**, 207 (1990).
5. H. C. Bazett and B. McGlone, Temperature gradients in the tissues in man. *Am. J. Physiol* **82**, 415 (1927).
6. H. C. Bazett, L. Love, M. Newton, L. Eisenberg, and R. E. Forster, Temperature changes in blood flowing in arteries and veins in man. *J. Appl. Physio.* **1**, 3 (1948).
7. H. C. Bazett, E. S. Mendelson, L. Love, and B. Libet, Precooling of blood in the arteries, effective heat capacity and evaporative cooling as factors modifying cooling of the extremities. *J. Appl. Physiol* **1**, 169 (1948).
8. C. Bernard, "Leçons sur la chaleur animale." Bailliére, Paris, 1876.
9. H. F. Bowman, Estimation of tissue blood flow. *In* "Heat transfer in Medicine and Biology" (A. Shitzer and R. C. Eberhart, eds.), pp. 193–230. Plenum Press, New York, 1985.
10. H. F. Bowman, The bioheat transfer equation and discrimination of thermally significant vessels. *Ann N.Y. Acad. Sci.* **335**, 155 (1980).

11. A. C. Burton, The application of the theory of heat flow to the study of energy metabolism. *J. Nutr.* **7**, 497 (1934).
12. A. C. Burton and O. G. Edholm, "Man in a Cold Environment." Williams & Wilkens, Baltimore, 1955.
13. A. C. Burton, "Physiology and Biophysics of the Circulation." Year Book Medical Publishers, Chicago, 1972.
14. F. S. Castellana, R. Skalak, J. M. Cho, and R. B. Case, Steady-state analysis and evaluation of a new thermal sensor for surface measurements of tissue perfusion, *Ann. Biomed. Eng.* **11**, 101 (1983).
15. C. K. Charny, M. J. Hagmann, and R. L. Levin, A whole body thermal model of man during hyperthermia. *IEEE Trans. Biomed. Eng.* **BME-34**, 375 (1987).
16. C. K. Charny and R. L. Levin, Simulations of MAPA and APA heating using a whole body thermal model. *IEEE Trans. Biomed. Eng.* **BME-35**, 362 (1988).
17. C. K. Charny and R. L. Levin, Heat transfer normal to paired arteries and veins embedded in perfused tissue during hyperthermia. *ASME J. Biomech. Eng.* **110**, 277 (1988).
18. C. K. Charny and R. L. Levin, Bioheat transfer in a branching countercurrent network during hyperthermia. *ASME J. Biomech. Eng.* **111**, 263 (1989).
19. C. K. Charny, S. Weinbaum, and R. L. Levin, An evaluation of the Weinbaum–Jiji bioheat equation for normal and hyperthermic conditions. *ASME J. Biomech. Eng.* **112**, 80 (1990).
20. J. C. Chato, Heat transfer to blood vessels. *ASME J. Biomech. Eng.* **102**, 110 (1980).
21. M. M. Chen and K. R. Holmes, Thermal pulse-decay method for simultaneous measurements of thermal conductivity and local blood perfusion rate of living tissues. *In* "1980 Advances in Bioengineering" (V. C. Mow, ed.), pp. 113–115. American Society of Mechanical Engineers, New York, 1980.
22. M. M. Chen and K. R. Holmes, Microvascular contributions in tissue heat transfer. *Ann. N.Y. Acad. Sci.* **335**, 137 (1980).
23. S. T. Clegg, R. B. Roemer, and T. C. Cetas, Estimation of complete temperature fields from measured transient temperatures. *Int. J. Hyperthermia* **1**, 265 (1985).
24. Z. Dagan, S. Weinbaum, and L. M. Jiji, Parametric studies on the three-layer microcirculatory model for surface tissue energy exchange. *ASME J. Biomech. Eng.* **108**, 89 (1986).
25. R. C. Eberhart, A. Shitzer, and E. J. Hernandez, Thermal dilution methods: estimation of tissue blood flow and metabolism. *Ann. N.Y. Acad. Sci.* **335**, 107 (1980).
26. L. T. Fan, F. T. Hsu, and C. L. Hwang, A review on mathematical models of the human thermal system. *IEEE Trans. Biomed. Eng.* **BME-18**, 218 (1971).
27. A. P. Gagge, C. A. Winslow, and L. P. Herrington, The influence of clothing on the physiological reactions of the human body to varying environmental temperatures. *Am. J. Physiol.* **124**, 30 (1938).
28. R. G. Gordon, R. B. Roemer, and S. M. Horvath, A mathematical model of the human temperature regulatory system—Transient cold exposure response. *IEEE Trans. Biomed. Eng.* **BME-23**, 434 (1976).
29. J. D. Hardy and E. F. DuBois, Basal metabolism, radiation, convection, and vaporization at temperatures of 22 to 35°C. *J. Nutr.* **15**, 477 (1938).
30. J. D. Hardy and G. F. Soderstrom, Heat loss from the nude body and peripheral blood flow at temperatures of 22°C to 35°C. *J. Nutr.* **16**, 493 (1938).
31. C. E. Huckaba, L. W. Hansen, J. A. Downey, and R. C. Darling, Calculation of temperature distribution in the human body. *AIChE J.* **19**, 527 (1973).
32. C. E. Huckaba, H. S. Tam, R. C. Darling, and J. A. Downey, Prediction of dynamic temperature distributions in the human body. *AIChE J.* **21**, 1006 (1975).

33. R. K. Jain, Analysis of heat transfer and temperature distributions in tissues during local and whole body hyperthermia. *In* "Heat Transfer in Medicine and Biology" (A. Shitzer and R. Eberhart, eds.), Vol. 2, pp. 3–54. Plenum Press, New York, 1985.
34. L. M. Jiji, S. Weinbaum, and D. E. Lemons, Theory and experiment for the effect of vascular microstructure on surface tissue heat transfer. Part II. Model formulation and solution. *ASME J. Biomech. Eng.* **106**, 331 (1984).
35. W. R. Johnson, A. H. Adbelmessih, and J. Grayson, Blood perfusion measurements by the analysis of the heated thermocouple probe's temperature transients. *ASME J. Biomech. Eng.* **101**, 58 (1979).
36. K. H. Keller and L. Seiler, An analysis of peripheral heat transfer in man. *J. Appl. Physiol.* **30**, 779 (1971).
37. H. G. Klinger, Heat transfer in perfused biological tissue. I. General theory. *Bull. Math. Biol.* **36**, 403 (1974).
38. H. G. Klinger, Heat transfer in perfused biological tissue. II. The macroscopic temperature distribution. *Bull. Math. Biol.* **38**, 183 (1976).
39. H. G. Klinger, Green's function formulation of the bioheat transfer problem. *In* "Heat Transfer in Medicine and Biology" (A. Shitzer and R. C. Eberhart, eds.), pp. 245–260. Plenum Press, New York, 1985.
40. J. J. W. Lagendijk, The influence of bloodflow in large vessels on the temperature distribution in hyperthermia. *Phys. Med. Biol.* **27**, 17 (1982).
41. D. E. Lemons, S. Weinbaum, and L. Jiji, Experimental studies on the role of the micro and macro vascular system in tissue heat transfer. *Am. J. Physiol.* **253**, R128 (1987).
42. R. L. Levin and M. J. Hagmann, A heat and mass transfer model for computing thermal dose during hyperthermic treatment of extremities. *In* "1984 Advances in Bioengineering" (R. L. Spilker, ed.), pp. 13–14. American Society of Mechanical Engineers, New York, 1984.
43. T. V. McCaffery and R. D. McCook, A thermal method for the determination of tissue blood flow. *J. Appl. Physiol* **39**, 170 (1975).
44. E. S. Mendelson, Measurement of the superficial temperature gradient in man. *Am. J. Physiol.* **114**, 642.
45. J. W. Mitchell and G. E. Myers, An analytical model of the countercurrent heat exchange phenomena. *Biophys. J.* **8**, 897 (1968).
46. H. H. Pennes, Analysis of tissue and arterial blood temperatures in the resting forearm. *J. Appl. Physiol.* **1**, 93 (1948).
47. W. Perl, Heat and matter distribution in body tissues and the determination of tissue bloodflow by local clearance methods. *J. Theor. Biol.* **2**, 201 (1962).
48. W. Perl and R. L. Hirsch, Local blood flow in kidney tissue by heat clearance measurements. *J. Theor. Biol.* **10**, 251 (1966).
49. R. B. Roemer and T. C. Cetas, Applications of bioheat transfer simulations in hyperthermia. *Cancer Res.* **44**, 4788s (1984).
50. P. F. Scholander and L. van Dam, Secretion of gases against high pressures in the swimbladder of deep sea fishes. I. Oxygen dissociation in blood. *Biol. Bull.* **107**, 247 (1954).
51. P. F. Scholander, Secretion of gases against high pressures in the swimbladder of deep sea fishes. II. The rete mirabile. *Biol. Bull.* **107**, 260 (1954).
52. P. F. Scholander and J. Krog, Countercurrent heat exchange and vascular bundles in sloths. *J. Appl. Physiol.* **10**, 405 (1957).
53. A. Shitzer and M. K. Kleiner, Thermal behavior of biological tissues—A general analysis. *Bull. Math. Biol.* **38**, 369 (1976).

54. A. Shitzer and J. C. Chato, Analytical solutions to the problem of transient heat transfer in living tissue. *ASME J. Biomech. Eng.* **100,** 202 (1978).
55. W. J. Song, S. Weinbaum, and L. M. Jiji, A theoretical model for peripheral tissue heat transfer using the bioheat equation of Weinbaum and Jiji. *ASME J. Biomech. Eng.* **109,** 72 (1987).
56. W. J. Song, S. Weinbaum, L. M. Jiji, and D. Lemons, A combined macro and microvascular model for whole limb heat transfer. *ASME J. Biomech. Eng.* **110,** 259 (1988).
57. J. A. J. Stolwijk and J. D. Hardy, Control of body temperature. *In* "Handbook of Physiology—Reactions to Environmental Agents" (D. H. K. Lee, ed.), pp. 45–67. American Physiological Society, Bethesda, 1977.
58. S. A. Victor and V. L. Shah, Steady state heat transfer to blood flowing in the entrance region of a tube. *Int. J. Heat. Mass Trans.* **19,** 777 (1976).
59. S. Weinbaum and L. M. Jiji, A two phase theory for the influence of circulation on the heat transfer in surface tissue. *In* "1979 Advances in Bioengineering" (M. K. Wells, ed.), pp. 179–182. American Society of Mechanical Engineers, New York, 1979.
60. S. Weinbaum, L. M. Jiji, and D. E. Lemons, Theory and experiment for the effect of vascular microstructure on surface tissue heat transfer. Part I. Anatomical foundation and model conceptualization. *ASME J. Biomech. Eng.* **106,** 321 (1984).
61. S. Weinbaum and L. M. Jiji, A new simplified bioheat equation for the effect of blood flow on local average tissue temperature. *ASME J. Biomech. Eng.* **107,** 131 (1985).
62. S. Weinbaum and L. M. Jiji, Discussion of papers by Wissler and Baish *et al.* concerning the Weinbaum–Jiji bioheat equation. *ASME J. Biomech. Eng.* **109,** 234 (1987).
63. S. Weinbaum and L. M. Jiji, The matching of thermal fields surrounding countercurrent microvessels and the closure approximation in the Weinbaum–Jiji equation. *ASME J. Biomech. Eng.* **111,** 271 (1989).
64. R. L. Whitmore, "Rheology of the Circulation." Pergamon Press, London, 1968.
65. E. H. Wissler, Mathematical simulation of human thermal behavior using whole-body models. *In* "Heat Transfer in Medicine and Biology" (A. Shitzer and R. C. Eberhart, eds.), pp. 325–373. Plenum Press, New York, 1985.
66. E. H. Wissler, Comments on the new bioheat equation proposed by Weinbaum and Jiji. *ASME J. Biomech. Eng.* **109,** 226 (1987).
67. E. H. Wissler, Comments on Weinbaum and Jiji's discussion of their proposed bioheat equation. *ASME J. Biomech. Eng.* **109,** 355 (1987).
68. E. H. Wissler, An analytical solution of countercurrent heat transfer between parallel vessels with a linear axial temperature gradient. *ASME J. Biomech. Eng.* **110,** 254 (1988).
69. W. Wulff, The energy conservation equation for living tissues. *IEEE Trans. Biomed. Eng.* **BME-21,** 494 (1974).
70. M. Zhu, S. Weinbaum, and D. E. Lemons, On the generalization of the Weinbaum–Jiji equation to microvessels of unequal size: The relation between the near field and local average tissue temperatures. *ASME J. Biomech. Eng.* **110,** 74 (1988).